Gas Sampling Using Convection and Humidity Stabilization to Improve Point Gas Sensor Responses

PAR

Emily Ann HAMMES

ÉCOLE POLYTECHNIQUE
FÉDÉRALE DE LAUSANNE

Suisse
2016

"I don't want advice."
"Nobody does. It's a giver's present. Go through the motions, Adam."
"What motions?"
"Act out being alive, like a play. And after a while, a long while, it will be true."
"Why should I?" Adam asked.
Samuel was looking at the twins. "You're going to pass something down no matter what you do or if you do nothing. Even if you let yourself go fallow, the weeds will grow and the brambles. Something will grow."
— John Steinbeck, East of Eden

To those who gave me advice even when I did not want to hear it: without their unyielding faith and love, I would have never learned to act, nothing good would have grown in me and the self that I love may have never been true. And to those who gave me the opportunities I needed to find my way back to myself and accomplish my ambitions.

Acknowledgements

Acknowledgements

cognitive abilities and disabilities can do amazing things, Ms. Skates for helping me overcome my fear of reading aloud in front of my peers and Mr. Royer for his positive attitude and teaching me mathematical modeling.

I would also like to thank Professor Papavasiliou and Professor Menhart for teaching me to love research and encouraging me to apply to top universities for my doctorate. I would like to acknowledge Professor Hall, for teaching me technical writing and using my essays as examples in her courses. I would like to thank Professor Tokuhiro, for being brave enough to let a 16 year old Emily, touch the controls on a nuclear reactor. I would also like to thank the late Robert Pritzker for financing the majority of my bachelors and masters degrees, and taking the time to teach me about his business philosophies and encouraging me to become a professor one day. I would also like to thank Professor Ogunnaike and Professor Akay for encouraging me in a time when I felt as if my world was falling apart around me. Additionally, I would like to thank Professor Jean-Marie Fuerbringer for teaching me about greco-latin squares and being supportive during my candidacy exam.

Lastly, I would like to acknowledge the people who have helped me edit this text: Professor Peter Ryser, Dr. Helmut Knapp, Simon Schubert, Virginia Hammes, Katherine Hammes, Professor Gemma Garcia Mandayo, Professor Yves Perriard, Dr. Martin Zimmermann, and Professor Jean-Louis Scartezzini.

Hergiswil, 17 April 2016   E. A. H.

Abstract

Many diseases including sick building syndrome, respiratory problems and cancers can be caused by exposure to high concentrations of toxins commonly used in modern building materials, paints, glues and furniture. To minimize exposure to these toxins, it is important to have air exchange with the outside environment. However, this is usually not energy efficient because the air must be heated or cooled.

The purpose of the Intasense project was to resolve this problem by creating an air quality monitor which could determine the current quality of air within the building. This information would then be used to control the ventilation system within an energy efficient building. The purpose of this Ph.D. thesis was both to build a system which could be used to test and calibrate sensors used in the air quality monitor as well as to build its final fluidic platform.

During this thesis, three fluidic platforms which include a humidity buffering system were designed, tested and constructed. The first platform was used to test an electrochemical sensor or metal oxide sensor in the laboratory. The second and third platforms held three electrochemical or metal oxide sensors, respectively. They are able to deliver equal quantities of gas to the sensors simultaneously. To date, the multisensor metal oxide platform has been used to create two versions of the Intasense Demonstrator and used to calibrate novel and commercial gas sensors.

In both of these applications simultaneous delivery of equal quantities of the sample gas are required for optimal gas sensor signal processing: equal quantities are required so that the amount of analyte in contact with each sensor is the same and simultaneous delivery allows all three sensors to respond concurrently. This was achieved by creating a computational model of gas flow through the system, conducting a parameter sweep and then selecting the optimal set. To confirm that the model and machine error were not significant, a Greco-Latin square design was used to test the platform. This test showed that gas delivery to each channel was equal within statistical boundaries.

Another major challenge was buffering humidity fluctuations without loss of analyte gas. This was necessary because metal oxide gas sensors are also sensitive to humidity fluctuations. To prevent a false positive caused by a rapid humidity increase, a reversible adsorbent was placed upstream of the gas sensors. However, there was concern that the adsorbent may

remove analyte gasses. To optimize the tradeoff between humidity buffering and loss or delay of analyte signal, a computational model of adsorption and desorption of gasses within the filtration system was developed. It was experimentally tested using benzene, carbon monoxide, formaldehyde and nitrogen dioxide.

To date ten platforms have been delivered to laboratories throughout Europe. Three are being used to test and calibrate gas sensors. The rest have been used to create demonstrators of the Intasense Air Quality Monitor.

Key words: Air Quality Monitoring, Computational Fluid Dynamics, Adsorption Modeling, Design of Experiments, Product Integration

Zusammenfassung

Viele Krankheiten, wie unter anderem das Sick-Building-Syndrom, Atemwegsprobleme und Krebs, können durch hohe Konzentrationen von Giftstoffen ausgelöst werden, die in modernen Baustoffen, Farben, Klebstoffen und Möbeln verwendet werden. Um den Kontakt mit diesen Giftstoffen zu minimieren, ist es wichtig, die Gebäudeluft mit der Umgebungsluft auszutauschen. Dieser Luftaustausch ist jedoch im allgemeinen nicht energieeffizient, da die Aussenluft geheizt oder gekühlt werden muss.

Das Ziel des Intasense-Projekts war dieses Problem mittels eines Luftqualitäts-Monitors zu lösen, der die aktuelle Luftqualität in einem Gebäude bestimmen kann. Diese Information würde dann verwendet, um das Belüftungssystem eines energieeffizienten Gebäudes zu steuern. Das Ziel dieser Doktorarbeit war es, sowohl ein System zu erstellen, um die Sensoren im Luftqualitäts-Monitor zu testen und zu kalibrieren, als auch die endgültige Fluidik-Plattform für den Luftqualitäts-Monitor zu erstellen.

Im Verlauf dieser Arbeit wurden drei Fluidik-Plattformen entwickelt, getestet und gebaut. Die erste Platform kann einen elektrochemischen oder Metall-Oxid-Sensor aufnehmen und wurde speziell zur Erprobung von neuen Sensoren entwickelt. Die zweite und dritte Plattform können jeweils drei elektrochemische, respektive drei Metall-Oxid-Sensoren aufnehmen. Diese Plattformen liefern gleichzeitig die gleiche Menge Gas an alle drei Sensoren. Die Plattform für mehrere Metall-Oxid-Sensoren wurde in zwei Versionen des Intasense-Demonstrators und zur Kalibrierung von neu entwickelten und von kommerziellen Gassensoren verwendet.

Sowohl bei dem Intasense-Demonstrator, als auch bei der Kalibrierung von Gassensoren ist es nötig die gleiche Menge des Probe-Gases gleichzeitig zu liefern, um eine optimale Signalverarbeitung der Gassensor-Signale zu erreichen: die gleiche Menge wird benötigt, damit jeder Sensor mit der gleiche Menge des Analyts in Kontakt kommt; die gleichzeitige Lieferung erlaubt es allen drei Sensoren gleichzeitig zu reagieren. Diese beiden Ziele wurden erreicht, indem ein numerisches Modell des Gasflusses durch das System entwickelt wurde und nach Simulationen ueber den Parameterraum die beste Lösung gewählt wurde. Die Plattform wurde mittels eines Tests, der ein lateinisches Quadrat verwendet, überprüft, um zu bestätigen, dass weder Modellfehler noch Herstellungsungenauigkeit statistisch signifikanten Einfluss auf die Gasversorgung der Sensoren haben.

Zusammenfassung

Eine weitere Herausforderung war das Puffern von Schwankungen der Luftfeuchtigkeit, ohne Analyt-Gas zu verlieren. Das Puffern ist nötig, da Metall-Oxid-Gassensoren auch auf Veränderungen der Luftfeuchte reagieren. Um Fehlalarme aufgrund eines abrupten Anstiegs der Luftfeuchte zu verhindern, wurde ein reversibles Adsorptionsmittel im Gasstrom vor die Sensoren platziert. Es bestand jedoch Verdacht, dass das Adsorptionsmittel auch Analyt-Gas entfernen könnte. Es wurde ein numerisches Modell von Adsorption und Desorption von Gasen innerhalb des Filtersystems entwickelt, um den Kompromiss zwischen dem Puffern der Luftfeuchtigkeit, und dem Verlust oder der Verzögerung des Analyt-Signals zu optimieren. Dieses Modell wurde experimentell für Benzol, Kohlenstoffmonoxid, Formaldehyd und Stickstoffdioxid überprüft.

Bisher wurden zehn Plattformen an Forschungslabore in ganz Europa ausgeliefert. Drei werden zum Testen und Kalibrieren von Gassensoren verwendet. Der Rest wurde verwendet, um Demonstratoren für den Intasense Luftqualiät-Monitor zu erstellen.

Stichwörter: Messung von Luftqualität, Numerische Strömungsmechanik, Modelierung von Adsorption, Gestaltung von Experimenten, Produktintegration

Contents

Contents

List of Figures

List of Tables

List of Abbreviations

AIChE American Institute of Chemical Engineers

C_6H_6 Benzene

CEIT Centro de Estudios e Investigaciones Tecnicas

CH_2O Formaldehyde

CO Carbon Monoxide

CSEM Centre Suisse d'Electronique et de Microtechnique S.A.

C-tech C-Tech Innovation Ltd

EC (organization) European Commission

EC (sensor) Electrochemical Sensor

EPFL École Polytechnique Fédérale de Lausanne

EU European Union

GUI Graphical User Interface

IAQ Indoor Air Quality

IEEE Institute of Electrical and Electronics Engineers

INTASENSE Integrated Air Quality Sensor for Energy Efficient Environment Control

IUPAC International Union of Pure and Applied Chemistry

MICS Metal Oxide Sensor

NBR Acrylonitrile Butadiene Rubber

NO_2 Nitrogen Dioxide

OSHA Occupational Safety and Health Administration

PCB Printed Circuit Board

List of Tables

PEEK Polyether Ether Ketone

PMx Particle Matter less than x micrometers in diameter

PMMA Poly(Methyl Methacrylate)

PPM Parts Per Million

PTFE Polytetrafluoroethylene

RH Relative Humidity

SiO$_2$ Silica Gel Bulk Formula

SiOH Silica Gel Surface Formula

SUVA Schweizerische Unfallversicherungsanstalt

Temp Temperature

TUIL Technische Universität Ilmenau Institut fur Mikro- and Nano-technologien

UV Ultraviolet

VOC Volatile Organic Compound

WHO World Health Organization

1 Introduction to Air Quality Monitoring

It is commonly accepted that air pollution causes respiratory illness and other medical problems. For example, the life expectancy of inhabitants of northern China is 5.5 years lower than their southern counterparts due to emissions from coal burning for heating [Chen et al., 2013]. However, what the general public often fails to realize is that many pollutants are generated within a building. These sources include general office supplies such as glues and printers, furniture, carpets, or occupant's clothing after a smoking break. In places where the air quality index is generally good, the easiest way to reduce an individual's exposure to chemicals from indoor sources is to increase the amount of fresh air entering the room. However, this increases the energy consumption of the building.

As energy costs increase and the environmental cost of carbon emissions becomes more apparent, there has been a trend toward designing low energy buildings. Within the European community, heating typically accounts for more than half of the total energy consumption of both public and residential buildings [Janssen, 2004]. Therefore, improving the climate control system in a building would reduce the energy consumption of that building.

With this in mind, modern buildings are often equipped with a central heating system which regulates the ratio of fresh air to recycled air. These systems moderate the humidity, however they often lack an air quality monitor. Thus, the ratio of fresh to recycled air is based on generic guidelines or regulations, not the quantity of pollutants in the air within the building.

The purpose of this doctoral thesis is to design and test the fluidic packaging and preconditioning unit for an air quality monitoring system, as presented in Chapters 2 and 3. The system was also used to test and calibrate multiple gas sensors simultaneously. Six of these devices have been incorporated into product demonstrators, as part of the Intasense project. These prototypes include electronics to run and record data from the pump, flow sensor, humidity sensors, temperature sensors, air filters and three metal oxide semiconductor sensors. This integration and an overview of the collaborative work is presented in Chapter 4.

1.1 What is Air Quality Monitoring?

Indoor air quality monitors are devices which report the current air quality of a gas sample based on a variety of parameters including the concentration of chemicals such as carbon dioxide, general volatile organic compounds (VOCs), temperature and humidity. Temperature and humidity are usually measured to determine occupant comfort. Carbon dioxide is frequently used as a proxy for building occupancy, as the only common sources within buildings are humans breathing and gas stoves in kitchens. VOC measurements are used to get a qualitative assessment of the smelliness of the air or the presence of hazardous gasses. These are not absolute measurements or chemical specific i.e. they do not differentiate between chemicals such as ethanol, expected from a broken bottle of vodka, and toxic cleaning fluids.

Sometimes these parameters are reported separately, sometimes they are grouped into one overall measurement, such as a green LED for "good" and a red one for "bad." The devices can be stand alone, such as a personal device which sits on an office desk and reminds the user to open the window, or they can be integrated into the building. Integration into the building allows for automated responses, such as opening a ventilation system or turning on a humidifier.

1.2 Sources of Chemicals and Particles and Their Effect on Human Health

Many of the pollutants which lead to poor air quality come from common household activities, chemicals and devices. In addition to human discomfort, they are associated with a variety of diseases. For example, nitrogen dioxide (NO_2), carbon monoxide (CO) and carbon dioxide (CO_2) which are produced by combustion processes, such as smoking or using a gas stove or heater, can cause a variety of diseases. Specifically, nitrogen dioxide is associated with respiratory problems [Belanger et al., 2006]. Carbon monoxide is a well-known poison which has a greater affinity for hemoglobin than oxygen does. Thus, when red blood cells are exposed to CO, the CO will inhibit oxygen transport within the body [Pace et al., 1950]. Unlike CO and NO_2, CO_2 is relatively innocuous: it only becomes toxic when it is in extreme excess [Ikeda et al., 1989]. However, because both humans and combustion reactions convert oxygen to CO_2, CO_2 can be a simple and useful gauge of indoor air quality.

Aside from combustion processes, there are many other pollutant sources within a home or office. Common office equipment and household products can create gaseous byproducts which lead to medical problems. Printers and copy machines produce ozone (O_3) which can alter the epithelial cells of the upper respiratory tract and lungs and cause a variety of respiration related problems including asthma [Tuomi et al., 2000]. Moth balls contain p-Dichlorobenzene ($C_6H_4Cl_2$), a cytotoxic and genotoxic chemical which has been correlated with increased risk of blood diseases such as aplastic anemia and hemolytic anemia [Tenenbaum, 2004]. Tobacco smoke can generate benzene (C_6H_6) and toluene (C_7H_8). Additionally,
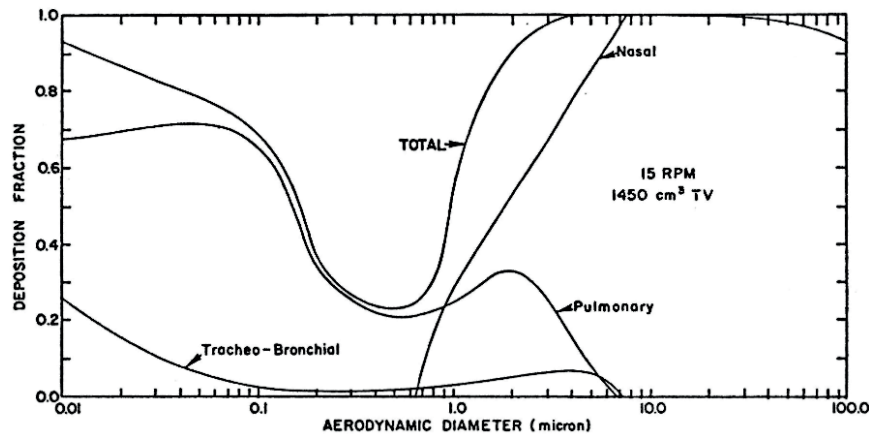
Figure 1.1 – Relative deposition of inhaled particles of various sizes, assuming a respiratory rate of 15 breaths per minute and a tidal volume of 1450 cm^3 [Phalen and Raabe, 1974].

benzene is found in fuels and toluene is found in paints and paint thinners. Benzene increases cancer risk. Toluene is associated with neurological damage [Wallace, 1989; Eisenberg, 2003]. Another potential carcinogen frequently found in buildings is formaldehyde (CH_2O). This is used in many fabrics, paints, cleaners, insulating materials and particle board [Cooke, 1991]. It is also emitted from printers [Tuomi et al., 2000].

Finally, small particles, roughly PM10, can enter the respiratory tract and cause irritation. Particles greater than PM8 are almost completely deposited in the respiratory airway between the nose and the larynx. These particles have a residence time of about 1-2 days and are removed by blowing the nose. A small fraction of particles below PM10 are deposited in the the tracheobronchial region, which extends from the trachea to the terminal bronchioles, is lined with cilia, small whip like protrusions which extend from a cell of the epithelium which lines the tubes of the lungs. The cilia propel these particles out of the lungs via a rhythmic motion. Thus, they will end up in the gut within 24 hours of inhalation. Particles smaller than about 7PM can make it past the nasal and tracheo-bronchial region, into the pulmonary region of the body to be deposited in the respiratory bronchioles, alveolar ducts and sacs, atria and alveoli. In this part of the body the residence time of particles can be years [Cooke, 1991] (Figure 1.1).

1.3   Regulations

Recognizing the detrimental health effects associated with the aforementioned gasses and particulates, the European Commission, the World Health Orginization (WHO) and the United States (OSHA) have set exposure limits for toxic gasses (Table 1.1) and particles (Table 1.2). Additionally, to calculate overall acceptable limits of multiple pollutants within a given time

Pollutant	Organization	Limit or Suggested Limit
CO	WHO:	$100\,\mathrm{mg\,m^{-3}}$ for 15 min
		$35\,\mathrm{mg\,m^{-3}}$ for 1 hour
		$10\,\mathrm{mg\,m^{-3}}$ for 8 hours
		$7\,\mathrm{mg\,m^{-3}}$ for 24 hours
	OSHA:	$<55\,\mathrm{mg\,m^{-3}}$ (50 ppm) 8 hour average
	EC:	$10\,\mathrm{mg\,m^{-3}}$ maximum daily 8 hour mean
CO_2	EU:	Measure up to 5000 ppm
	OSHA:	$<9000\,\mathrm{mg\,m^{-3}}$ (5000 ppm) 8 hour average
CH_4		$<20\%$ of lower explosive limit. Equivalent to 1% CH_4
	OSHA:	No limit per se. O_2 must remain above 18%
O_3	EC:	$120\,\mathrm{\mu g\,m^{-3}}$ maximum daily 8 hour mean
	WHO:	$100\,\mathrm{\mu g\,m^{-3}}$, 8-hour mean
	OSHA:	$<0.2\,\mathrm{\mu g\,m^{-3}}$ (0.1 ppm) 8 hour average
NO_2	WHO:	$200\,\mathrm{\mu g\,m^{-3}}$ 1 hour average
		$40\,\mathrm{\mu g\,m^{-3}}$ annual average
	EC:	$200\,\mathrm{\mu g\,m^{-3}}$ 1 hour average
		$40\,\mathrm{\mu g\,m^{-3}}$ annual average
	OSHA:	$<5\,\mathrm{mg\,m^{-3}}$ (0.9 ppm) ceiling limit
Benzene	EC:	$5\,\mathrm{\mu g\,m^{-3}}$, 1 year averaging
	OSHA:	<10 ppm 8 hour average
		acceptable ceiling concentration 25 ppm
		maximum peak above the ceiling concentration per 8 hours: 50ppm
	WHO:	No safe level of exposure can be recommended
		Unit risk of leukemia per $1\,\mathrm{\mu g\,m^{-3}}$ air concentration is $6e-6$
		The concentrations of airborne benzene associated with an excess lifetime risk of 1/10,000, 1/100,000 and 1/1,000,000 are 17, 1.7 and $0.17\,\mathrm{\mu g\,m^{-3}}$ respectively
Formaldehyde	OSHA:	<2 ppm for 15 minutes
		<0.75ppm for an 8 hour average
	WHO:	$0.1\,\mathrm{mg\,m^{-3}}$, 30 min. average
Toluene	OSHA:	<200 ppm 8 hour average
		acceptable ceiling concentration 300 ppm
		maximum peak above ceiling concentration per 8 hours: 500ppm
P-dichlorobenzene	OSHA:	$<75\,\mathrm{mg\,m^{-3}}$ (450 ppm), 8 hour average

Table 1.1 – Regulations on gas exposure. World Health Organization (WHO) data was reprinted from [WHO Regional Office for Europe, 2010]. Occupational Safety and Health Administration (OSHA) data was reprinted from [OSHA, 2006b,c]. European Commission data was reprinted from [European Union (EU), 2015]. European Union (EU) data was reprinted from European Recommendation (EN-45544-1).

Particles	Organization	Limit
PM2.5:	EC:	$25\,\mu g m^{-3}$, 1 year average
		starting in 2015: $20\,\mu g m^{-3}$, 3 year average
		starting in 2020: $18\,\mu g m^{-3}$, 3 year average
	WHO:	$10\,\mu g m^{-3}$, annual mean
		$25\,\mu g m^{-3}$, 24-hour mean
PM10:	EC:	$50\,\mu g m^{-3}$, 24 hour average
		(permitted exceedences per year: 35)
		$40\,\mu g m^{-3}$, 1 year average
	WHO:	$20\,\mu g m^{-3}$, annual mean
		$50\,\mu g m^{-3}$, 24-hour mean
Reparable fraction:	OSHA	$<5\,mg m^{-3}$, 8 hour average
Total Dust:	OSHA	$<15\,mg m^{-3}$, 8 hour average

Table 1.2 – Regulations on particle exposure. World Health Organization (WHO) data was reprinted from [World Health Organization, 2006]. Occupational Safety and Health Administration (OSHA) data was reprinted from [OSHA, 2006d]. European Commission data was reprinted from [European Union (EU), 2015].

OSHA gives the following formula [OSHA, 2006a]:

$$Em = ([A]/L_A + [B]/L_B + \ldots + [N]/L_N) \tag{1.1}$$

Where Em is the equivalent exposure for the mixture, $[N]$ is the concentration of chemical N and L_N is the exposure limit for substance N in an 8 hour period. Thus, Em values smaller than 1 are within acceptable limits.

Note: the chemical concentration and exposure limit for any given substance must be in the same units. Different chemicals and their exposure limits can be in different units, i.e. chemical A and chemical B can be in different units. This is because the ratio between the chemical and its limit will unitless. Thus, Em is a unitless parameter.

1.4 Commercial Benefit

Due to the risk of disease and illness from toxins which are generated within a building and the potential liability to the employer or building owner if these exposure limits are exceeded [Icard, 1994], it is absolutely necessary to have some kind of ventilation in buildings. However, excess ventilation reduces energy efficiency. Thus, there is a trade-off between energy efficiency and air quality. Table 1.3 shows the energy savings potential for various location types, when a real time air quality monitor is used to optimize the trade-off between energy efficiency and air quality.

Location	Potential Energy Savings (%)
Lecture Hall	20 to 50
Open Plan Offices	
40% occupancy	20 to 30
90% occupancy	3 to 5
Entrance Halls, Airport Check-in Areas, Booking Halls	20 to 60
Exhibition Halls or Arenas	40 to 70
Theaters, Cinemas, Conference Rooms, Assembly Rooms	20 to 60
Restaurants and Canteens	30 to 70

Table 1.3 – Potential energy savings after air quality monitor is installed [Siemens Building Technologies, 2015].

1.5 Overview of Air Quality Monitors

To optimize this trade-off between indoor air quality and energy efficiency, a variety of air quality monitors have been introduced to the market. They fall into three broad categories: personal or desktop devices, portable professional devices and devices which are integrated into the building.

1.5.1 Personal Devices

Personal air quality monitors are low cost ($100 to $300) devices designed to be purchased by an individual. Despite what user reviews on these products might indicate, they are not safety devices. They are not intended to replace fire detectors or carbon monoxide detectors in homes. Neither are they intended to guide health choices such as whether or not to open a window while painting a room or working with other household chemicals where ventilation is recommended.

Some integrate with a smart phone, while others have a digital display. They vary in what they measure and can include any combination of sensors targeting carbon dioxide, general VOCs, temperature, humidity and particles of various sizes. These devices are not always well calibrated. Users frequently report that devices intended to measure the same things do not report the same overall air quality or quantitative values.

1.5.2 Portable Devices

In contrast to personal devices, portable devices measure the largest array of gasses. This is reflected in their high price. Devices which measure a single toxin range from $250 to $1,000, while systems which detect multiple contaminants cost between $6,000 to $10,000. Generally, they are used by companies which specialize in ventilation installation in order to confirm that the ventilation system in a building is sufficient. Additionally, they could be

Product	Measures: VOC	CO_2	PM	Temp.	RH
Foobot	X	X	2.5	X	X
Withings Home	X				
Netatmo Indoor Module		X		X	X
Awair	X	X	2.5 and 10	X	X
UNI-T UT938C	X		2.5	X	X
Dylos DC1100			X		
Indoor Air Quality Meter by CO2METER		X		X	X
Blueair Aware	X	X	2.5	X	X
Sper Scientific 800048		X		X	X

Table 1.4 – Examples of personal devices labeled as Indoor Air Quality monitors sold on Amazon.

Device name	Measures	Mounting	Battery
DustTrack II	PM	Hand	Rechargeable
DRX aerosol monitors	PM	Desktop	Rechargeable
Testo 361-1	CH_4	Hand	5h
Testo 435	CO_2, RH, Temp., Pressure	Hand	200h
Testo 400	CO_2, RH, Temp., Pressure	Hand	18h
Testo 535	CO_2	Hand	6h
Kanomax IQM 60	PM, CO, CO_2, VOC, O_3, RH, Temp.	Desktop	Optional
Quest Technologies—EVM-7	PM, CO_2, VOC, RH, Temp.	Portable	Rechargeable
Grey Wolf DirectSense IQA	CO, CO_2, VOC, RH, Temp.	Portable	120h

Table 1.5 – Examples of portable professional Indoor Air Quality monitors.

used by companies specializing in air quality in order to confirm that toxins do not exceed local legislative guidelines. These portable devices are designed for short term data collection: they typically have a battery life between a few hours and a week. As such, they are not suited for permanent installations. Examples of portable air quality monitoring devices are listed in Table 1.5.

1.5.3 Permanent Devices

Permanent air quality monitors are also intended for professional use. They range in price from about $700 to $1,000. These devices integrate with the ventilation system of a building to dynamically control the ratio of fresh to recycled air. The monitors can either be mounted directly in the air ducts or on the wall of a specified room, depending on user preference and device model. Similar to the personal devices, these systems usually only monitor a few components of air quality. However, unlike the personal devices, their accuracy is quantified.

Product	Measures: VOC	CO_2	Temperature	Humidity
Honeywell IAQPoint2 with CO_2 sensor		X	X	X
Honeywell IAQPoint2 with VOC sensor	X		X	X
Siemens QPA84	X			
Siemens QPA200		X		
Siemens QPA2002	X	X		
Siemens QPA2060		X	X	
Siemens QPA2062		X	X	X
Greystone Air41	X	X	(optional)	
BAPI VOC duct	X			
BAPI CO2 duct		X		
BAPI VOC room	X			
BAPI CO2 room		X		

Table 1.6 – Examples of Indoor Air Quality monitors designed for permanent installment into buildings.

Examples of such products can be seen in Table 1.6.

1.5.4 Ways to Improve the State of the Art

Undoubtedly some air quality monitoring is preferable to none. However, simply monitoring general CO_2, temperature and humidity is a better indicator of physical comfort than chemical exposure. Simply adding a generic or total VOC sensor is not sufficient because the exposure limits vary by orders of magnitude between chemically similar VOCs, such as toluene and benzene. Therefore, there is a place in the market for an indoor air quality monitor which would permanently and continuously measure the quality of air as a function of specific combustion gasses (i.e. NO_2, CO, CO_2), specific VOCs (i.e. benzene, toluene, formaldehyde and p-dichlorobenzene), humidity and temperature. Moreover, it would be best to develop the device so that sensors could be selected based on the end location of the device and switched out or added without need for a device redesign or replacement. For example, combustion gasses may be of more interest in buildings in large cities or near highways while toluene could be of greater concern in a new building or one undergoing renovations. Fortunately, many commercial sensors, with a given working principle, come in standardized packages and have similar pinouts. Thus, with the turn of a potentiometer, or the addition of a resistor, the same platform could be populated with gas sensors designed to measure different target gasses.

1.6 Overview of Gas Sensing Technologies

Gas sensor technologies are both well-established commercially and are an active research topic. They are frequently used in a wide range of commercial devices. For example, oxygen

sensors are used to optimize and control the efficiency of combustion engines; carbon monoxide detectors, which incorporate sensors, are used to detect toxic gas within homes. Companies such as Figaro, SGX (once e2v) and City Technology provide dozens of gas sensing options which use multiple technologies. Additionally, research organizations such as the European Commission are investing in basic research in hopes of developing new sensors which are more specific than those currently available on the market. Some of the most common technologies currently used in sensors, both commercially and by academic research groups, include electrochemical, pellistor, metal oxide and infrared detection.

1.6.1 Sensors on the Market

Electrochemical gas sensors, also called solid electrolyte gas sensors, work by forming a galvanic cell which reacts with the analyte of interest. This reaction creates a small current which is proportional to the concentration of the gas of interest. These sensors can be both temperature and humidity sensitive due to the chemical composition of and the reactions between the sensing electrode, the reference electrodes and the salt bridge. Additionally, many designs require oxygen influx from the sensed gas in order to work properly [Azad et al., 1992; Yamazoe, 2005; E2v, 2007c].

Similar to electrochemical gas sensors, catalytic pellistor sensors also rely on changes in electrical properties. Sometimes referred to as catalytic combustion or solid state sensors, pellistor sensors contain a wire, often platinum, which is coated with an alumina bead doped using a dispersed catalyst such as platinum or palladium. The wire is heated to a few hundred degrees Celsius by an electric current and gas is allowed to diffuse through the bead to the wire where it combusts. This combustion causes an increase in the temperature of the wire and thus an increase in its resistance. The resistance change can then be correlated to the amount of gas burned [Fanget et al., 2011; E2v, 2007b; Azad et al., 1992].

Metal oxide sensors, sometimes called semi-conductor sensors, also use changes in resistance to detect gases. However, these sensors do not use combustion, but rather use the oxidative state of a porous material to detect gases. They are commonly used for detecting low concentrations of combustible gases. Three factors control the sensitivity of these sensors: receptor function, transducer function and utility. Receptor function involves the chemical properties of the sensor and how these influence the interaction between the oxide surface of the sensor and the analyte of interest. Sensors of this type use oxidation or reduction to sense gases, so humidity, which acts as a reducing agent, influences the reactivity of the sensor surface. The transducer function describes the conversion of this chemical interaction to an electrical signal. Finally, utility describes the transport phenomena which determine how the analyte reaches the surface of the sensor and diffuses into its pores. The reactivity of these sensors is dependent on the microstructure of the metal oxide surface and the activation energy required by the oxidative or reductive reaction. As such, many of these sensors must operate at high temperatures (i.e. a few hundred degrees Celsius) [Yamazoe, 2005; E2v, 2007a;

Azad et al., 1992; Chang et al., 2002].

Unlike electrochemical, pellistor or metal oxide sensors, infrared sensors do not use changes in electrical properties to detect gases. Rather, they measure light absorbed by chemical bonds within the sample. This works because infrared radiation of specific wavelengths can be absorbed by dipoles within gaseous molecules. The wavelengths which the molecules absorb are dependent on the chemical bonds within the molecule. For example, a single bond between carbon and oxygen (C-O) will absorb different wavelengths than a double bond between carbon and oxygen (C=O) or a single bond between carbon and hydrogen (C-H). Based on this absorption pattern, the chemicals present within a sample can be identified. When the chemical species within a sample are unknown, a dispersion spectrum must be taken to determine all of the chemical bonds within the sample. However, when the sample content is known, a whole spectrum does not need to be taken and thus nondispersive infrared may be used. Nondispersive infrared does not check for the whole spectrum of bond types, but rather uses limited wavelengths and IR detectors to only check for the bond types of interest. If the desired spectrum includes a single bond between oxygen and hydrogen (O-H) bonds, then the humidity of the gas sample needs to be taken into account. Moreover, water's absorption spectrum can be strong enough to hide the analyte's signal below 3 microns, between 5 and 8 microns and above 16 microns [Fanget et al., 2011; E2v, 2007d].

In addition to these sensor types, novel gas sensor technologies are presented yearly at conferences such as the American Institute of Chemical Engineers (AIChE), Institute of Electronics and Electrical Engineers Sensors (IEEE Sensors) and Sensors Exposition and Conference. Frequently, these sensors are designed to be more specific than those currently on the market. One popular method of increasing specificity is to combine multiple sensors with different properties in the same package. This results in a sensor with multiple signals which can then be analyzed using a mathematical model to determine more precisely which gases are in the sample.

1.6.2   Sensor Testing and Calibration

Both in the laboratory and in the field, there is high demand for specific and robust gas sensors which operate efficiently under application defined conditions. These conditions can include temperature, humidity, flow, reaction rates and cross sensitivities. Often, multiple sensors will work for a given application, so comparisons must be made to select the best option. However, although there are a wide variety of sensors for gases of particular interest, such as carbon monoxide, oxygen, combustion gases or volatile organic compounds (VOCs), there are not standardized methods for comparing or optimizing operating parameters for sensors. Furthermore, publications frequently do not report sufficient data to recreate the fluid dynamics within the sensor testing chamber, which means that it is unclear how much gas was in contact with the sensor surface. Additionally, the standard relative humidity used for calibration varies between manufacturers. Therefore, it is frequently impossible to accurately

Gas/parameter	Commercial Sensors (not exhaustive list)
Humidity & Temperature	Sensiron: SHT21, SHT75
Pressure	MEAS: MS5540C
O_2	E2V: 410
	City Technology: 2FO, 2FO-N, 5FO
O_3	E2V: MICS-2614, MICS-2610, MICS-2611;
	City Technology 3OZ, O3 3E 1, O3 3E 1 F, A3OZ
NO_2	E2V: EC4-20-NO2
	City Technology: multiple options
CO_2	E2V: (16 different options)
	City Technology IRceLCO2
CO	E2V: EC4-500-CO
	City Technology ECOSURE
Benzene	E2V and City Technology
	(multiple, for nonspecific combustible gasses)
Toluene	E2V and City Technology
	(multiple, for nonspecific combustible gasses/hydrocarbons)
Formaldehyde	E2V and City Technology
	(multiple, for nonspecific combustible gasses/hydrocarbons)
p-dichlorobenzene	E2V and City Technology
	(multiple, for nonspecific combustible gasses/hydrocarbons)
Particles (general)	Seeedstudios groove dust sensor
	SHARP GP2Y1010AU0F

Table 1.7 – Commercially available air quality sensors.

compare sensors based on published data. Thus, when an end user is designing a product which requires a gas sensor, a variety of sensors must be tested in order to determine optimal fluid dynamics for a given sensor in a particular application. Additionally, the end user must determine optimal operating parameters such as temperature, influences of humidity, etc. Only after these parameters have been determined can a sensor be selected and a product designed for an industrial application.

1.6.3 Ways This Could be Improved

Both sensor selection for product design and the sensor optimization process could be expedited if standardized methods for comparing and testing gas sensors were developed. However, this is nontrivial because of the fluid dynamic requirements, humidity sensitivity and operating temperatures of the sensors. Therefore, in the course of this thesis, I developed multiple gas sensor testing platforms which operate in a controlled, plug and play fashion, so that experiments using many different operating conditions and many different sensor types could be easily conducted using the same device with known and therefore comparable, operating parameters.

The single sensor version of the gas sensing platform was integrated into the Intasense product prototype. This version was used by collaborators in England and Spain to test and calibrate sensors. Three different methods for collecting and analyzing sensor data were developed for this platform and are presented in Section 4.3. Additionally, a multisensor version of this platform was developed and published in *Urban Climate*. Finally, a miniaturized multisensor fluidic platform was developed which houses three gas sensors in TO8 packages. This platform was integrated into the final Intasense Demonstrator. It was used by laboratories in Spain, the Netherlands, Switzerland and England to test and calibrate both commercial gas sensors and laboratory prototype sensors.

1.7 Research Questions and Device Requirements

Before the first prototype could be designed, there were many research questions which needed to be explored and device requirements which needed to be defined. These included gas delivery, material properties, size, fluid dynamics and chemical adsorption.

1.7.1 Sensor Comparison and Testing Methods

Currently, literature containing standardized methods for comparing various sensors is not readily available, so further experimentation and methodology development are required. Most likely, this lack of methods stems from the motivational differences between industry, whose objective is to sell their products and protect intellectual property, and basic research institutions, whose goals are to disseminate information in peer reviewed journals. This has resulted in a gap between what is published in academic literature and the tests which must be done to make a marketable product. Specifically, for publication purposes, it is sufficient to demonstrate a proof of concept. However, this level of testing may not accurately emulate the conditions of the real world or the longevity required for a marketed product. Due to this, the sensor technologies reported in peer reviewed journals are frequently not ready to be transferred to an industrial prototype. Thus, comparisons between sensors are largely left to industry. However, industry has no motivation to publish this data—rather it is often left as a trade secret and the consumer is instructed to call a sales associate for further information prior to ordering. It is unclear, therefore, based on both information from data sheets for commercially available sensors and from peer reviewed journals, what the optimal method for comparing sensors would be. Furthermore, it is often unclear which sensor would be ideal for a given application. For example, e2v sells many VOC sensors; however, based on published data, it is impossible to determine which sensor would be best for a given application without experimentation because selectivity, or cross-sensitivity, data is unavailable.

Although methods for comparison are not standardized, methods for validating concepts in the basic research phase are well documented. In both academic and industrial settings, gas sensing technologies are commonly tested using a small amount of the gas of interest diluted in either a base gas mixture like synthetic air (i.e. 79% nitrogen and 21% oxygen, by

volume) or a pure nonreactive gas like nitrogen. Occasionally, a second contaminant gas is added to demonstrate some specificity to the sensing target. As this is the common way that most sensors are tested, and because laboratories in the field are set up to work with such mixtures, the device is able to use similar inputs. Additionally, the device was designed to use ambient air from the surroundings, as this is sometimes also used in laboratories. To minimize rapid humidity fluctuations, which can cause problems for many sensor types, an optional preconditioning unit can be added to the device.

1.7.2 Device Requirements

In order to compare sensors it is necessary to create a device with controlled and yet modifiable properties which will be suited to multiple sensor technologies. Specifically, differences in humidity, temperature, flow rates and gas delivery method (i.e. convection or diffusion) can influence how the sensor operates so these parameters must be known or controlled. In order to safely test toxic gases, it must also be airtight and small enough for the entire testing apparatus to easily fit under a hood as an extra precaution. Additionally, materials were selected so that the gas of interest does not react with components within the device. Similarly, the device must be able to withstand the operating temperatures of the sensors and allow light of various wavelengths to reach the sensor surface, as some sensors are activated using LEDs. Finally, it was necessary to be able to conduct experiments using both gas standards or ambient air, so humidity stabilization and particle filtration are optionally included. Particle filtration was included to prevent dust or dirt from blocking the sensor surface. Additionally, because the humidity is not constant in ambient air and humidity fluctuations can cause many sensors to give inaccurate measurements, it was necessary to include humidity stabilization. However, this is challenging because it is difficult to selectively remove water, without removing toxins, from the air.

1.7.3 Device Materials

The materials used in the device were selected to prevent chemical reactions between the gas of interest and the housing materials. Also, the materials were selected to support the environmental requirements of the sensors. As such, the device was designed so that light can pass through the sensor housing to the sensor surface. Additionally, the housing is able to withstand high temperatures, is relatively inert and is easily machined.

As there is no single material which possesses all of these properties, identical housings were made using a range of materials optimized for specific sensor types in order to produce comparable data. For example, some sensors needed light activation, with the light source optimally being external to the fluid path so as to prevent altered fluid dynamics based on its presence or absence. In this case the material was selected so that the light can pass through the device to the sensor surface. For this purpose poly(methyl methacrylate) (PMMA) was used for the base of the device.

Additionally, temperature also plays a role in the material used for various components. Many sensors have operating temperatures in the range of hundreds of degrees Celsius. However, very few plastics have melting points above these temperatures. Therefore, it was necessary to make some components out of polyether ether ketone (PEEK) which has an acceptable melting point (maximum operating temperature of 250 °C [Oberbach et al., 2001]). Additionally, it was necessary to design the device so that heat transfer was minimized.

Finally, and most importantly, the material was selected to prevent loss of analyte due to reaction with or long desorption times from the surfaces within the device. This is especially true for the preconditioning unit which is designed to be adsorbent. To quantify this problem, many experiments were conducted and are fully presented in Chapter 3.

1.7.4   Active Versus Passive Sampling

When designing the device the pros and cons of both convective (active) and diffusive (passive) sampling need to be considered. Although many household gas detection systems, such as smoke detectors, use diffusion to sample gases from the environment, it is also common for gas sensors to be designed to receive samples by convection. Furthermore, convection is required if the gas needs to be preconditioned. This includes particle filtration, dehumidification or humidity stabilization. Additionally, it is much simpler to switch between gas samples if the device can be purged via convection. The drawbacks to using convection are that some sensors operate best with very low flow rates, with small gas samples or with the use of diffusion. This can be the case with chemical sensors which are limited by the catalytic activity of the electrodes [E2v, 2007c]. However, this can be accounted for when designing the sensor chamber or selecting a pump speed.

1.7.5   Device Fluid Dynamics

Three types of flow across the sensor surface were considered: maximized convective flow, uniform convective flow and diffusion. Which flow type is appropriate for a specific sensor is a function of the sensor type and whether that type is optimal under diffusive or convective transport. The first flow type to be considered was maximized convective flow to the sensor surface. To achieve this, the flow direction was changed within the sensor chamber so that more air was pushed up to the sensor than would be possible at a similar flow rate in a tube. The one drawback of this design is that the flow is uniform across the sensor surface, although it will be bilaterally symmetric. When this is a problem, uniform convective flow can be used. To do this the sensor is placed flat against the wall of a channel with a fully developed flow profile. Although less of the gas sample is pushed against the sensor surface, the flow becomes uniform across it. Finally, some sensors require diffusion. In this case, the sensor needs to be intentionally placed in a dead volume. However, for preconditioning to work, gas still needs to pass through the chamber by convection, so the sensor itself must be some distance from the main flow. However, this distance must be minimal so that diffusion times do not prevent

the sensors from working in real time. After much deliberation with gas sensor designers, the maximized convective flow was selected for all the platform prototypes because it minimizes the amount of air which needs to be preconditioned.

1.7.6   Design of the Preconditioning Unit

When using gas samples with uncontrolled water content, such as ambient air, humidity stabilization is often an important feature. Most sensors cannot operate in condensing environments and are optimized for only specific ranges of humidity. Furthermore, water can interfere with some sensor's operation by disrupting IR signals or acting as a reducing agent in chemical sensors [E2v, 2007c,d]. Therefore, it is necessary to account for the humidity in the system and to avoid any rapid fluctuations which could occur. Additionally, dust accumulation on the sensor surface can shorten its life span so particle filters are included in the preconditioning unit.

Silica gel was chosen as the primary candidate for the humidity stabilization units because it is chemically inert. However, because of its chemical structure it adsorbs and desorbs polar chemicals at its surface by hydrogen bonding with them [Scott, 2000]. This has been extensively studied, mathematically modeled and exploited in liquid chromatography, where chemicals are separated by polarity based on how long it takes them to travel down the length of a column under a continuous flow of liquid [Golshan-Shirazi and Guiochon, 1989; DeVault, 1943; Guiochon and Lin, 2003; Finlayson, 2006; Bird et al., 2007].

Although silica gels adsorptive properties in liquids and for gaseous water are well studied [Pesaran and Mills, 1987a,b; Pesaran, 1983; San and Jiang, 1994], the kinetics of the adsorption process vary. Additionally, there is relatively little published literature on its adsorption kinetics of various gases. However, there are a few studies on ammonia NH_3 [Kuo et al., 1985; Davidheiser, 1921; Bliznakov and Polikarova, 1966], benzene C_6H_6 [Wang et al., 2004], nitrogen dioxide NO_2 [Izumi et al., 2002], carbon monoxide CO [Markham and Benton, 1931] and acetylaldehyde C_2H_4O [Yang et al., 2005; Weinstock et al., 2005]. Although these studies give insight into how to design the system, available data was not extensive enough to gain a complete perspective. Therefore, experimental studies were conducted to determine the reaction rates for water and the mathematical model for gas transport which best fits the target gases' interaction with silica gel.

1.8   Thesis Outline

Chapter 1 gave an overview of the current state of the art in air quality monitoring. It included an introduction to the sources of pollutants and their effects on human health. Then an overview of the regulations and suggestions for exposure to various chemicals and particulates were discussed. This was followed by a discussion of the three main types of air quality monitoring devices currently on the market: personal devices which give a poorly calibrated

indication of air quality and are marketed toward individuals for use in the home, portable air quality monitors which are used by professionals to assess the air quality in a room and make decisions such as how much ventilation is needed in a given location, and permanent devices which are designed to integrate with the ventilation system in a building and dynamically control the ventilation system. Next, an overview of sensing technologies was given. Lastly, an overview of the research questions and objectives of this thesis were were discussed. These research questions are investigated and tested in the following chapters.

Chapter 2 focuses on the fluidic platform design. Throughout this thesis, three platforms were developed: a single sensor platform and two multisensor platforms. Each serves a slightly different purpose in the project. To create each of these platforms, the transport phenomena within the device needed to be studied prior to manufacture. After assembly, the platforms were tested to confirm that accuracy of the simulation. The design differences between each platform, the heat and mass transport studies and the platform testing methods are covered in this chapter.

Chapter 3 gives an in-depth analysis of the preconditioning unit. It begins by discussing the device design. Then the working principle and the material choices are discussed. An overview of the literature is also given in this chapter. Next, the preconditioning unit is experimentally validated. The methods and results of these experiments are discussed. Then gas transport through the preconditioning unit is modeled. The model is then compared to the experimental results.

Chapter 4 is a synopsis of the integration and use of the platforms by laboratories throughout Europe. Various electronics platforms and computer programs used in data acquisition are discussed. Two experimental methods are shown: one using gas standards from a tank and another using an environmental chamber to mimic a real world test. Lastly, the manufacturing plan for the device is given.

Chapter 5 is a short conclusion and outlook. It gives an overview of the results of the project as a whole and discusses the steps which would need to be taken to bring this platform to market

The **Appendix** should not be skipped. It contains useful information which does not belong in the body of the text, but should be considered by anyone interested in reproducing the results of this thesis. Additionally, it contains information about the experiments conducted on formaldehyde and why the model and the experimental results are not conclusive enough to be incorporated into the main body of the text.

2 Fluidic Platform Design

Three platforms were designed throughout the course of this project: a single sensor platform and two multisensor platforms. The first was designed to house a single electrochemical sensor. This platform is used to house the electrochemical sensors in experiments described in Section 3.2. Additionally, this is the version which was used in the masters thesis referenced in Section 4.3.2. Lastly, the first prototype electronics platforms were designed for use with this system.

In the second platform, the system is expanded to hold three electrochemical sensors. This was used in publication (Mandayo et al. [2015]). It is the intermediate step between the first prototype and the final demonstrator in the Intasense project.

The last design houses three metal oxide sensors. It was used to collect the metal oxide sensor data in Section 3.2. It was also used by CEIT and C-tech Innovation to collect data using prototype sensors developed at CEIT. Additionally, Advantic developed an electronics platform which integrates with this platform design. This was packaged by Gooch and Housego to create the Intasense demonstrator described in Section 4.4.3.

2.1 Single Sensor Platform Design

An overview of the flow path through the single sensor testing platform can be seen in Figure 2.1. This platform (Figures 2.2 and 2.3) houses a sensor with a maximum radius of 10 mm. It was designed so that my collaborators and other gas sensor designers would have sufficient space and flexibility to alter individual components or parameters without changing the overall design. For example, flow rates, sensor size, filtration and method of sensor activation are not fixed. Sensor sizes were changed using a small plastic washer and an alternative configuration of the sensor holder lid (Figure 2.4). Two electronics boards have been developed for this platform. One is designed for use with electrochemical sensors and the other works with metal oxide semiconductor sensors. These integrated platforms are presented in Chapter 4.

Figure 2.1 – Flow chart of the fluid path through the single sensor platform. For a flow chart of the components in the preconditioning unit see Figure 2.5.
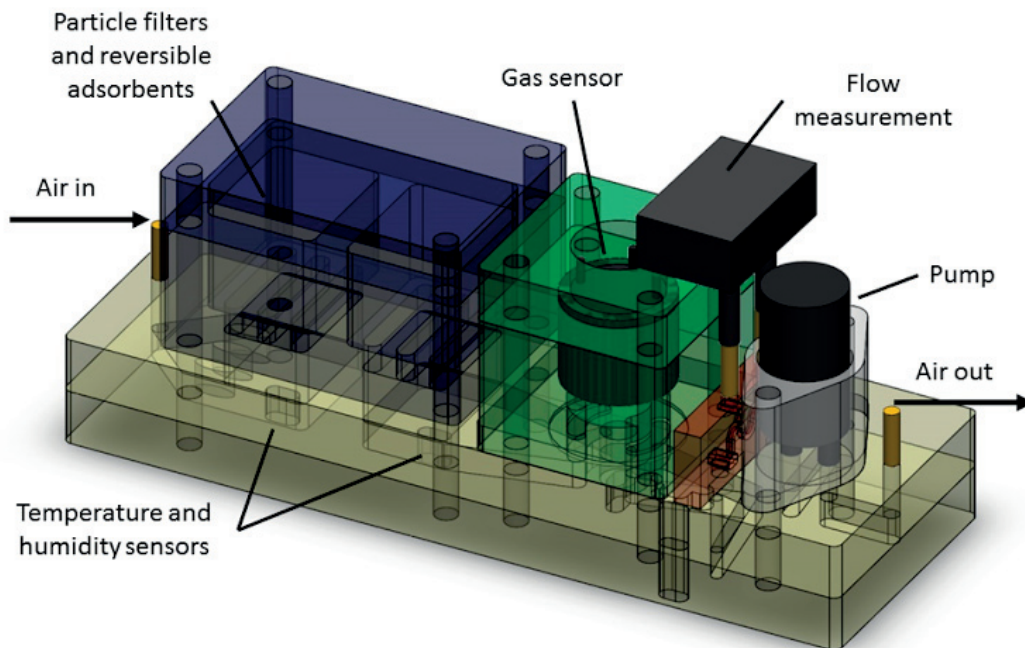
Figure 2.2 – Above is a 3D rendering of the single sensor device. The yellow base is 145 mm long. Air enters from the left and moves right. It first passes a temperature and humidity sensor before moving up into the preconditioning unit (purple) and back down into the base of the device where the humidity and temperature are sensed again. Then the air moves into the sensor chamber (green). The sensor can be activated via electronics or an LED installed in the base of the device. The differential pressure is then read as the air passes through a small restriction (red). Finally, the air is pumped out of the device. A cutaway showing this flow path can be found in Figure 2.3.
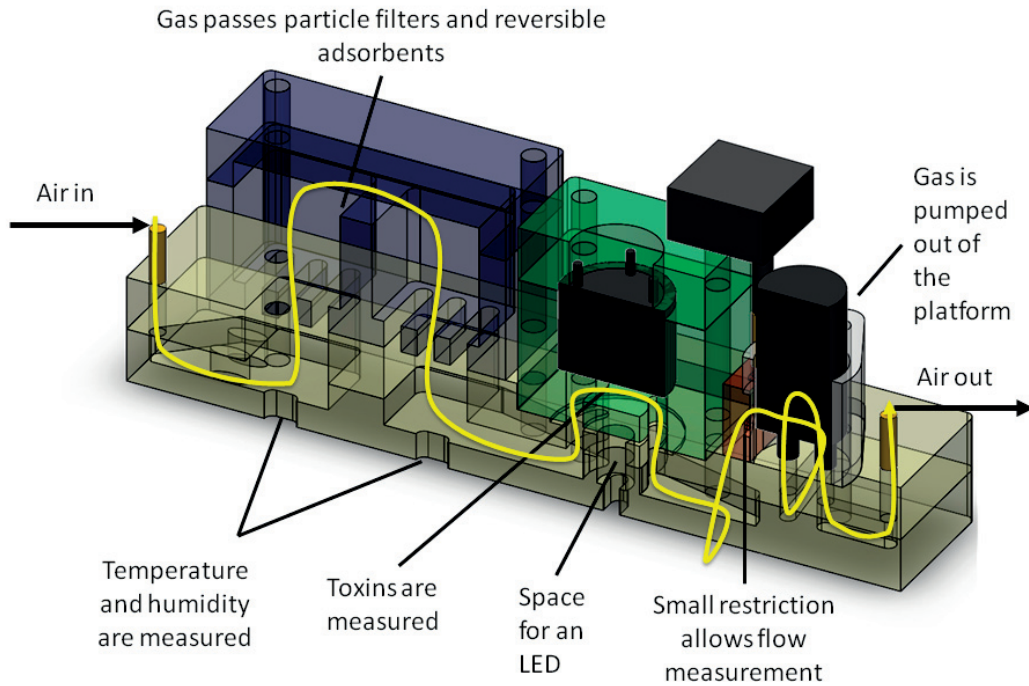
Figure 2.3 – Cutaway of Figure 2.2 showing fluid path through the device.
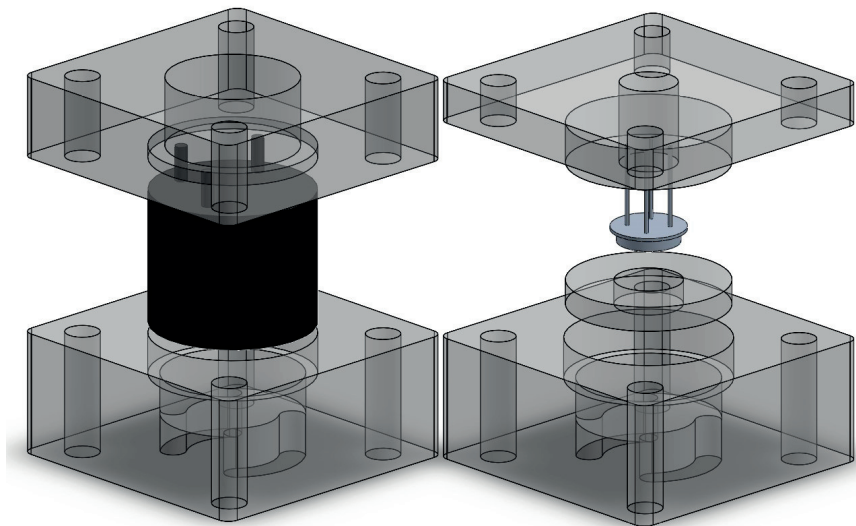
Figure 2.4 – Two examples of sensor holders compatible with the single sensor platform. On the left is a typical electrochemical package shown in black (radius = 10 mm). On the right is a TO8 package shown in silver (radius = 4 mm). These are commonly used to mount metal oxide sensors.

To manufacture these prototypes, first a list of requirements was made by my collaborators. Then designs were made using SolidWorks. Next, the fluid dynamics within the system were studied to determine an optimal device design. Once an optimal design had been found, these platforms were milled, using a 2.5D STEP4 mill, from Poly(methyl methacrylate) (PMMA) blocks. Gaskets were made from nitrile rubber (NBR) of various thicknesses and were cut with a Trumpf nanosecond laser. Gas connectors were made of stainless steel tubing and components were connected using either silicone or Polytetrafluoroethylene (PTFE) tubing. Components were glued using UHU sekundenkleber (super glue) or UHU 5 minute epoxy. After assembly, multiple platforms were tested to ensure that the device was working as expected.

In this platform air first passes by a Sensirion SHT75 temperature and humidity sensor to get a measurement of the external air. It then goes through a bed of silica gel held in place by a PM10 and a PM1 particle filter. Next, air passes by a second Sensirion SHT75 temperature and humidity sensor. All of these components combined are called the preconditioning unit. A flow chart of the preconditioning unit is given in Figure 2.5. Upon leaving the preconditioning unit the gas is sucked into the gas sensor chamber. Once leaving the gas sensor chamber, the air flows through a narrow restriction where differential pressure–and thus flow rate–is measured by a Sensirion SDP610-500Pa sensor. The sample gas then leaves the device.

Flow is generated by either a pump or a gas tank. When a pump is used, the air is sucked through the platform using a Schwarzer Precision SP 135 FZ miniature vane pump. A miniature vane pump was chosen in order to minimize oscillations in the flow. Oscillations, such as those generated by a peristaltic or syringe pump, could cause fluctuations in analyte concentration if the gas of interest is consumed by interacting with the sensor surface. Additionally, if the sensor is heat activated, changes in flow rate can lead to temperature changes of the sensor surface. In either of these cases, fluctuations in flow rate can lead to unstable sensor signals which are a combination of the change in flow rate and the analyte of interest (Figure 2.6). Alternatively, the pump can be removed and the whole system can be connected to a gas tank or mixer. This allows gas standards to be propelled through the system for experimental purposes.

The device also contains a space for an LED of up to 5.5 mm, which is external to the flow chamber. This allows the sensor designers to quickly change activation methods for their sensors without redesigning the device. All of the components can be easily accessed and changed by the user. Additionally, many components such as the differential pressure sensor, pump or early part of the preconditioning unit can be easily bypassed during experiments.

Fluid dynamics played a crucial role in the design of the platform. The sensor housing topology was created by redesigning and optimizing the flow trajectory through a design suggested by a sensor specialist at C-tech Innovation (Figure 2.7a). Their design placed the sensor in a dead volume. By reorienting and enlarging the openings to the chamber and decreasing the chamber height, a more efficient design was achieved (Figure 2.7b). Although this design
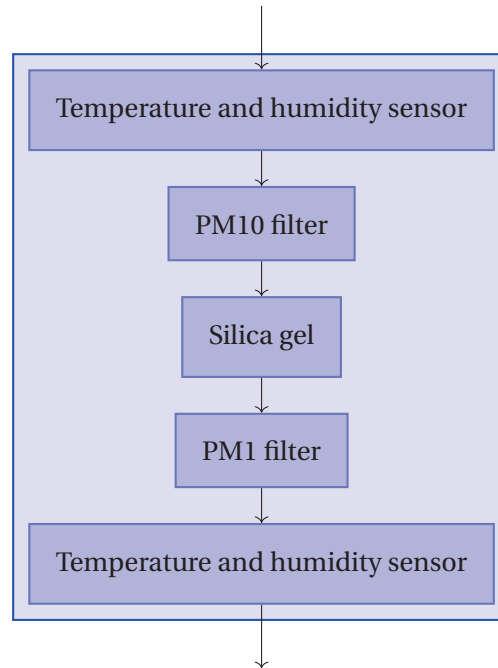
Figure 2.5 – The preconditioning unit is composed of an inlet temperature and humidity sensor which monitors the ambient air as it enters the system, a large particle filter, silica gel, a small particle filter, and an outlet temperature and humidity sensor, which monitors air flowing out of the preconditioning unit. All of the components in the preconditioning unit are optional.

is optimized, it is important to note that the flow across the sensor surface will be axially symmetric but not centered for a flow rate of $0.4\,\mathrm{L\,min^{-1}}$. This could cause uneven wearing or non-comparable data if the sensor is not placed properly into the chamber. The chamber holds sensors with a diameter less than or equal to $20\,\mathrm{mm}$ in diameter. After construction, this housing design was tested using an e2v oxygen sensor. Using a flow rate of approximately $0.15\,\mathrm{L\,min^{-1}}$ the sensor housing cleared in about 15 s (Figure 2.8), indicating that the gas is efficiently reaching the sensor surface. This is because the housing before the oxygen sensor contains about 35 mL of air. Thus, in a design with this volume and non-fully developed flow profile, we would expect to see the whole system clear in about 14 s.

Throughout the Intasense project, nine devices were delivered to six laboratories across Europe. Before they were shipped, five of the devices were tested to determine which components needed to be calibrated and which had no effect on the fluid dynamics or readings generated by the system. To do this, a five by five Latin Square analysis was conducted to investigate the effects of the base of the device, the small pressure channel and the commercial pressure sensors (2.1). Each of the twenty-five system combinations were tested using a syringe pump to generate repeatable flow rates. The pressure differential was measured at each flow rate and a mean flow was found. Then a 3-way ANOVA test was used to determine which components
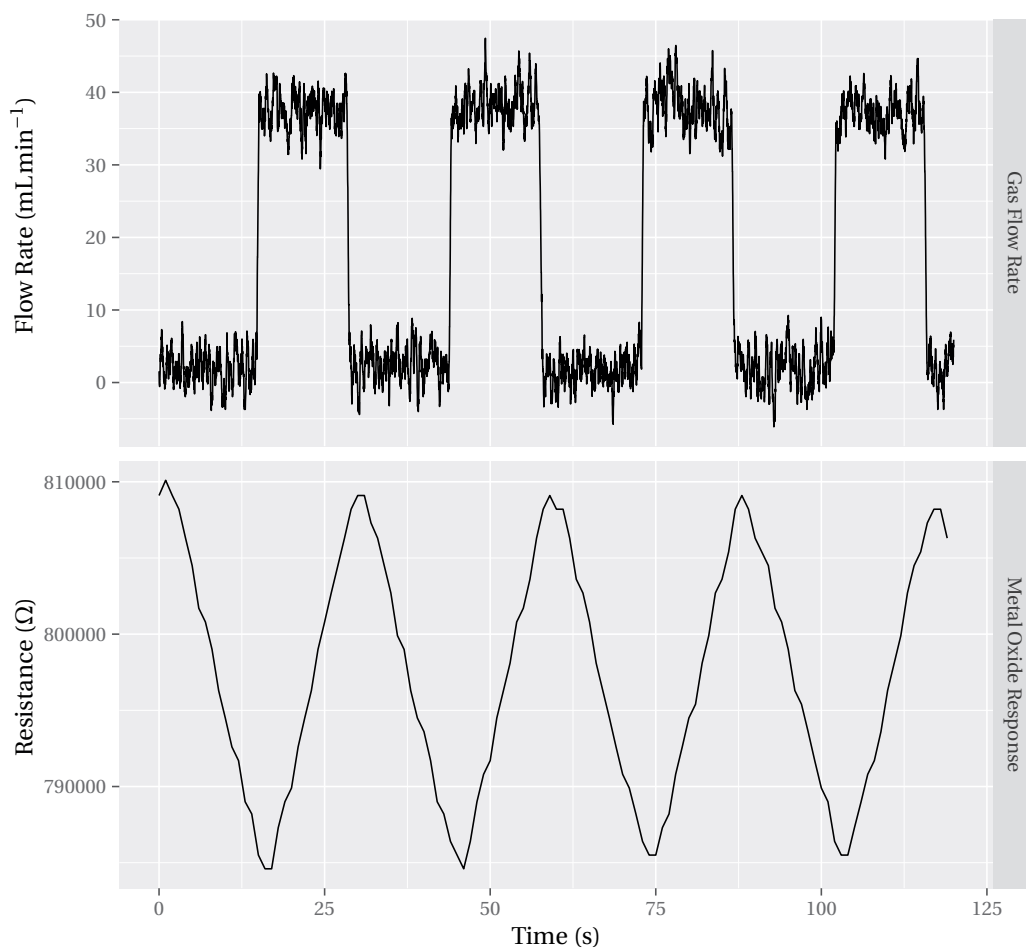
Figure 2.6 – Example of oscillating flow leading to an unstable sensor signal. Flow in this figure was created using a syringe pump which propelled clean humid air through the metal oxidesensor platform (presented later in this chapter). The flow rate was monitored using a Sensirion mass flow meter (Item number: SFM4100). The metal oxide data was collected using an e2v 5521 sensor.
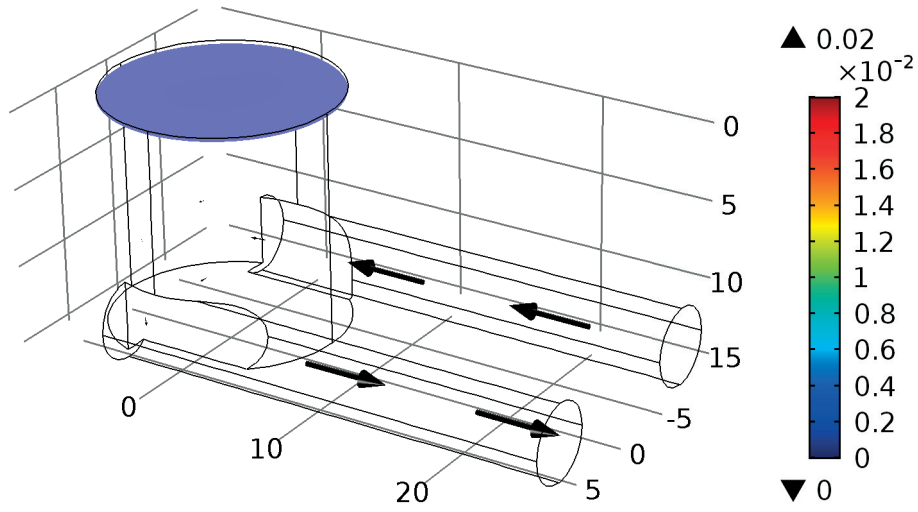
(a) Collaborator Design
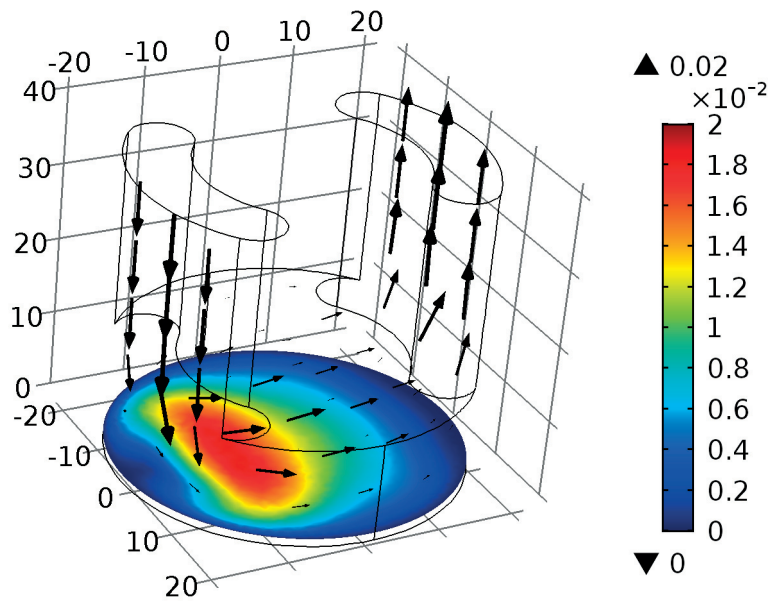
(b) CSEM Design

Figure 2.7 – Results of fluid dynamic simulations for sensor chamber designs. The amount of air going into each system is equal and the scales on both images are the same. For both images, the colored disk represents flow near the sensor surface (in $\mathrm{m\,s^{-1}}$). Figure (a) shows a computational fluid dynamic simulation of the CAD drawing proposed by a collaborator; Figure (b) is the optimized design which is used in the single sensor platform. The flow rate across the sensor is greatly increased in Figure (b) by reducing the volume of the sensor chamber, increasing the area of the openings and changing the orientation of the inlet and outlet relative to the sensor.
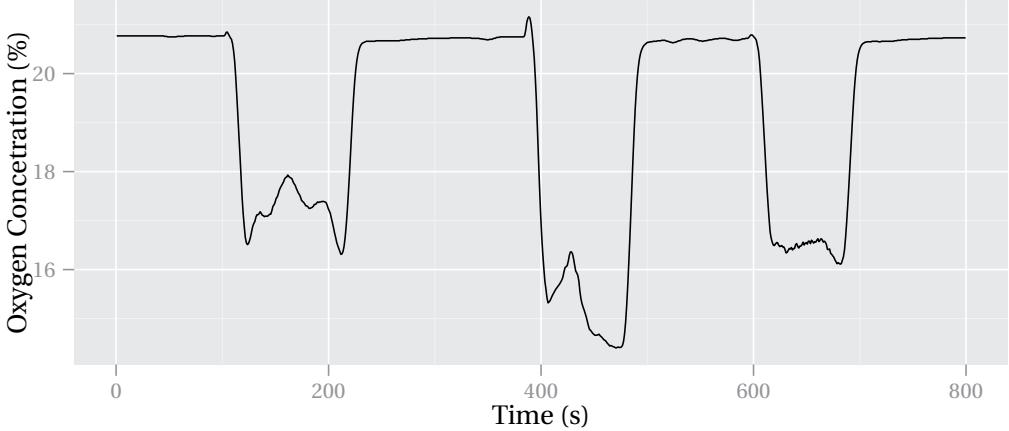
(a) Complete run
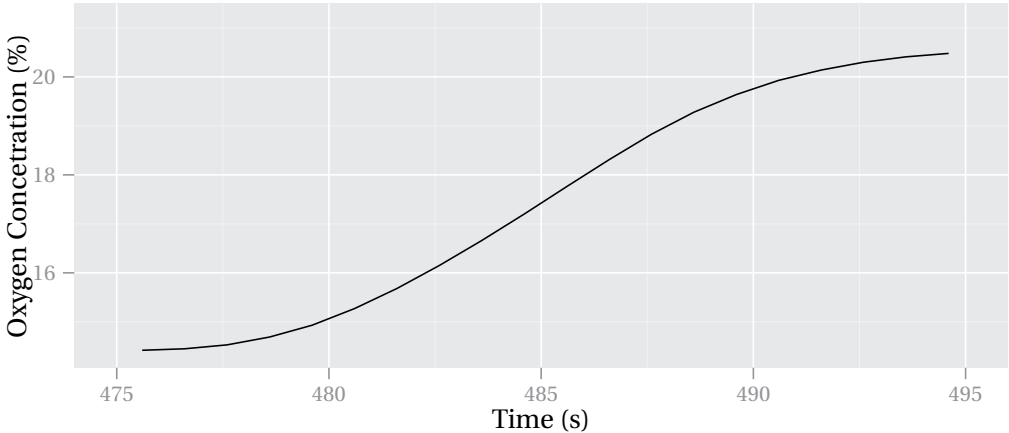
(b) Detail showing internal gas clearance

Figure 2.8 – Experiment to quantify clearance time of the platform. A partially filled balloon of exhaled air was placed at and removed from the inlet of our single sensor testing platform. Figure (a) shows the complete run which includes 3 periods of exposure to exhaled air; the lower values fluctuate because there is variation in the amount of oxygen exhaled by a person. Figure (b) is a detail view as the gas is being changed from exhaled air to ambient air. This figure shows that gas in the platform is exchanged in about 15 s.

		Platform or Base Channel				
		1	2	3	4	5
	1	1	2	3	4	5
	2	2	3	4	5	1
Pressure Sensor	3	3	4	5	1	2
	4	4	5	1	2	3
	5	5	1	2	3	4
		Differential Pressure Channel				

Table 2.1 – The experimental design (5x5 Latin Square) used to test the null hypothesis that all components are the same, is displayed above. From this it can be seen that each component is only used 1 time with each other component, to generate a total of 25 data sets, which were later analyzed using least squares methods and ANOVA tests.

Flow Rate $mL\,min^{-1}$	Platform	Restriction	Sensor
157	0.98	0.0042	1.5×10^{-8}
139	0.98	0.0038	1.1×10^{-8}
122	0.99	0.0029	1.4×10^{-8}
105	1.00	0.0025	7.4×10^{-9}
87	0.99	0.0014	6.9×10^{-9}
70	0.99	0.0014	9.5×10^{-9}
52	0.99	0.00021	3.6×10^{-9}
35	0.98	0.000008	1.7×10^{-9}

Table 2.2 – P-values for Latin Square analysis show that the platforms are statistically similar while the other components are not.

were significantly different from each other (Figure 2.2). The effects of both the pressure sensor and the channel were significant while the bases were interchangeable. To resolve this, the pressure channel was redesigned (Figure 2.9). In the new design the dimensions of the channel between each side of the differential pressure sensor were constant. However, the channel was changed from a curve to a meander, which allows for a more compact design. Additionally, rather than milling the pressure channel from two pieces of plastic and gluing them together, the pressure channel was milled from one piece of plastic and sealed with an adhesive foil. This prevented excess glue from flowing into the channel and changing its dimensions. Statistical analysis of the new channel showed that there was not a significant difference between each of the new channels (Table 2.3).

2.2 Multisensor Prototype Device Design

The multisensor prototype platform (Figures 2.10 and 2.11), presented in [European Environment Agency, 2013; Mandayo et al., 2015], was designed to deliver equal quantities of gas to three sensors simultaneously. It was built using the same materials as the single sensor
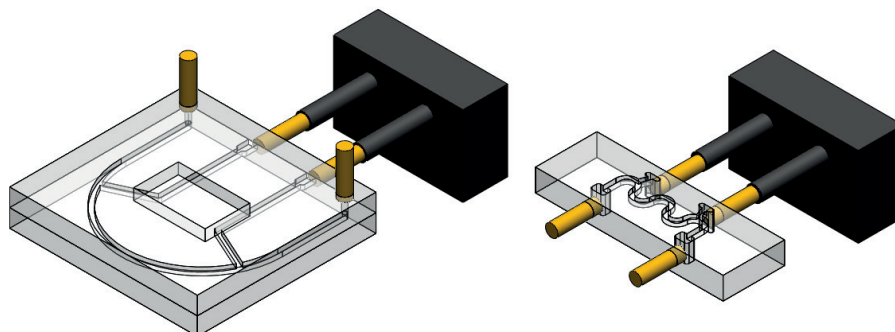
Figure 2.9 – Images of the two versions of the differential pressure channels. On the left is the first version, on the right is the second. The second version is closed with an adhesive foil, rather than glue, making production more repeatable.

Flow Rate mL min^{-1}	P value
157	0.35
139	0.31
122	0.32
105	0.29
87	0.30
70	0.35
52	0.33
35	0.33

Table 2.3 – Results of the Anova test on the second version of the pressure restriction show that all p-values are greater than 0.05, indicating that the channels are working similarly.
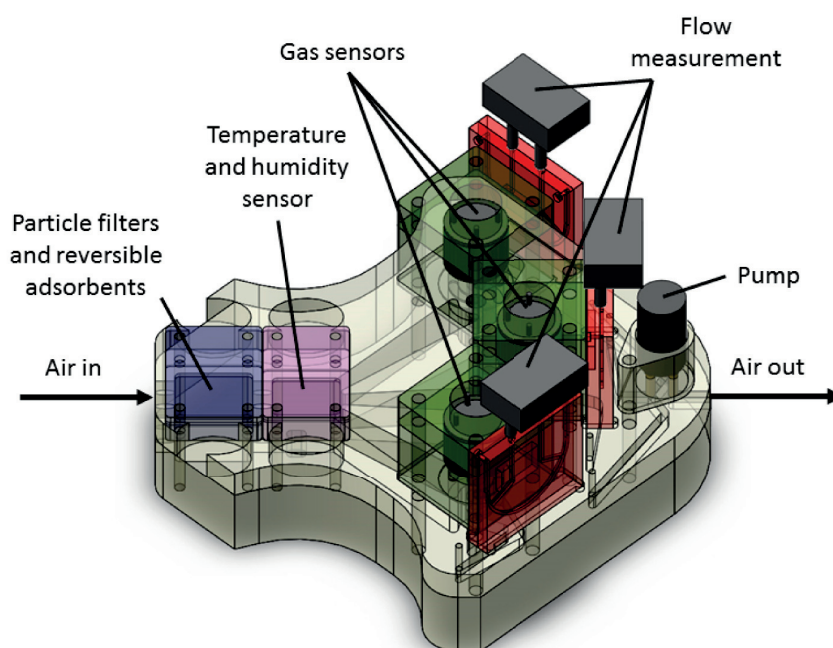
Figure 2.10 – Above is a three dimensional rendering of the three sensor housing unit. The base of this housing unit (yellow) measures 145 by 145 mm. Its design is based on the single sensor housing pictured in Figure 2.2. Similarly air enters the device on the left, where it is filtered (dark purple section) and the temperature and humidity are measured (light purple section) before the gas path trifurcates. Gas is then delivered to three sensor chambers in parallel (green). Then the flow rate is measured (red and black) before being sucked into the pump (black) and out of the device. A cutaway of this device, showing the fluid path can be seen in Figure 2.11.

platform, and recycles many of it's components. Specifically, both platforms use the same manufacturing equipment, sensor holders, differential pressure channels and commercial electronics. However, the expected flow rate through the system is $0.6\,\mathrm{L\,min^{-1}}$ instead of $0.4\,\mathrm{L\,min^{-1}}$, meaning that flow to each of the three sensors is half of what was shown in Figure 2.7b. The flow patterns through the chamber at $0.2\,\mathrm{L\,min^{-1}}$ are shown in Figure 2.14. The order of events in the device are also the same: gas is still filtered, humidity measured, toxins are sensed, then flow is measured before it exits the device. However, in this platform, the gas is split after the preconditioning unit and is recombined after the flow is measured. The fluid path can be seen in image 2.13.

To guarantee that each sensor received the same amount of air, the fluid transport through the system was modeled prior to construction using COMSOL Multiphysics 4.4. Specifically, the flow through the sensor chamber, the geometry of the trifurcation point and the dimensions of
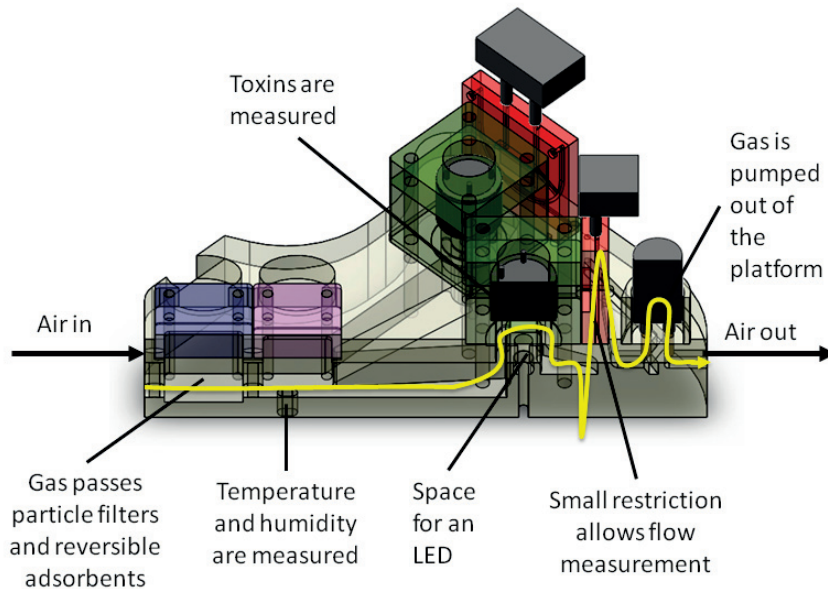
Figure 2.11 – Cutaway of Figure 2.10 showing fluid path through the device.

the unequal gas outlets were simulated to determine an optimal geometry. At the trifurcation it was important that the mean velocity at the entry point of each channel was equal. As the geometry of the exit channels controls the pressure drop through the system, it was also important to make the pressure drop through each of these channels as close to equal as possible. A variety of geometries were simulated until an optimal solution was found. In the final design each of these channels has a different cross sectional area and length. The combination of these parameters allows the pressure drop through each path–and thus the overall flow rate through each sensor chamber–to be functionally identical.

To test the performance of the system, three commercial oxygen sensors (e2V EC410) and corresponding electronics testing platforms (e2v ECVQ-EK3 sensor evaluation kits) were installed into the sensor chambers of the system. Oxygen levels at the inlet were allowed to vary throughout the experiment. The results of the test performed in the fluidic platform show simultaneous response times, indicating that the gases arrive at the sensor with comparable delays, and similar peak heights, indicating that the amount of gas flowing through the device is also comparable (Figure 2.15).
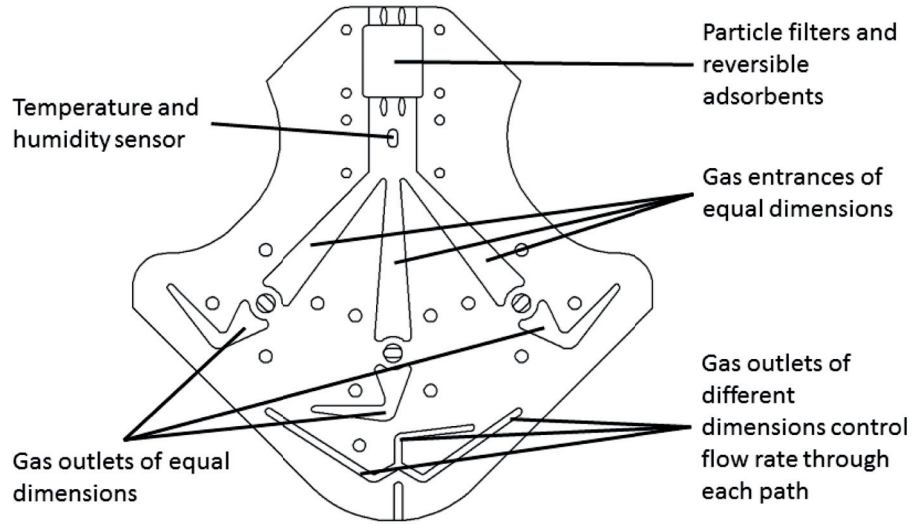
Figure 2.12 – CAD drawing of the base of the device.
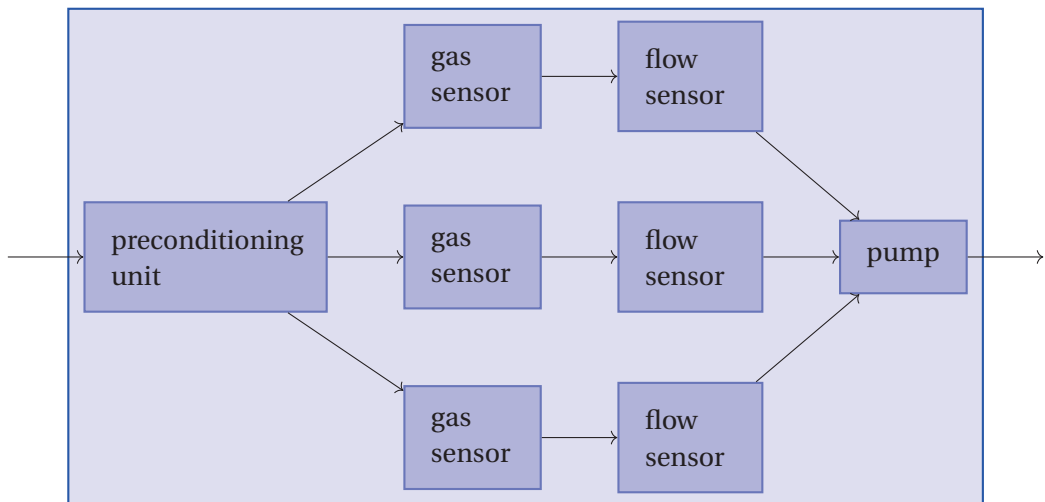
Figure 2.13 – Flow chart of the fluid path.
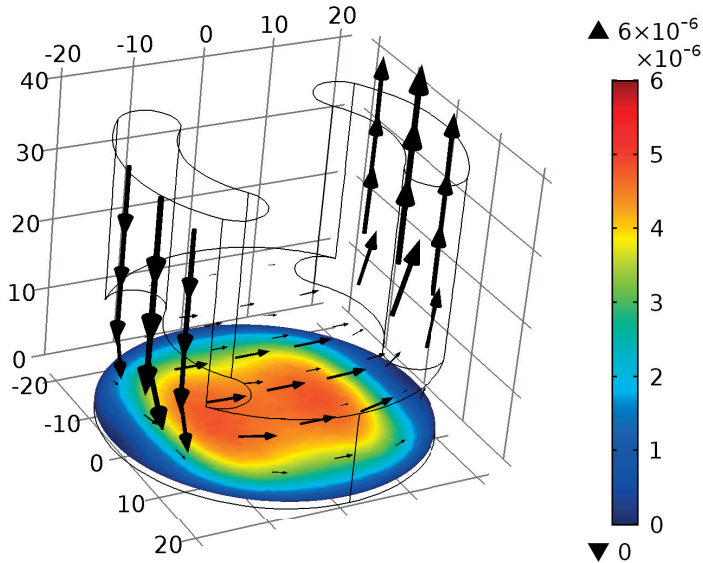
Figure 2.14 – Results of flow simulation through the gas sensor chamber at $0.2\,\mathrm{L\,min^{-1}}$ (in the previous platform flow was $0.4\,\mathrm{L\,min^{-1}}$). Arrows are proportional to the velocity and direction of flow (in $\mathrm{m\,s^{-1}}$) and colored disk represents the flow near the sensor surface.
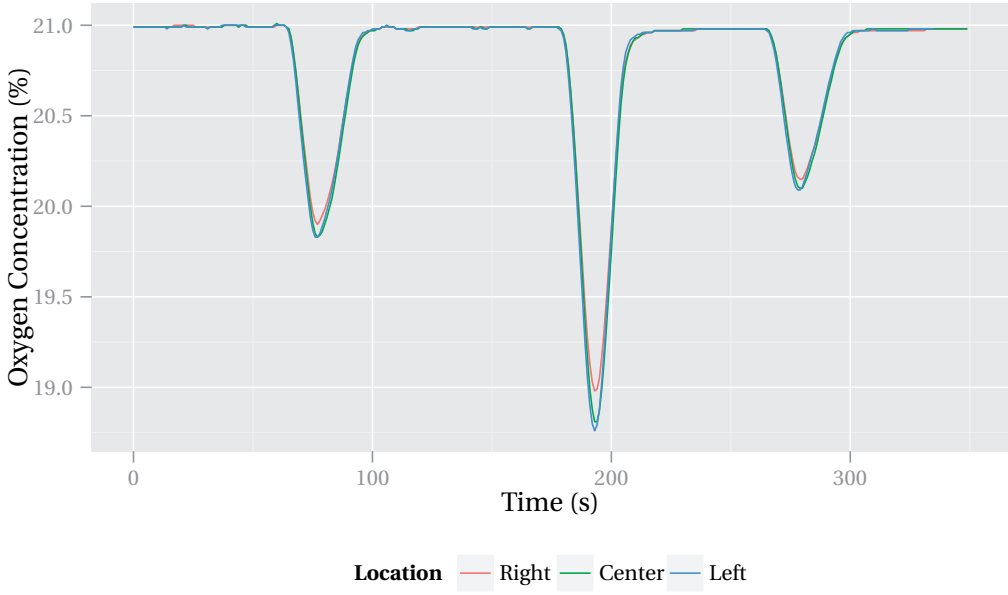
Figure 2.15 – The above graph of sensor response v. time shows that the responses of 3 O_2 sensors are simultaneous and of similar magnitudes.
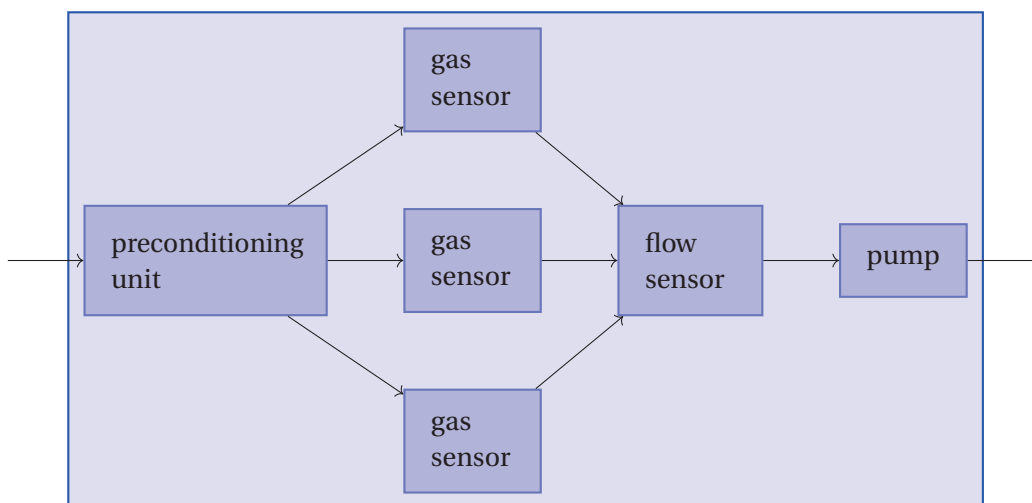
Figure 2.16 – Flow chart of the fluid path.

2.3 Metal Oxide Sensor Platform

Using the feedback of the sensor designers who received the single sensor prototype, a smaller and more integrated platform was developed specifically for metal oxide sensors in TO-8 packages (Figures 2.16, 2.17, 2.18, and 2.19). Although this device could be used for other sensor types, the sensor must be 8 mm in diameter or smaller. Additionally there is not an explicit place for an LED, so it is not suitable for light activated sensors. Many of these design changes stem from the purpose of each platform: namely, the previously described platforms were designed to be easily adaptable and test sensors of sizes up to 20 mm radius, whereas this platform is optimized for a set of up to 3 sensors in TO8 packages. Because this device delivers equal amounts of air simultaneously to all sensor chambers it is ideal for testing the responses of three sensors of the same type to confirm that they are acting similarly, testing similar sensors at different temperatures to find an ideal operating temperature, or testing three different types of sensors to determine their specificity. Additionally, this version is smaller and lighter than the previous platforms, which reduces material costs, but the smaller components are more difficult to change.

The fluid dynamics of the entire system was a primary concern when designing the metal oxide sensor platform. Specifically, it was important that the same amount of air was arriving at each sensor simultaneously. If the flow rates were different it would be possible that the sensor responses would not be comparable because different amounts of analyte would reach each sensor. If the gas did not reach each sensor simultaneously then the sensors would not respond simultaneously. This could make the signal processing or gas fingerprinting more computationally intensive. Lastly, it was also important that the gas flow was centered on the sensor. If the flow was not centered, in the short term this could cause unusual responses because the temperature could be uneven across the sensor surface or part of the sensor could receive more analyte. In the long run variance in analyte concentration or temperature could
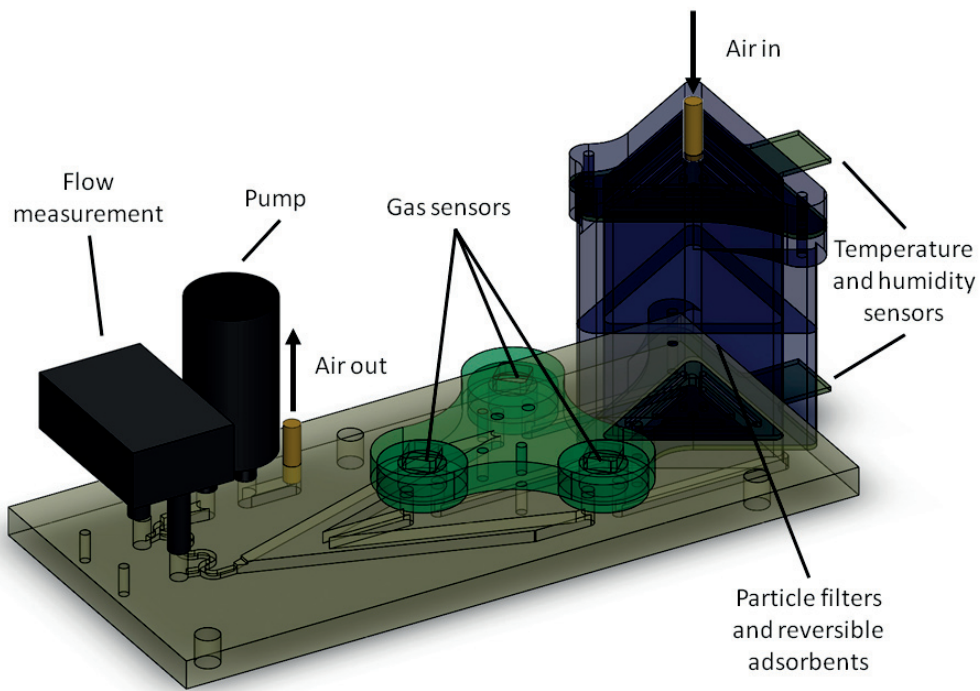
Figure 2.17 – Above is a 3D rendering of the metal oxide sensor platform. Air enters from the top right and moves left. It first passes through the preconditioning unit (purple). Then the air moves into the sensor chamber (green). The differential pressure is then read as the air passes through a small restriction in the base of the platform. Finally, the air is pumped out of the device. The longest side of the platform base (yellow) is 145 mm. A cutaway showing this flow path can be found in Figure 2.18.
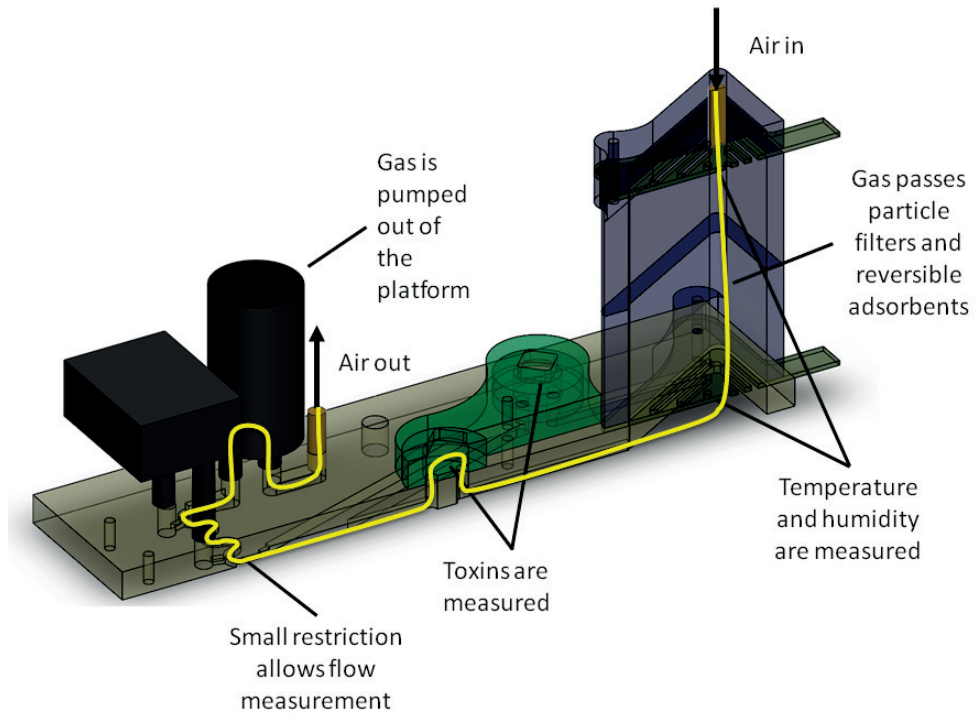
Figure 2.18 – Cutaway of Figure 2.17 showing the fluid path through the device.

Figure 2.19 – Above is the metal oxide sensor platform. This design was specifically created to hold 3 of CEIT's TO8 packaged sensors. However, because TO8 is an industry standard package, the device can be adapted to hold commercial sensors. It was also designed to be smaller and more integrated than the single sensor version.

		Platform or Base Channel		
		1	2	3
	1	1	3	2
Pressure Sensor	2	3	2	1
	3	2	1	3

Differential Pressure Channel

Table 2.4 – The experimental design (3x3 Latin Square) used to test the null hypothesis that all channels are the same, is displayed above. From this it can be seen that each component is only used 1 time with each other component to generate a total of 9 data sets, which were later analyzed using least squares methods and ANOVA tests.

cause uneven wear of the sensing material leading to a shorter sensor lifespan.

To deliver equal quantities of gas to each sensor, the device was divided into three subsections: the channels before the sensor, the channels after the sensor, and the compartment which housed the sensor. The channels before the sensors and the sensor housings were designed and fabricated to be as identical as possible. Then a parameter sweep over channel lengths and outer channel widths (Figure 2.20) was conducted by coupling Comsol simulations to SolidWorks models. Because the Reynolds number is low, these models assume laminar flow through the system. Using these simulations, the average pressure at the exit of the sensor chamber was determined. The percent pressure difference was then calculated. The optimal set of solutions–where the percent pressure difference between the gas outlets of the sensor housings was zero–could then be determined (Figure 2.21). In this plot, the white line represents the most optimal parameter set from a fluid dynamic perspective. In addition to fluid dynamics, packaging properties needed to be considered. This added a constraint on the maximum width and maximum length that the channels could be. Final dimensions were chosen from this optimal set and a prototype was constructed. However, because inaccuracies can arise in both the numerical simulations and the manufacturing process, tests were then conducted to confirm that each channel was receiving the same gas flow.

Specifically, an Anova test was conducted using a Latin Square design [Box et al., 1978], [Fischer, 1960]. This method was chosen because it minimizes the number of experiments which need to be conducted in order to determine which components of the system cause significant measurement errors. In this case, the error could arise from the optimized manufactured device or the flow sensors which were composed of a differential pressure sensor and a restriction.

In the experiment the three test objects—channels in the platform, differential pressure sensors and restrictions—were each assigned a number from 1 to 3. They were then grouped so that each object was used exactly once with each other object (Table 2.4). The platform was then set up so that the restrictions were connected directly to the exit of the gas sensor chamber. Using a syringe pump, gas was pulled through the system at a known flow rate.
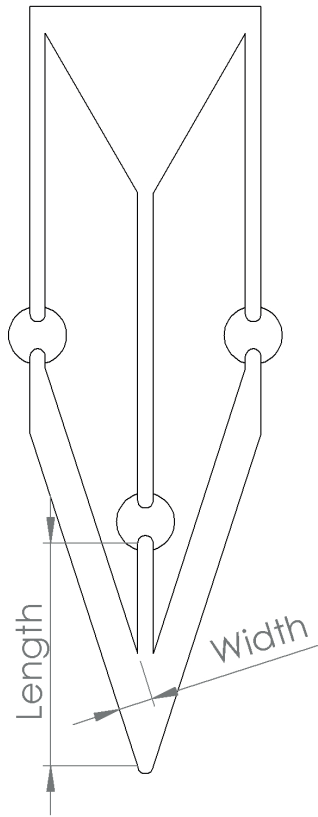
Figure 2.20 – 2D image of fluidics highlighting length and width variables.
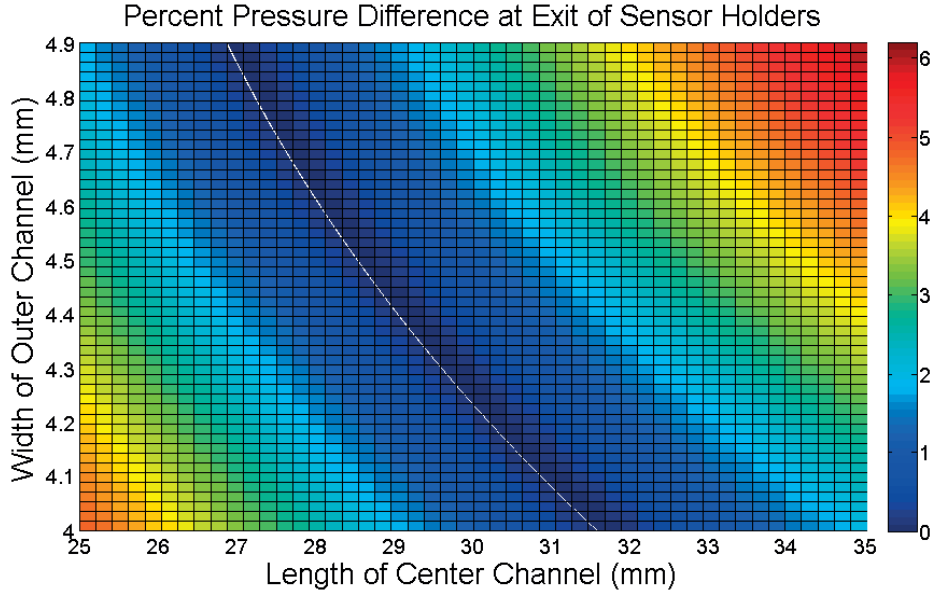
Figure 2.21 – Results of the optimization simulation. The white line represents the optimal parameter set.

The differential pressure for each sensor was then averaged for each flow rate. Once all 9 experiments had been completed, statistical analysis could begin. The first step was to decompose the orthogonal components by computing the values for the Anova model of the Latin Square design. Mathematically this takes the form:

$$Y_{ij(k)} = \mu + \alpha_i + \beta_j + \gamma_k + \epsilon_{ij(k)} \quad \text{for } i, j, k = 1, 2, ..., m \tag{2.1}$$

where i, j, and k represent specific channels, pressure sensors and restrictions respectively. Y is the average flow result from an experiment, μ is the average of all results at a given flow rate, α_i is the main effects factor for the channel i, β_j is the main effects factor for pressure sensor j, γ_k is the main effects factor for restriction k, $\epsilon_{ij(k)}$ is the residual or noise and m is the number of items of each type. In this case, $m = 3$. This equation becomes:

$$\begin{bmatrix} Y_{1,1} & Y_{2,1} & Y_{3,1} \\ Y_{1,2} & Y_{2,2} & Y_{3,2} \\ Y_{1,3} & Y_{2,3} & Y_{3,3} \end{bmatrix} = \begin{bmatrix} \mu & \mu & \mu \\ \mu & \mu & \mu \\ \mu & \mu & \mu \end{bmatrix} + \begin{bmatrix} \alpha_1 & \alpha_2 & \alpha_3 \\ \alpha_1 & \alpha_2 & \alpha_3 \\ \alpha_1 & \alpha_2 & \alpha_3 \end{bmatrix}$$

$$+ \begin{bmatrix} \beta_1 & \beta_1 & \beta_1 \\ \beta_2 & \beta_2 & \beta_2 \\ \beta_3 & \beta_3 & \beta_3 \end{bmatrix} + \begin{bmatrix} \gamma_1 & \gamma_3 & \gamma_2 \\ \gamma_3 & \gamma_2 & \gamma_1 \\ \gamma_2 & \gamma_1 & \gamma_3 \end{bmatrix} + \begin{bmatrix} \epsilon_{1,1} & \epsilon_{2,1} & \epsilon_{3,1} \\ \epsilon_{1,2} & \epsilon_{2,2} & \epsilon_{3,2} \\ \epsilon_{1,3} & \epsilon_{2,3} & \epsilon_{3,3} \end{bmatrix} \tag{2.2}$$

Flow rate (L/min)	P value for channel	P value for sensor	P value for restriction
.157	0.0315	0.0196	0.0207
.139	0.0548	0.0344	0.0371
.122	0.0390	0.0251	0.0271
.105	0.0387	0.0279	0.0327
.087	0.0231	0.0170	0.0239
.070	0.0196	0.0118	0.0229

Table 2.5 – P values for all components and flow rates are greater than .01, indicating systems are comparable.

in matrix form. Values for α, β, and γ were computed using the following formulas:

$$\alpha_i = \frac{1}{m} \sum_{j=1}^{m} Y_{i,j} - \mu \tag{2.3}$$

$$\beta_j = \frac{1}{m} \sum_{i=1}^{m} Y_{i,j} - \mu \tag{2.4}$$

$$\gamma_k = \frac{1}{m} \sum_{i=1}^{m} Y_{i,k} - \mu \tag{2.5}$$

and values for ϵ were solved by substituting all numerical values back into the matrix form of the equation or by computing residuals.

Once the model was found, an Anova test was conducted. After all of these values were calculated, the critical F-value for a given confidence level could be determined using a lookup table. When the F-value for an item type was greater than critical F-value, then the null hypothesis was rejected, meaning that the items within the group–pressure sensors, channels or restrictions–are statistically different from each other. Alternatively, p-values can be calculated using the Anovan function in Matlab.

Table 2.5 reports the p-value for each item type at each flow rate. In this experiment, p values less than .01 were considered significant. Because all values are greater than .01, we cannot reject the null hypothesis that each item performs identically. Thus, we conclude that the device design is sufficiently accurate despite any numerical errors in the optimization calculations and/or inaccuracies in machining.

Once the platform design had been optimized and analyzed, the sensor housing chamber was designed. Initially, mathematical models for the system needed to account for gas transport in order to maximize and center the flow on the sensor surface of commercial sensors. Once prototype sensors were ready for incorporation into the platform, heat transport needed to
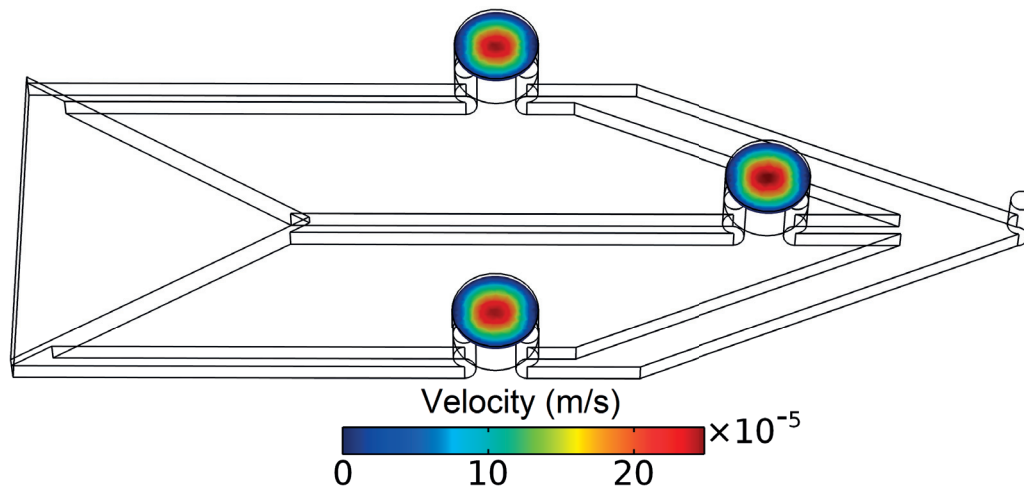
Figure 2.22 – Velocity of gas near sensor surface shows that the transport is optimally centered.

be accounted for because metal oxide sensors have a sensor surface operating temperature of up to about 450 °C. In commercial products this is not a problem as the sensor surface is very small and well insulated from the sensor packaging. However, part of sensor prototype development is perfecting this insulation. Therefore, housing components in contact with the prototype sensor packaging needed to be able to withstand 100 °C. Additionally, heat transport to PMMA (poly(methyl methacrylate)) components needed to be controlled so that they would not exceed their long term operating temperature of about 70 °C.

So that the gas flow would be centered on the sensor surfaces, Comsol simulations began by investigating flow within a variety of sensor housing chamber designs. Heat transport from the sensor to the gas and plastics in the sensor housing chamber was then studied using a simplified model. The optimized gas transport can be seen in Figure 2.22, which shows the velocity of the gas near the sensor surface. From this image it is clear that gas transport is centered on the sensor surface.

The simplified model of heat and gas transport through the sensor housing chamber can be seen in Figure 2.23. Figure 2.23a is a cross-section of the system, while Figure 2.23b and Figure 2.23c show the heat transport through the system when it is composed entirely of PMMA, or of both PMMA and PEEK (polyether ether ketone), respectively. In each simulation, air at 20 °C enters the chamber and follows the path depicted by the arrows in Figure 2.23. To determine the maximum allowable temperature of the insulation layer, the insulation layer (red, Figure 2.23) is modeled as a constant temperature heat source. The sensor packaging (yellow, Figure 2.23) does not generate heat, and starts the simulation at 20 °C. Green components in Figure 2.23 are made of PMMA in both simulations, while blue components are made of PMMA in Figure 2.23b and PEEK in Figure 2.23c. Heat transport simulations were conducted without gaskets because they act as insulators and the device should not be damaged even when the gaskets are not used.
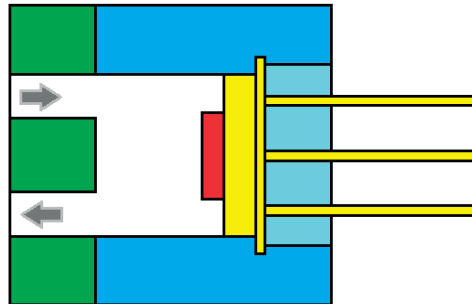
(a) Cross-section of Housing.
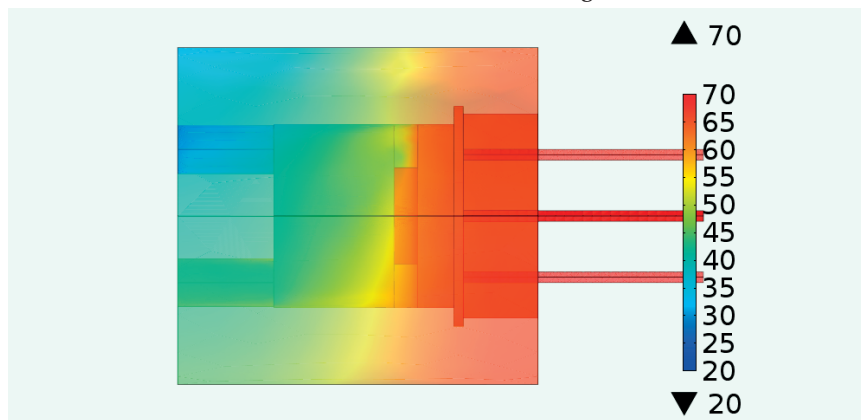
(b) Heat transport though the sensor housing with PMMA components only.
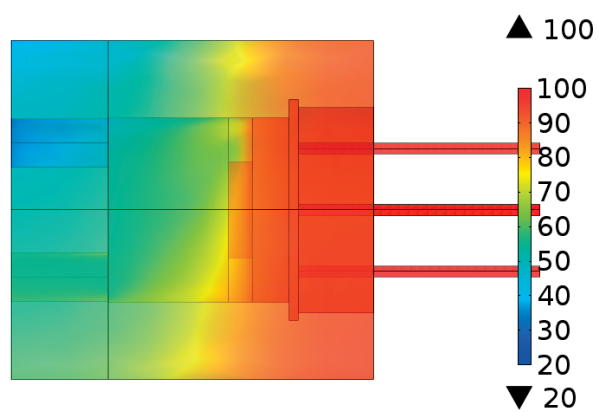
(c) Heat transport though the sensor housing with some PEEK components.

Figure 2.23 – Simulations used to find the maximum operating temperature of the insulation layer before heat from the sensor causes the metal oxide platform to melt. Measurements are in degrees Celsius.
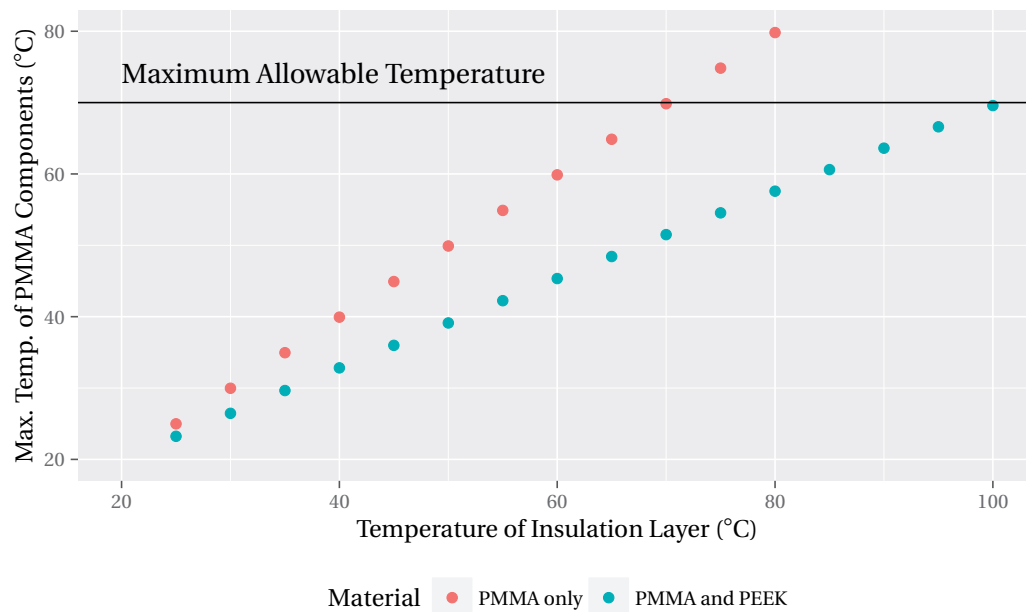
Figure 2.24 – Results of Comsol simulation show the maximum temperature of PMMA components for both sensor housing designs.

A parameter sweep was conducted for both systems by varying the temperature of the insulation. This technique allows us to understand how efficient the insulation must be for a given sensor temperature and platform material. Based on the results in Figure 2.24, it is clear that the PMMA only system can withstand insulation temperatures below about 70 °C. However, when components in direct contact with the sensor packaging are replaced with PEEK components the device can withstand insulation operating at about 100 °C. These simulations were confirmed experimentally using thermographic images taken during insulation studies (Figure 2.25).

Once these studies were completed, seven devices were integrated with electronics platforms developed by Advantics. Two of these were housed and made into demonstration units. An overview of the integrated product is given in Chapter 4. In addition to these platforms, four more were created for experimental studies. Some were used to evaluate prototype chemical sensors, while others were used to study adsorption in the preconditioning unit. The adsorption studies are documented in the next chapter.

In the previous designs the temperature and humidity sensor holder was very difficult to seal completely. In the new design this was remedied by incorporating a PCB directly into the filtration packaging. This decision saved space by allowing the temperature and humidity sensor unit to serve both as a mechanical and electrical component: the humidity sensor PCB also secures the particle filters. Lastly, the sensor base was covered with an adhesive foil rather than a milled component in order to save space and reduce the weight of the device.
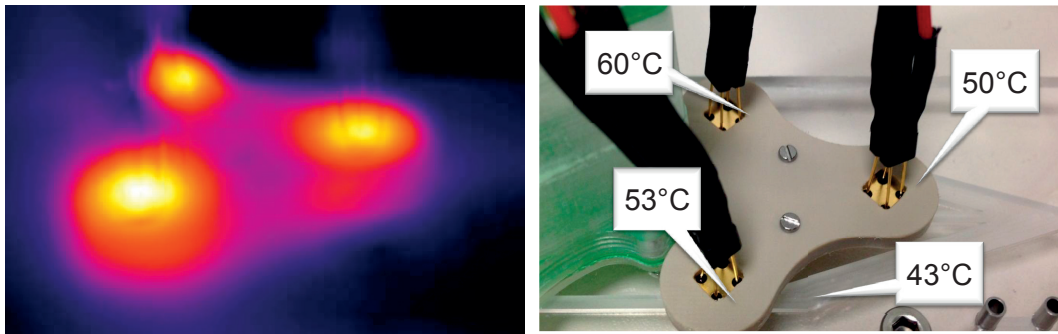
Figure 2.25 – Thermographic image of sensor housing during experiments (left) and photo of the same section with temperatures labeled (right). Images taken by Jurgi Gonzalez-Chavarri.

3 Preconditioning Unit Design

Convection is required because air needs to be preconditioned prior to contact with the gas sensor. The preconditioning types used in this system include particle filtration and humidity stabilization. Particle filtration is necessary because dust can block sensor surfaces, reducing their lifespan [E2v, 2007a]. Humidity stabilization is important because most gas sensors cannot operate in condensing environments and are optimized for only specific ranges of humidity [E2v, 2007a; Figaro, 2007; Alphasense Ltd., 2015]. Furthermore, metal oxide sensors are sensitive to humidity fluctuations [Hammes et al., 2015; E2v, 2007a; Figaro, 2007]. Additionally, when a humidity stabilizer is used, it is important to confirm that the materials in the device and the method used to add or remove humidity do not change the amount of gas which reaches the sensor or significantly delay the sensor reaction time. For this project, the goal was to have sensors react to carbon monoxide in less than one minute and react to nitrogen dioxide and benzene in less than ten minutes.

3.1 Device Design

Electrochemical sensors frequently require influx of humidity from the environment to operate correctly and metal oxide semiconductor sensors are cross sensitive to humidity fluctuations. As a result, humidity stabilization without analyte removal is the most important and most challenging feature of the device. This is because it is difficult to selectively remove chemicals from the air. Additionally, humidity control systems on the market are designed for applications where toxic gas removal could potentially be beneficial. Therefore, it was necessary to design, test and model a humidity stabilization unit with a particular focus on minimizing the delay between the gas of interest entering the system and reaching the sensor, and minimizing the loss of analyte due to reaction with the materials in the preconditioning system. It was also important that the system could do this as cheaply as possible in terms of materials, components and energy costs.

3.1.1 Overview of Drying Methods

Humidity in a building is more likely to rapidly increase than rapidly decrease. This is because people enter buildings with rain-soaked clothing. Designs for the humidity stabilization unit began by creating an overview of various types of drying systems and their drawbacks in regard to this application. A brief summary of these are listed below:

1. In water or air cooled aftercoolers humid air is passed over a cooling coil filled with either a gas or a liquid. This causes gaseous water to form particles. The water particles can then be removed by either a centrifugal filter or by slowing the velocity of the air and allowing it to fall out by gravity [Lee and Schmidt, 1995].

2. Deliquescent dryers use a chemical adsorbent, such as silica gel or carbon, to adsorb water. They require no electricity. However when the adsorbent becomes saturated it must be changed [Lee and Schmidt, 1995].

3. Regenerative desiccant dryers also use a material such as silica gel to adsorb water. However, instead of replacing the chemical adsorbent, the adsorbent goes through a drying cycle. These dryers usually have two desiccant beds so that one can be used for drying air while the other is being regenerated [San and Jiang, 1994].

4. In membrane dryers water transport out of the sample gas is promoted by a humidity differential between the inlet gas, which passes on one side of the membrane, and either a purge gas or some hydrophilic material on the other. The membrane must be selected so that analytes are not lost, which is why nafion is frequently used for the membrane in cases where concentrations of reactive gases are measured such as gas chromatography [Leckrone and Hayes, 1997].

5. Other drying methods exist, such as refrigerated dryers or cold traps, but these will not be considered either because of the cost of various components or energy expense.

The problem with using an aftercooler to stabilize humidity is that it removes water by condensation. Any system which would cool air enough to remove significant amounts of water would also remove significant quantities of benzene (boiling point 80.1 °C) and nitrogen dioxide (boiling point 21.2 °C). Although it might be possible to quantify the gas loss, this would make accurate measurement of the toxic gases more difficult and require more sensitive sensors. Thus, a system which buffers rather than removes the humidity would be better.

Deliquescent dryers, regenerative desiccant dryers and membrane dryers all use an adsorbent which is not at equilibrium with the ambient air to remove humidity. Once this adsorbent reaches equilibrium with the ambient air it must either be replaced or regenerated because it can no longer dry the air. However, in this application we are not interested in drying the air: rather we need to buffer rapid humidity fluctuations. So, rather than using a dry adsorbent, we can use a reversible adsorbent–a material which can easily adsorb or desorb
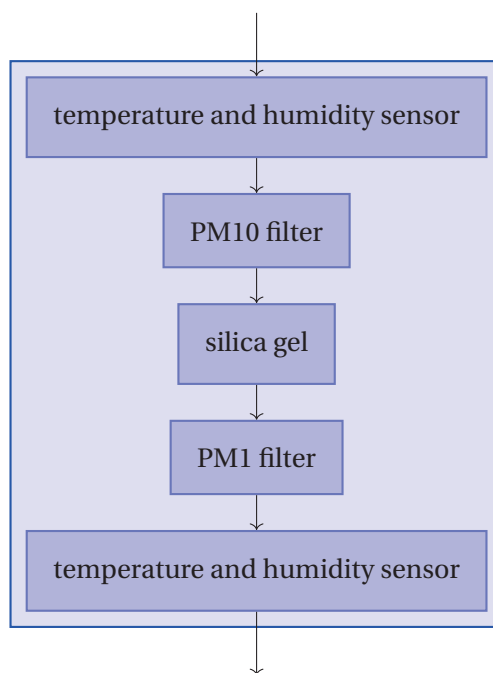
Figure 3.1 – The preconditioning unit is composed of an inlet temperature and humidity sensor which monitors the ambient air as it enters the system, a large particle filter, silica gel, a small particle filter and an outlet temperature and humidity sensor, which monitors air flowing out of the preconditioning unit. All of the components in the preconditioning unit are optional.

water–operating at equilibrium with the humidity in the ambient air. This way the materials never need a regeneration cycle. Additionally, assuming the gas of interest and the adsorbent are not reactive and that the adsorbent analyte pair are not able to non-covalently interact, the system will not cause loss or delay of analyte gases.

3.1.2 Overview of the components in the Preconditioning Unit

A flow chart of the gas through the preconditioning units is given in Figure 3.1. Images of the preconditioning units in the single sensor and the metal oxide sensor platforms are given in Figure 3.2. In the single sensor version, Figure 3.2a, air enters through the slats in the bottom right. It then passes by a Sensirion SHT 75 temperature and humidity sensor, which takes a reading of the ambient air. The gas then passes up through the PM10 filter, across a layer of silica gel (pink), and then down through the PM1 filter. Finally, the exiting air is read by another Sensirion SHT 75 temperature and humidity sensor. The image shown is a special ambient air only version, so it does not contain an entry port for gas standards.

The metal oxide sensor version mimics the flow chart: gas perpetually moves down the column. It can be seen in Figure 3.2b. In this platform gas standards or ambient air enter the system
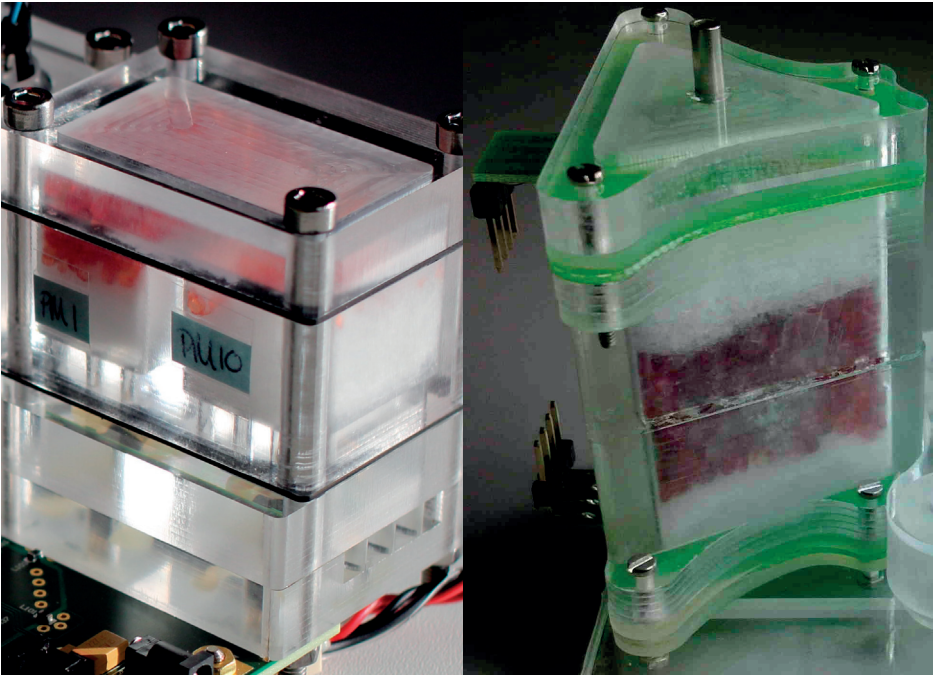
(a) Single sensor version   (b) Metal Oxide sensor version

Figure 3.2 – Preconditioning units on the single sensor and metal oxide sensor platforms. The following experiments were conducted using the metal oxide sensor version.
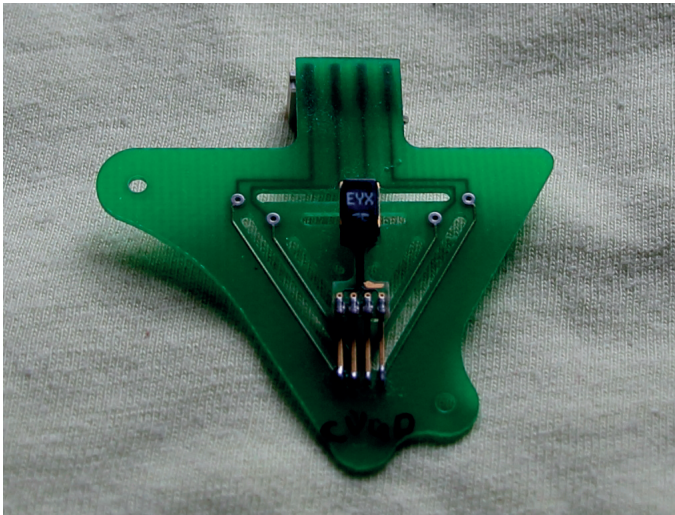
Figure 3.3 – A close up of the PCB which mechanically holds the filters in place while allowing gas to pass through the preconditioning unit and contains a temperature and humidity sensor.
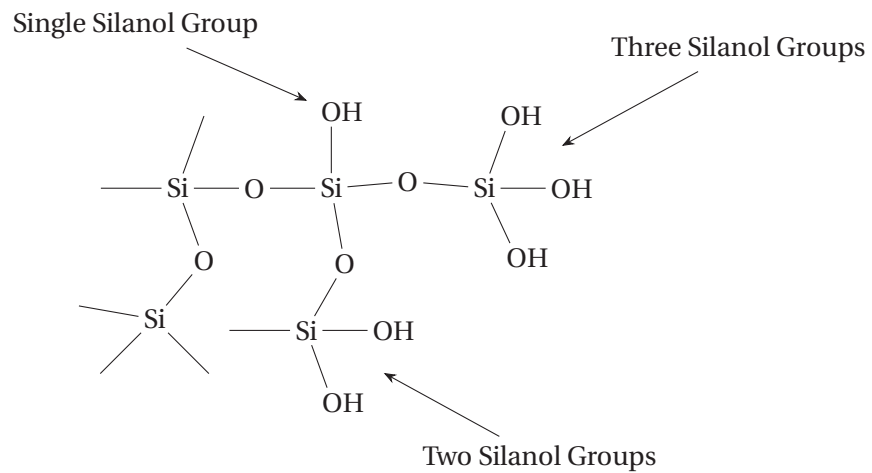
Figure 3.4 – Chemical structure of silica gel.

through the metal tube in the upper center of the image. The gas then passes a SHT 75 temperature and humidity sensor which is soldered directly onto the green pcb. This PCB contains holes which allow gas to pass through the system, and it also holds the particle filters in place. A close up of the PCB can be seen in Figure 3.3. After passing through the holes in the PCB, the gas passes through a PM10 filter, a layer of silica gel (red) and then a PM1 filter. The gas exits through holes in a second PCB which also contains a temperature and humidity sensor.

3.1.3   Material Choice

Silica gel is used as the adsorbent in the humidity stabilization unit because it is a reversible adsorbent at room temperatures and does not react with most chemical species. This property makes it an ideal candidate for the solid phase in liquid chromatography. Additionally, silica gel is a very low cost material and its ability to dehumidify air has been extensively studied.

Silica gel is an amorphous solid with the chemical formula $[SiO_2]$, where each oxygen atom is connected to two silicon atoms and each silicon atom is connected to four oxygen atoms, all with single bonds. The result is a large stable molecule with no overall dipole. However, at the surface of the gel this lattice structure is incomplete. Surface oxygen atoms are bound to hydrogen. This allows the silica gel to physically adsorb polar molecules such as water by forming hydrogen bonds. A planar projection of this can be seen in Figure 3.4. However, because the internal structure of the gel is nonpolar, the gel cannot absorb polar molecules such as water. Therefore, water binding to the silica gel is only a surface phenomenon [Scott, 2000].

The process of a chemical reversibly adsorbing onto a material is usually quantified by the pair's isotherm equation. For gases, the isotherm equation relates the amount of a chemical species adsorbed onto the surface of the adsorbent to the amount in gas at equilibrium. It is specific to a given temperature, hence its name.

The isotherm equation can take several forms. The International Union of Pure and Applied Chemistry (IUPAC) classifies these into 6 main types shown in Figure 3.5. Type I usually describes monolayer formation on porous solids. These isotherms can be described by the Langmuir equation. Type II isotherms usually describe non-porous or macroporous adsorbents and adsorbates which can bind to themselves to form multilayers. Point B is the transition between monolayer and multilayer formation. Type III occurs when there are strong adsorbate-adsorbate interactions. Type IV is similar to type II. However, it contains a hysteresis loop as a result of capillary action within the pores of the adsorbent. Type V occurs in porous systems with adsorbate-adsorbate interactions. Lastly, Type VI results from multilayer formation on a non-porous surface. The number of steps indicate how many layers can be formed [Sing, 1985].

Silica gel and water have been found to have Type I, II and V isotherms [Yildirim, 2011]. The reason there is so much discrepancy in the literature is that the type of curve that gives the best fit is a result of the surface properties of the gel used, not the bulk properties [Li et al., 2007]. The surface structure (i.e. size, number and depth of pores) and ratios of types of silanol groups vary between silica gel manufacturers. Additionally, the operating temperature has been shown to have an effect not only on the type of curve [Naono et al., 1980] but also on its magnitude [Ahlberg, 1939].

Once an isotherm has been measured, it is important to find the best fit equation for the data. Some researchers simply apply a best fit curve such as a polynomial to the data. This was done by Pesaran et al. for two types of silica gel and water as part of a model of a desiccant dryer system [Pesaran, 1983; Pesaran and Mills, 1987a]. Other researchers apply models whose parameters have chemical significance. This was the case when Jury et al. used the Langmuir isotherm to describe the binding of water on silica gel [Jury and Edwards, 1971].

Although there are dozens of equations used to describe isotherms [Foo and Hameed, 2010], only two will be used in the body of this thesis: the Langmuir isotherm and the Hill Equation. The Langmuir isotherm is used to describe Type I isotherms. The Hill Equation, which was originally used to describe the binding of oxygen to hemoglobin, is used to describe Type V isotherms because they exhibit cooperative binding [Hill, 1910]. Both of these equations are derived below.

3.1.4 Derivation of the Langmuir Isotherm

The Langmuir equation is derived from the basic chemical reaction scheme:
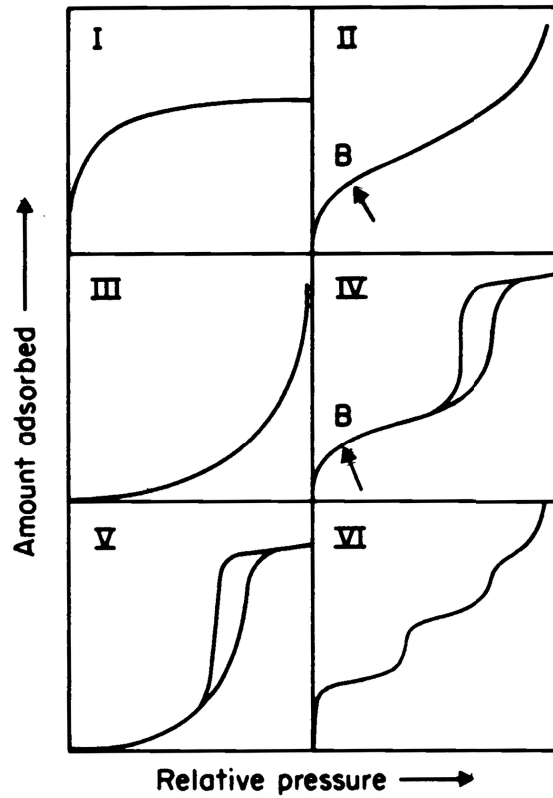
Figure 3.5 – IUPAC classification of isotherm types. Image source [Sing, 1985].

$$\text{SiOH} + \text{H}_2\text{O} \underset{k_r}{\overset{k_f}{\rightleftharpoons}} \text{SiOH} \cdots \text{H}_2\text{O}$$
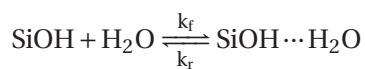
where the hydrogen on the OH group of the silica gel hydrogen bonds reversibly with the unpaired electrons on the oxygen of the water molecule with the forward reaction rate of k_f and the reverse reaction rate of k_r. The changes in concentration of each species with respect to time are described by the following differential equations:

$$\frac{d[\text{SiOH}]}{dt} = k_r [\text{SiOH} \cdots \text{H}_2\text{O}] - k_f [\text{SiOH}] \cdot [\text{H}_2\text{O}] \tag{3.1}$$

$$\frac{d[\text{H}_2\text{O}]}{dt} = k_r [\text{SiOH} \cdots \text{H}_2\text{O}] - k_f [\text{SiOH}] \cdot [\text{H}_2\text{O}] \tag{3.2}$$

49

$$\frac{d[\text{SiOH}\cdots\text{H}_2\text{O}]}{dt} = -k_r[\text{SiOH}\cdots\text{H}_2\text{O}] + k_f[\text{SiOH}]\cdot[\text{H}_2\text{O}] \tag{3.3}$$

where brackets represent species concentration. Additionally, at equilibrium the concentrations of all species are not changing with respect to time so the following equation is true:

$$k_r[\text{SiOH}\cdots\text{H}_2\text{O}] = k_f[\text{SiOH}]\cdot[\text{H}_2\text{O}] \tag{3.4}$$

Additionally, the amount of silica gel in the system is not changing with respect to time so it is known that $[\text{SiOH}]_{empty} + [\text{SiOH}\cdots\text{H}_2\text{O}]_{bound} = [\text{SiOH}]_{total}$ so this equation can be rewritten:

$$k_r[\text{SiOH}\cdots\text{H}_2\text{O}] = k_f([\text{SiOH}]_{total} - [\text{SiOH}\cdots\text{H}_2\text{O}]_{bound})\cdot[\text{H}_2\text{O}] \tag{3.5}$$

The kinetic constants can be replaced by the relation $K = k_f/k_r$ and the concentrations can be replaced by the ratio $\theta = [\text{SiOH}\cdots\text{H}_2\text{O}]/[\text{SiOH}]_{total}$. This can be rearranged to give the Langimuir equation:

$$\theta = \frac{K\cdot[\text{H}_2\text{O}]}{1 + K\cdot[\text{H}_2\text{O}]} \tag{3.6}$$

This can be rearranged to the form which is useful in mass transport studies. By noting that the maximum amount of water which can adsorb onto the silica gel, $[\text{SiOH}\cdots\text{H}_2\text{O}]_{max}$ is equal to the number of binding sites $[\text{SiOH}]_{total}$, for the case where only a monolayer can form on the surface of the adsorbent, the following relation can be derived:

$$[\text{SiOH}\cdots\text{H}_2\text{O}] = \frac{K\cdot[\text{SiOH}\cdots\text{H}_2\text{O}]_{max}\cdot[\text{H}_2\text{O}]}{1 + K\cdot[\text{H}_2\text{O}]} \tag{3.7}$$

The Langmuir equation in this form will be used again in future studies.

3.1.5   Derivation of the Hill Equation

The derivation of the Hill Equation is analogous to the Langmuir derivation. However, the Hill Equation includes one extra effect: the binding of a molecule to silica gel affects the affinity of

a molecule to the neighboring binding site. The result is that two balances must be written:
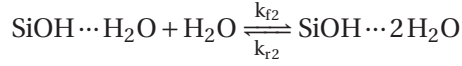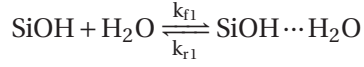
$$\text{SiOH} + \text{H}_2\text{O} \underset{k_{r1}}{\overset{k_{f1}}{\rightleftharpoons}} \text{SiOH} \cdots \text{H}_2\text{O}$$

$$\text{SiOH} \cdots \text{H}_2\text{O} + \text{H}_2\text{O} \underset{k_{r2}}{\overset{k_{f2}}{\rightleftharpoons}} \text{SiOH} \cdots 2\,\text{H}_2\text{O}$$

The changes in concentration of each species with respect to time are described by the following differential equations:

$$\frac{\text{d}[\text{SiOH}]}{\text{d}t} = k_{r1}[\text{SiOH} \cdots \text{H}_2\text{O}] - k_{f1}[\text{SiOH}] \cdot [\text{H}_2\text{O}] \tag{3.8}$$

$$\frac{\text{d}[\text{H}_2\text{O}]}{\text{d}t} = k_{r1}[\text{SiOH} \cdots \text{H}_2\text{O}] - k_{f1}[\text{SiOH}] \cdot [\text{H}_2\text{O}]$$
$$- k_{r2}[\text{SiOH} \cdots 2\,\text{H}_2\text{O}] - k_{f2}[\text{SiOH} \cdots \text{H}_2\text{O}] \cdot [\text{H}_2\text{O}] \tag{3.9}$$

$$\frac{\text{d}[\text{SiOH} \cdots \text{H}_2\text{O}]}{\text{d}t} = -k_{r1}[\text{SiOH} \cdots \text{H}_2\text{O}] + k_{f1}[\text{SiOH}] \cdot [\text{H}_2\text{O}]$$
$$- k_{r2}[\text{SiOH} \cdots 2\,\text{H}_2\text{O}] + k_{f2}[\text{SiOH} \cdots \text{H}_2\text{O}] \cdot [\text{H}_2\text{O}] \tag{3.10}$$

$$\frac{\text{d}[\text{SiOH} \cdots \text{H}_2\text{O}]}{\text{d}t} = -k_{r2}[\text{SiOH} \cdots 2\,\text{H}_2\text{O}] + k_{f2}[\text{SiOH} \cdots \text{H}_2\text{O}] \cdot [\text{H}_2\text{O}] \tag{3.11}$$

Similarly, at equilibrium the following relations are true:

$$k_{r1}[\text{SiOH} \cdots \text{H}_2\text{O}] = k_{f1}[\text{SiOH}] \cdot [\text{H}_2\text{O}] \tag{3.12}$$

$$k_{r2}[\text{SiOH} \cdots 2\,\text{H}_2\text{O}] = k_{f2}[\text{SiOH} \cdots \text{H}_2\text{O}] \cdot [\text{H}_2\text{O}] \tag{3.13}$$

And the total available binding sites is constant:

$$[\text{SiOH}] + [\text{SiOH} \cdots \text{H}_2\text{O}] + [\text{SiOH} \cdots 2\,\text{H}_2\text{O}] = [\text{SiOH}]_{total} \tag{3.14}$$

By rearranging and combining the equilibrium relationships, we find:

$$\frac{k_{r1} \cdot k_{r2}}{k_{f1} \cdot k_{f2}} \cdot \frac{[\text{SiOH} \cdots 2\,\text{H}_2\text{O}]}{[\text{SiOH}]} = [\text{H}_2\text{O}]^2 \tag{3.15}$$

Then replacing $\frac{k_{r1} \cdot k_{r2}}{k_{f1} \cdot k_{f2}}$ with K and substituting in the equation for the total binding sites yields:

$$K \cdot \frac{[\text{SiOH} \cdots 2\,\text{H}_2\text{O}]}{[\text{SiOH}]_{total} - [\text{SiOH} \cdots \text{H}_2\text{O}] - [\text{SiOH} \cdots 2\,\text{H}_2\text{O}]} = [\text{H}_2\text{O}]^2 \qquad (3.16)$$

Rearranging this equation yields:

$$K \cdot [\text{SiOH} \cdots 2\,\text{H}_2\text{O}] + [\text{H}_2\text{O}]^2 \cdot ([\text{SiOH} \cdots \text{H}_2\text{O}] + [\text{SiOH} \cdots 2\,\text{H}_2\text{O}])$$
$$= [\text{SiOH}]_{total} \cdot [\text{H}_2\text{O}]^2 \quad (3.17)$$

When binding is cooperative, the concentration of the intermediate state is usually negligibly small such that $[\text{SiOH} \cdots \text{H}_2\text{O}] + [\text{SiOH} \cdots 2\,\text{H}_2\text{O}] \approx [\text{SiOH} \cdots 2\,\text{H}_2\text{O}]$. Applying this approximation gives the Hill Equation for a system where one binding site can effect exactly one other binding site:

$$[\text{SiOH} \cdots 2\,\text{H}_2\text{O}] = \frac{[\text{SiOH}]_{total} \cdot [\text{H}_2\text{O}]^2}{K + [\text{H}_2\text{O}]^2} \qquad (3.18)$$

The above method can be used to find the Hill Equation for any system which exhibits cooperative binding. In the generalized case, where one binding site can effect n other binding sites, the Hill Equation becomes:

$$[\text{SiOH} \cdots 2\,\text{H}_2\text{O}] = \frac{[\text{SiOH}]_{total} \cdot [\text{H}_2\text{O}]^n}{K + [\text{H}_2\text{O}]^n} \qquad (3.19)$$

3.1.6 Potential Problems with Design

Although silica gel is ideal from a water sorption perspective, it could also interact with the analyte of interest. This would both increase the time it takes for the toxic gas to reach the sensor and, in the case of short exposures, reduce the maximum quantity of toxic gas which arrives at the sensor surface. This is particularly a concern for polar molecules which can hydrogen bond. An overview of functional groups and their ability to interact with polar substrates is given in Figure 3.6. Irrespective of a chemical's ability to adsorb onto to silica gel, the total quantity of the toxin which reaches the sensor should, theoretically, be the same. The signal will just be delayed and spread over time. Thus, continuous exposure measurements should not be effected.

To test the working principle of the preconditioning unit before a large investment was made in this design, two quick screenings were conducted. First, unquantified amounts of isopropanol and smoke were individually allowed to pass through a layer of silica gel before coming into contact with either a metal oxide sensor or an electrochemical sensor. The sensors all showed responses, indicating that the silica gel was not removing all of the gases of interest. The second screening was more scientific. A simple adsorption model was built in Comsol, using available literature data for the adsorption isotherms of a few toxic gases. The results of this

Most Adsorbent

Carboxilic Acids
↓
Alcohols, Amines, Thiols
↓
Aldehydes, Ketones, Esters
↓
Halogenated Hydrocarbons
↓
Unsaturated Hydrocarbons
↓
Saturated Hydrocarbons

Slowest

Least Adsorbent

Fastest

Figure 3.6 – Chromatographic adsorbabilities of some functional groups and their relative residence times when silica gel is used as the solid phase.

model showed that silica gel might be able to buffer humidity while allowing toxic gases to pass through the system. However, there was a small delay caused by adsorption and desorption of the analyte gases. To fully understand this trade off between buffering and signal delay, the system needed to be experimentally studied and computationally modeled. For both the experiments and models, the preconditioning unit from the second version of the multisensor platform (Section 2.3) was used. The results of these experiments are not shown because they were qualitative and not quantitative.

3.2 Experimental Validation of the Preconditioning Unit

To experimentally confirm that it is possible to use silica gel to buffer rapid humidity fluctuations without delaying the toxic gas sensor signal, gas mixtures with known quantities of analyte need to be made. Two methods of doing this were tried. First, gas samples were made in Tedlar sample bags by serial dilution. This method did not work because the bags are not humidity tight. For more information see the the failed experiments section of the Appendix. Later, a mass flow controller system was employed to make these samples. At first this method also had humidity problems, which are also presented in the failed experiments section of the Appendix. However, eventually these problems were solved.

Experiments were conducted at CEIT in San Sebastian, Spain and Siemens Building Technologies in Zug, Switzerland using analogous mass flow controller setups. To create toxic gas mixtures at various relative humilities, $0.4 \, \mathrm{L\,min^{-1}}$ of various mixtures of gas were propelled though the system using a set of 3 Bronkhorst EL-Flow Select mass flow meter/controllers. These controllers deliver a maximum of $0.5 \, \mathrm{L\,min^{-1}}$ air at 2 bar. Synthetic air, composed of 20% oxygen and 80% nitrogen by weight, was connected to two of these controllers, while the third controller was used for the toxic gas line. One of the air lines passed through a bubbler, which added water to the dry air until it was almost saturated (i.e. approximately 95

53
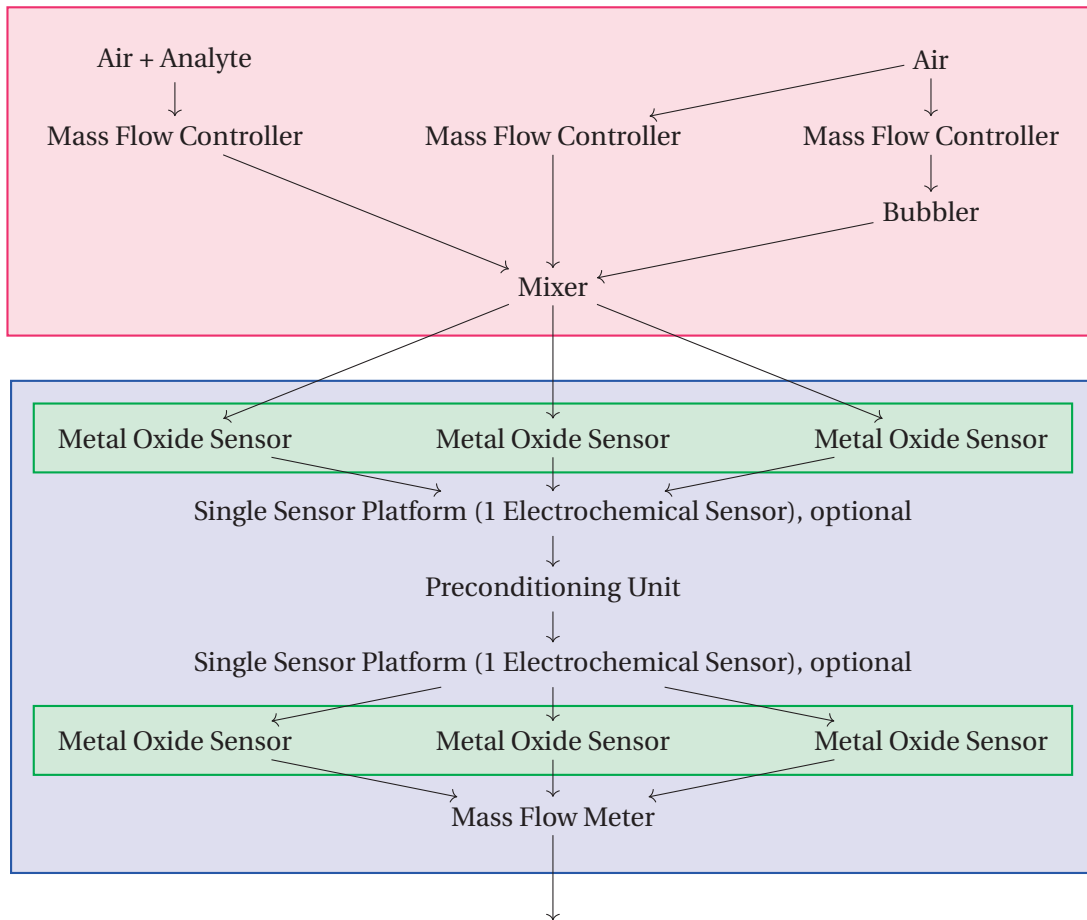
Figure 3.7 – Flow chart of the fluid path through both the gas sample mixing system (pink) and the gas sensor system (blue). The pink components in this system are shown in Figure 3.8 and the blue and green components are shown in Figure 3.10.

Figure 3.8 – One of the gas mixing systems at CEIT. The silver box contains all of the components in the pink box in Figure 3.7, with the exception of the gas tanks.

Figure 3.9 – Toxic gas experiments being setup with the help of a collaborator.
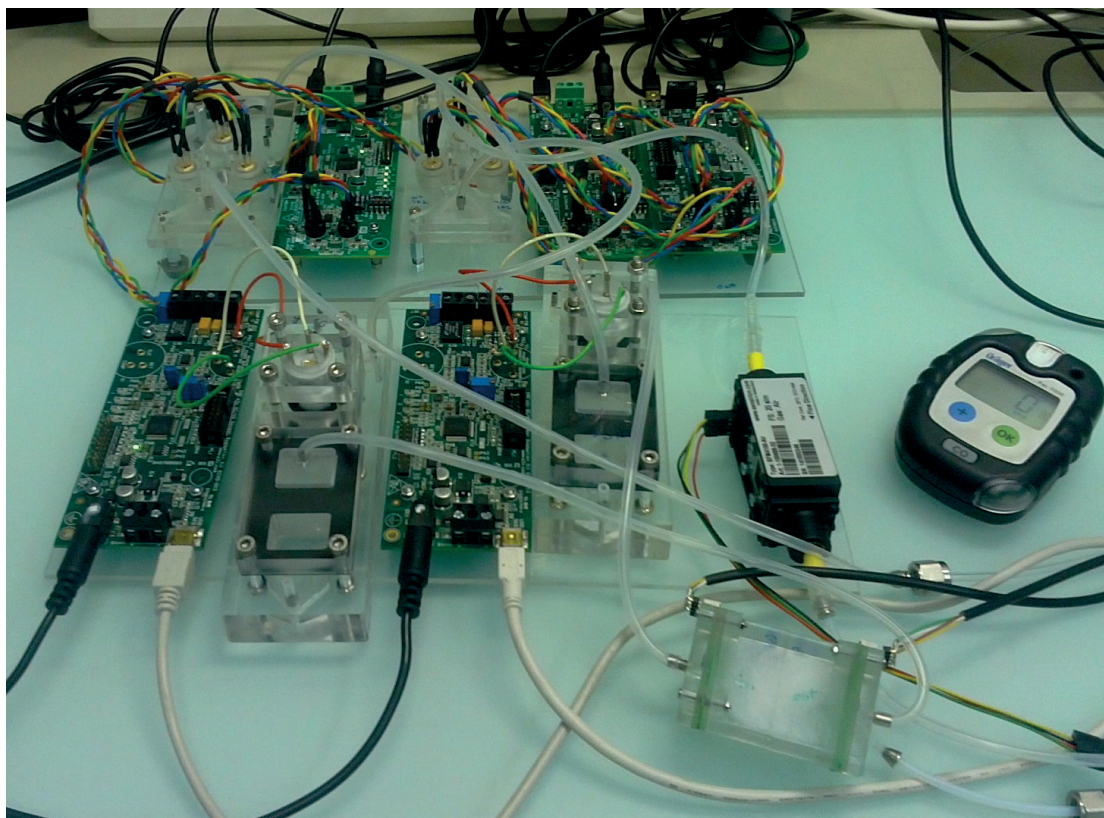
Figure 3.10 – Image of multisensor platform system, one metal oxide multisensor platform is before the preconditioning unit, another is after. Together they use 3 electronics boards to run and read data from 6 metal oxide sensors. Both of these platforms and their corresponding electronics platforms are in the back of the hood. The optional electrochemical sensors are in the front of the image. Each of their electronics boards can run one electrochemical sensor. The preconditioning unit has been removed from the board, and is located in the lower right of the image. The mass flow meter is behind it. Lastly, the CO alarm is right of the mass flow meter and reads 0 ppm.

to 99% relative humidity. Then all lines were fed into a mixer where the gases were combined (Figure 3.7,top and Figure 3.8). By changing the proportions of gas passing through each mass flow controller, both the relative humidity and the amount of toxic gas in a sample could be controlled. The mixed gas was then run through the sensor system.

The outlet of the mixer was fed into two multisensor platforms operating in series. These platforms were populated with six metal oxide sensors (e2v mics-5521). The device setup can be seen in Figure 3.10. In this setup gas first passed through the gas sensor only platform (Figure 3.10, left) and then passed into the normal platform (Figure 3.10, right). Thus, it was possible to obtain gas data from before the silica gel and after. Figure 3.9 shows Jurgi Gonzalez de Chavarri, a collaborator at CEIT, helping me setup and troubleshoot the gas mixing equipment.

Gas	Relative Humidities	Concentration (PPM)
CO	30, 45 and 60	20, 40, 60, 80 and 100
Benzene	30, 45 and 60	2, 4, 6, 8 and 10
NO_2	30, 45, and 60	4, 8, 12, 16 and 20

Table 3.1 – Concentrations of gas and humidity used in experiments.

To confirm that the correct flow rate was being output by the mass flow controllers and that the system did not contain leaks, a Sensirion mass flow meter (Item number: SFM4100), calibrated for air, was placed at the exit of the whole system. Data was continuously collected from this mass flow meter throughout all of the experiments to verify their accuracy. In addition to the mass flow controller, during carbon monoxide experiments, a Draeger Pac 700 Carbon Monoxide sensor was placed in the chemical hood with the system to confirm that the system was gas tight.

Additionally, for both nitrogen dioxide and carbon monoxide, electrochemical sensors were added to the setup for some experiments. When electrochemical sensors were used, two single sensor platforms containing a pair of carbon monoxide sensors (SGX EC4-500-CO) or a pair of nitrogen dioxide sensors (SGX-4NO2) and their corresponding electronic platforms were added to the setup. One of the single sensor platforms was placed between the exit of the inlet side of the multisensor system and the preconditioning unit. The other system was placed between the exit of the preconditioning unit and the outlet metal oxide sensors. The overall schematic of the system setup can be seen in Figure 3.7.

Once the system was set up, the sensors were allowed to stabilize in clean air at 45% relative humidity. Humidity experiments were then conducted to verify that the metal oxide sensors were responding to humidity fluctuations, and that the silica gel was acting as a reversible adsorbent to buffer out these false positives. To do these experiments pulses of clean air containing various concentrations of water were sent through the system. Pulses ranged from 5 minutes to 6 hours and from 0% to 80% relative humidity. Experiments were done both with and without silica gel in the preconditioning unit. All silica gel experiments were conducted using 2 ± 0.2 g of silica gel type II suitable for desiccation from Sigma Aldrich (lot #MKBQ4408V).

In addition to the humidity study, toxic gas studies were also performed both with and without 2 ± 0.2 g of silica gel in the preconditioning unit. Each experiment began with sensors at equilibrium with clean air at 45% relative humidity. Toxic gas pulses and humidity fluctuations were applied simultaneously, so that all combinations in Table 3.1 were tested. Once the sensor reached equilibrium with the toxic gas, clean air at 45% relative humidity was run through the system until the sensor returned to baseline. The data from the empty preconditioning unit experiments at 45% relative humidity was used to calibrate the sensors.

Once the experiment was complete, data was analyzed using matlab. First all data points were

| | | Signal and Baseline Delays (s) | | | |
| | | Metal Oxide | | Electrochemical | |
Gas	Relative Humidity	Signal Delay	Baseline Delay	Signal Delay	Baseline Delay
CO	30	-14 ± 10	-2 ± 1	23 ± 52	5 ± 37
	45	3 ± 4	-1 ± 1	5 ± 8	-17 ± 16
	60	6 ± 10	0 ± 2	7 ± 32	-12 ± 26
Benzene	30	23 ± 13	38 ± 9		
	45	21 ± 15	35 ± 5		
	60	43 ± 3	23 ± 5		
NO$_2$	30	197 ± 176	201 ± 28	6 ± 18	55 ± 78
	45	103 ± 145	155 ± 52	17 ± 49	2 ± 58
	60	108 ± 79	137 ± 37	13 ± 15	38 ± 46

Table 3.2 – Additional time required to reach 90% sensor response and 90% baseline return when silica gel is used, relative to experiments without silica gel. Each metal oxide value is the mean of a minimum of 15 sensor reading sets ± a standard deviation. The electrochemical data is similar but each value is the mean of 5 sensor reading sets.

aligned. Then, the metal oxide sensor data and electrochemical data were calibrated using the techniques outlined on the product data sheets. This calibrated data was then used to determine the effects of silica gel on signal delay (Table 3.2) and sensor response (Table 3.3). The delay data was calculated using the following formula:

$$\text{Delay} = \text{RT}_{\text{SiO}_2,\text{ out}} - \text{RT}_{\text{no SiO}_2,\text{ out}} - (\text{RT}_{\text{SiO}_2,\text{ in}} - \text{RT}_{\text{no SiO}_2,\text{ in}}) \tag{3.20}$$

Where RT stands for the 90% response time, in seconds for a given sensor. The subscripts SiO$_2$ or noSiO$_2$ refer to the experiments with and without silica gel in the preconditioning unit, respectively. The in and out subscripts are in relation to the preconditioning unit–in gas is going to be fed into the preconditioning unit and out gas is coming out of the preconditioning unit. In theory only the out data is necessary for this equation and the in data should be zero. However, occasionally the mass flow controllers take slightly longer to create a consistent gas stream. This means that there was a slightly different delay between the two experiments. This delay was only a few seconds. However, to compensate for it, the difference in inlet side responses–which should be zero–was removed. Once this data was found for all sensors in all runs, the values at a given humidity were grouped. Then their mean and one standard deviation was determined. These are reported in the Table 3.2.

Variation in mass flow controller response times does not effect the equilibrium value of the sensors. Therefore, the response values were calculated using the out data from the experiments with and without silica gel. These data were grouped by toxic gas concentration and are presented in Table 3.3.

Overall, the response times in Table 3.2 and the response values in Table 3.3 are sufficient for our application. For carbon monoxide, the goal was to take a sensor reading every minute. As

| | | PPM detected | | | |
| | | Metal Oxide | | Electrochemical | |
Gas	PPM gas	no SiO_2	SiO_2	no SiO_2	SiO_2
CO	20	8.2 ± 2.0	$10.0 \pm .9$	18.1 ± 3.2	22.9 ± 4.0
	40	37.1 ± 2.7	$40.3 \pm .8$	38.6 ± 2.1	44.7 ± 2.8
	60	47.4 ± 2.5	50.1 ± 1.0	56.9 ± 3.1	58.4 ± 2.8
	80	60.8 ± 3.5	63.2 ± 1.8	77.1 ± 4.4	86.7 ± 3.8
	100	69.4 ± 4.3	71.7 ± 2.3	100.3 ± 5.6	110.9 ± 3.8
Benzene	2	$2.5 \pm .7$	$1.7 \pm .3$		
	4	5.8 ± 1.2	$3.5 \pm .6$		
	6	8.9 ± 1.6	$5.2 \pm .6$		
	8	11.9 ± 2.1	$6.9 \pm .8$		
	10	14.5 ± 2.6	8.5 ± 1.1		
NO_2	4	2.0 ± 1.0	$2.9 \pm .9$	$3.7 \pm .3$	$3.9 \pm .6$
	8	3.4 ± 1.4	4.4 ± 1.4	7.4 ± 1.0	$6.6 \pm .9$
	12	6.9 ± 1.9	8.5 ± 1.9	13.6 ± 2.6	11.0 ± 1.0
	16	11.8 ± 2.5	14.7 ± 1.8	18.2 ± 3.2	16.0 ± 1.6
	20	18.1 ± 3.3	18.5 ± 2.5	20.0 ± 3.5	17.5 ± 3.9

Table 3.3 – Calibrated sensor responses at equilibrium. Each metal oxide value is the mean of a minimum of 9 sensor reading sets ± a standard deviation. The electrochemical data is similar but each value is the mean of 3 sensor reading sets.

Figure 3.11 shows, it is very difficult to see a difference between the sensor response with silica gel (red solid line) and the sensor responses without silica gel (other lines). According to the measurements from the metal oxide sensors, delays caused by carbon monoxide adsorbing onto or desorbing from silica gel are negligible. The electrochemical sensors act similarly, but are very noisy. The manufacturer recommends resolving this problem by taking a running average of the sensor data. However, even with a 20 second running average, the signal can be more than 10 ppm different than the gas it is exposed to. Thus, if the noise is causing the value to be low at the beginning of the pulse, it can take much longer for for the signal to reach the average equilibrium value for that sensor (Figure 3.11 left). The result is a much larger spread on the signal delay data. The carbon monoxide sensor responses for the elctrochemical data show much less variance than the sensor delay data because these are averages over 100 seconds rather than a single time point. The sensor responses for metal oxide sensors seem prone to calibration curve errors. The manufacturer states that the calibration curve is linear on a log log scale–but this did not seem to be true across the 20 to 100 ppm CO range. Additionally, the equilibrium value for the metal oxide sensors has a smaller standard deviation for the silica gel data than the no silica gel data. This is because the effects of humidity fluctuations during the gas pulse were less significant when the humidity was buffered. This trend was true across all gases, not just for carbon monoxide. An example for benzene can be seen in Figure 3.12.
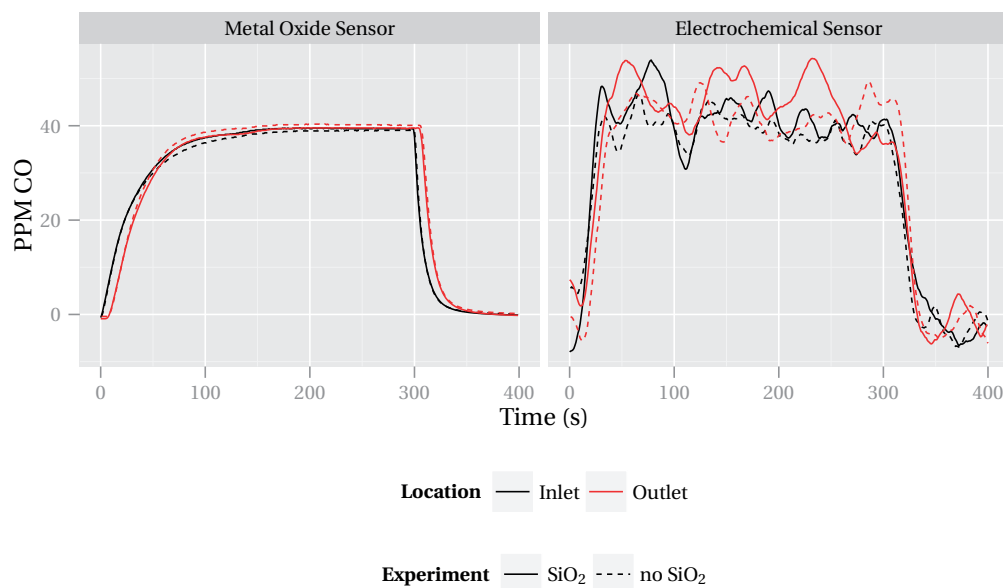
Figure 3.11 – Responses of metal oxide semiconductor sensors (left) and electrochemical sensors (right) to a 40 ppm pulse of carbon monoxide. Silica gel has a minimal effect on the response time or the equilibrium values of the sensors. The electrochemical sensors show a similar trend but are much nosier.

The benzene data was taken every ten minutes in this project. Therefore, the sensor delays, which are less than 1 minute, are sufficiently small for our application. Additionally, the sensor responses from the buffered experiments are more accurate and have a smaller standard deviation than the unbuffered experiments. The reason the buffered values are more accurate and have a smaller deviation is that the error from the humidity fluctuation is removed. In this case the low humidity sensor reading is consistently higher than the high humidity reading. The result is that the buffered sensors give a more consistent toxic gas reading than the unbuffered sensors.

The nitrogen dioxide data was also within the 10 minute mark. However, there is a very large variance in response time for the metal oxide sensors to pulses of toxic gas. This is because the metal oxide sensors in the NO_2 experiments frequently overshot the equalibrium concentration value at the beginning of the pulse. This type of response has been published elsewhere in literature [Nayak et al., 2015; Gole and Laminack, 2013], and occurred sporadically throughout the experiments. This inconsistency in the overshoot causes the variance in the NO_2 signal delay to be large. The electrochemical sensors did not have the same problem. However, they did have the same noise issues that the carbon monoxide electrochemical sensors had, hence their large variances. Lastly, the equilibrium sensor readings to NO_2 for both the electrochemical and metal oxide sensors seem slightly better when the gas is buffered, but not significantly so.
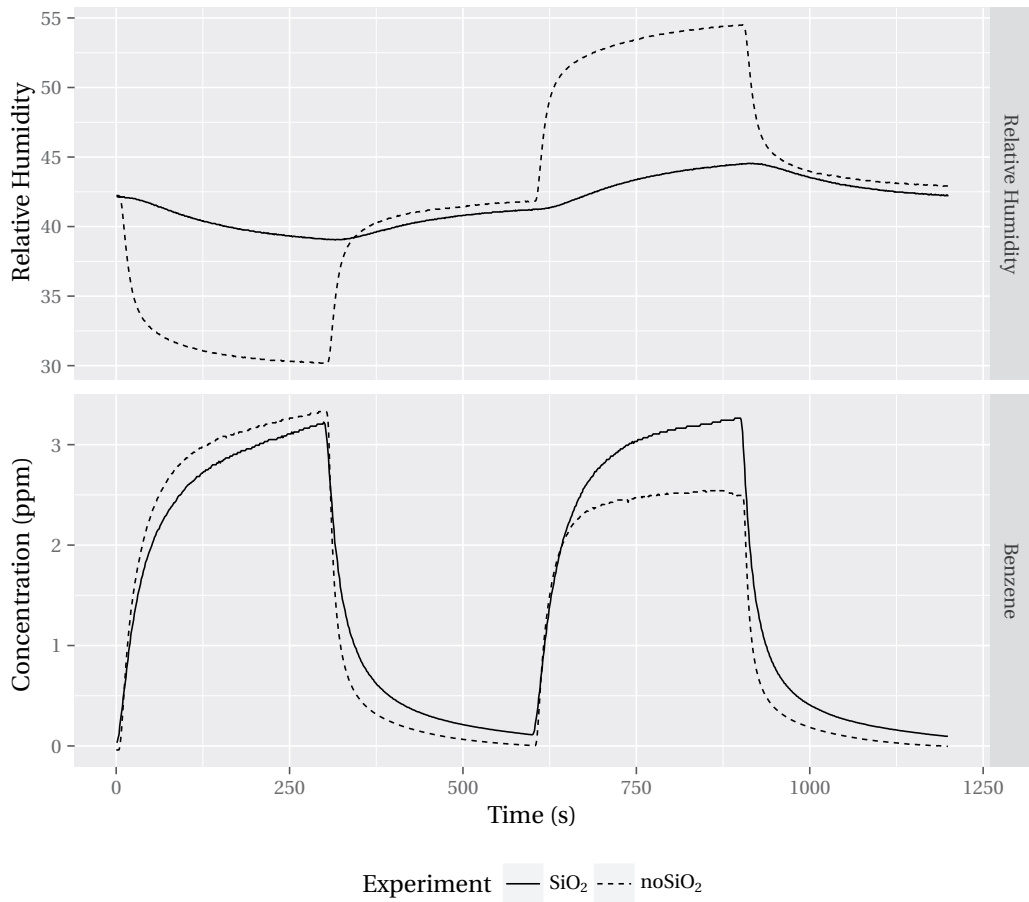
Figure 3.12 – Example of the effects of humidity on sensor response. The sensor without humidity buffering (dashed line) shows different responses to 4ppm of benzene, whereas the sensor buffered with silica gel shows a repeatable response.

In addition to the experiments above, experiments using metal oxide sensors operating in dry conditions were also conducted. These experiments gave inconclusive results because the sensors were not designed to operate in dry conditions. Additionally, experiments using formaldehyde were conducted and are included in the Appendix (Section 6.1). These experiments are inconclusive because the formaldehyde, which is stored in dry nitrogen, was probably reacting with the oxygen and water in the mixer and on the surface of the gel. Efforts were made to find lab equipment which could be used to quantify these reactions, but the only lab with this equipment found in Switzerland needed thousands of francs to repair the device.

3.3 Computational Model of the Preconditioning Unit

In addition to the experimental studies, the adsorption and desorption of toxic gases and water on silica gel were computationally modeled. Two methods were used. The first assumes that the heat of adsorption can be neglected, because the quantity of analyte adsorbed is so small that the temperature does not change. The second model includes heat of adsorption. These models give us a better understanding of the adsorption process. They could be used to minimize the experiments required in order to optimize the system for other applications, such as sensor response time or magnitude of humidity fluctuations.

3.3.1 Isotherm Values

Independent of which model is used, the first step is to determine the isotherm equation. As explained in Section 3.1.3, the isotherm equation correlates a concentration of an analyte on the surface of the silica gel to the quantity in the air at equilibrium at given temperature. For the toxic gases, curves were fit to literature data. However, because there is a wide variation in the affinity of various types of silica gel for water (see Section 3.1.3), the humidity data was experimentally measured.

Literature Values

Benzene data was taken from [Wang et al., 2004], nitrogen dioxide data was taken from [Izumi et al., 2002] and carbon monoxide data was taken from [Markham and Benton, 1931]. The raw data from these papers was converted to the units used in the computational model. A number of isotherm equations were fit to the data. The best fit curve for the best fit iostherm model was then selected for use in future models. The benzene data (Figure 3.13) had a best fit curve of:

$$[\mathrm{SiOH}\cdots\mathrm{C_6H_6}] = \frac{K_{\mathrm{C_6H_6}} \cdot [\mathrm{SiOH}\cdots\mathrm{C_6H_6}]_{max} \cdot [\mathrm{C_6H_6}]}{1 + K_{\mathrm{C_6H_6}} \cdot [\mathrm{C_6H_6}]} \qquad (3.21)$$
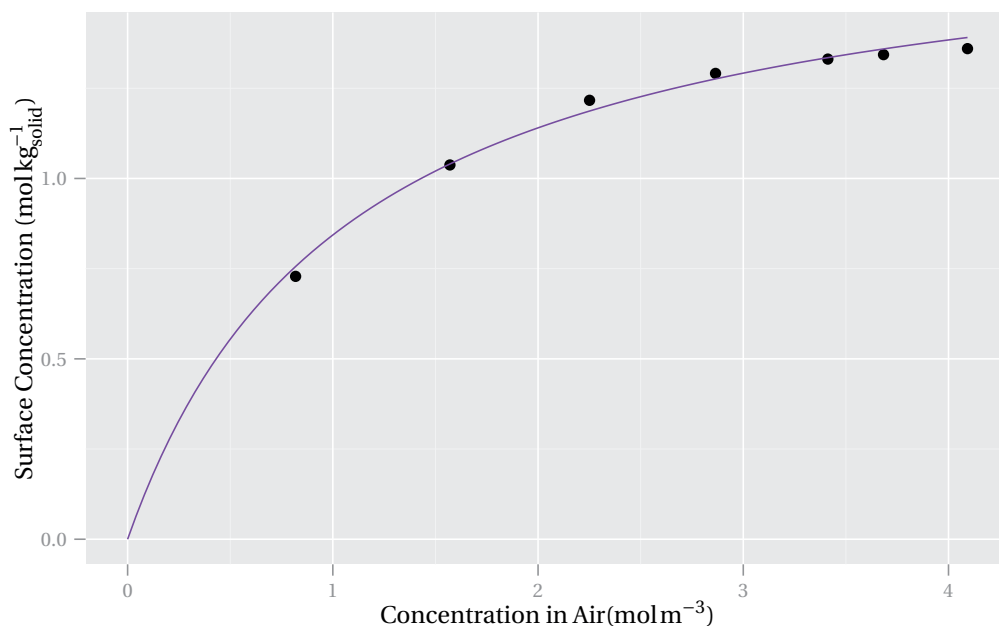
Figure 3.13 – Isotherm for Benzene (C_6H_6), found using data from [Wang et al., 2004].

where $[\text{SiOH} \cdots \text{C}_6\text{H}_6]_{max} = 1.8$ and $K_{\text{C}_6\text{H}_6} = .92$

Similarly, the NO_2 data, seen in Figure 3.14, had the following best fit curve:

$$[\text{SiOH} \cdots \text{NO}_2] = \frac{K_{\text{NO}_2} \cdot [\text{SiOH} \cdots \text{NO}_2]_{max} \cdot [\text{NO}_2]}{1 + K_{\text{NO}_2} \cdot [\text{NO}_2]} \tag{3.22}$$

where $[\text{SiOH} \cdots \text{NO}_2]_{max} = 55$ and $K_{\text{NO}_2} = .047$

Lastly, the best fit curve for the CO data, which is depicted in Figure 3.15 was:

$$[\text{SiOH} \cdots \text{CO}] = \frac{K_{\text{CO}} \cdot [\text{SiOH} \cdots \text{CO}]_{max} \cdot [\text{CO}]}{1 + K_{\text{CO}} \cdot [\text{CO}]} \tag{3.23}$$

where $[\text{SiOH} \cdots \text{CO}]_{max} = .74$ and $K_{\text{CO}} = .0043$.

Each of these curves uses the Langmuir equation (Equation 3.7) as described in Section 3.1.4.

Humidity Measurements

To find the isotherm for water on silica gel, two different methods were tried. The data collected using the first method contained errors, so it was not used. The errors in this data set are not obvious so they are included in the Appendix under failed experiments. The other method generated the isotherm curve by measuring the humidity of the air in a sample and then measuring the change in mass when the adsorbed analyte was removed by heat. This
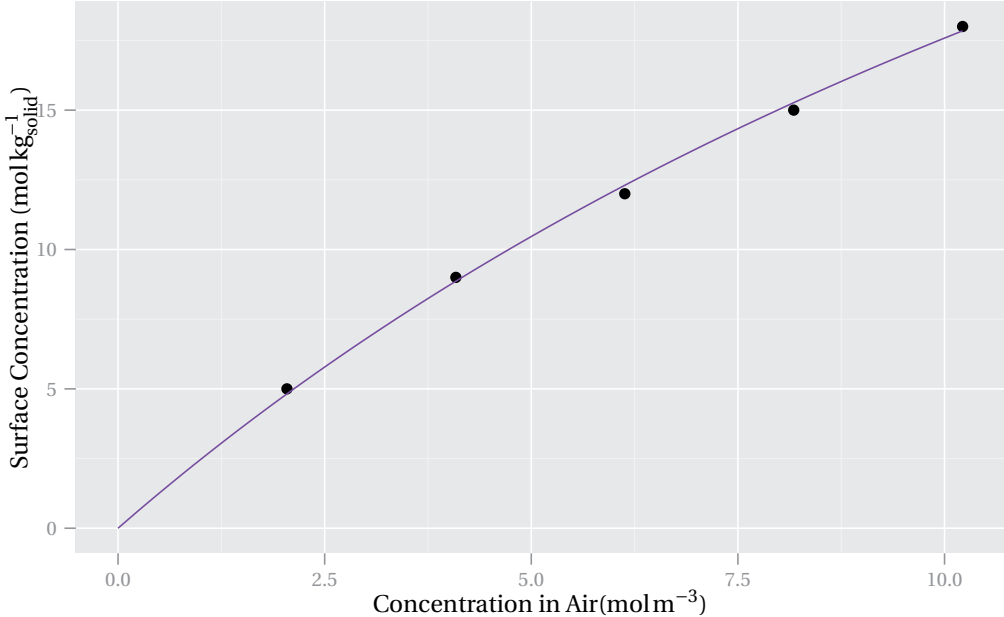
Figure 3.14 – Isotherm for Nitrogen Dioxide (NO_2), found using data from [Izumi et al., 2002].
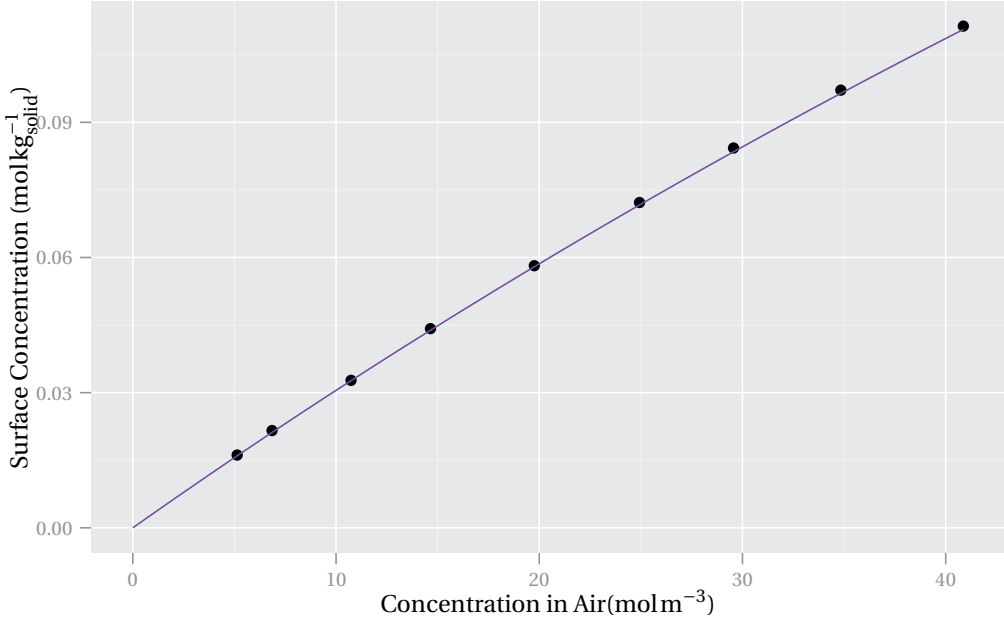
Figure 3.15 – Isotherm for Carbon Monoxide (CO), found using data from [Markham and Benton, 1931].

was successful, and is used in the models.

The first step in this method is to generate samples of silica gel at equilibrium with air at various humidities. To create these samples, two holes were drilled into the caps of 50 mL centrifuge tubes. Silicone tubes were placed through these holes and fixed using epoxy glue. These silicone tubes allow air to exit and enter the system. The centrifuge tubes were then filled with silica gel taking care to ensure that the air entrance was at the bottom of the centrifuge tube and the exit placed above the silica gel. Air was run through a bubbler and into the silica gel until samples with a variety of adsorbed concentrations had been made. These samples were then moved to glass containers and left for a few days to ensure equilibrium. Each was assigned a number and a random number generator was used to determine the order in which the samples were measured. The humidity in the container was then measured. Once equilibrium with the sensor system was found, the data point was recorded. This data point became the x value for a given point on the isotherm curve. The corresponding y value was found using a Mettler Toledo Halogen moisture analyzer. The moisture content:

$$\text{moisture content} = \frac{\text{wet weight} - \text{dry weight}}{\text{dry weight}} \cdot 100 \tag{3.24}$$

was found for each sample by heating the silica gel to 105 °C [Ng et al., 2001] and waiting until there was less than 1mg loss in 140s (settings in Table 3.4). This data was used to create the y value in the isotherm curve. The resulting plot gives the correlation between the amount of water in the air and the amount on the surface of the silica gel.

An example of the raw data collected during these experiments can be seen in Figure 3.17. In this figure the top, red curve is the value of the relative humidity in air as it reaches equilibrium. The values between the black points were averaged to find the relative humidity at equilibrium. The green curve is the moisture content change as the silica gel is heated in the drying unit. The adsorbed quantity is the last point on this curve. Many experiments like this were conducted on two types of silica gel: Rubin gel which contains an indicator and non-indicating silica gel which is designed to be used as a desiccant. This data was then used to create an adsorption isotherm curve of the raw data. Then the raw data was converted to units which the computational model could use (Figure 3.18).

Finally, a number of best fit curves were tried using matlab. In the end, the best fit for water on nonindicating silica gel, in the correct units for the mass transport only model was found to be:

$$c_{pi} = \frac{17.9 \cdot c_i^{2.4}}{0.155 + c_i^{2.4}} \tag{3.25}$$

where $c_p i$ is the concentration of water on silica gel ($\text{mol}\,\text{kg}^{-1}$) and c_i is the concentration of

(a) place silica gel in bubbler system

(b) leave in glass container then measure humidity

(c) place sample in moisture analyzer
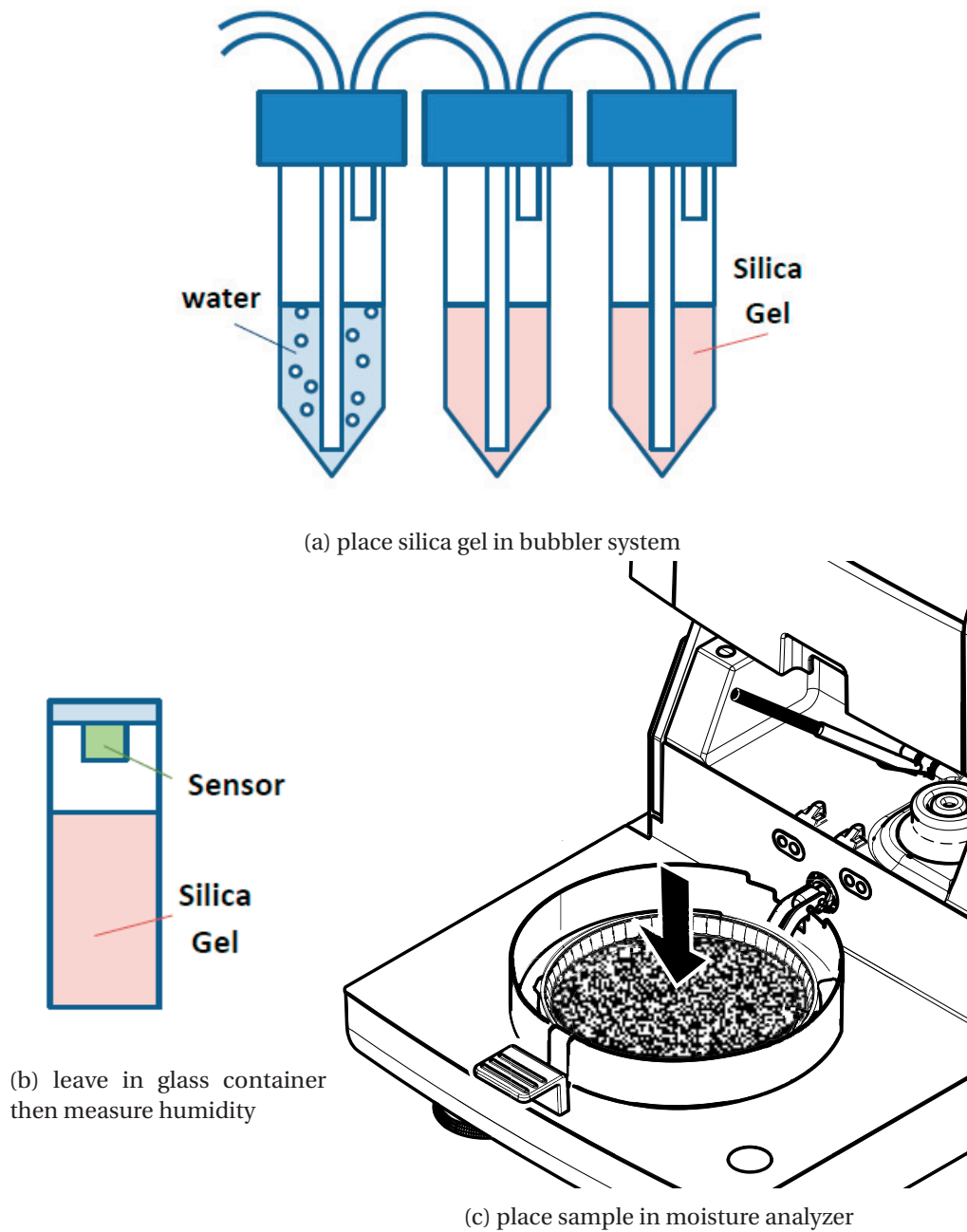
Figure 3.16 – Overview of experimental setup for determining the adsorption isotherm for water on silica gel. First, dry silica gel is placed in containers and humid air is run through them to create samples with various amounts of adsorbed water. The samples are then left for a few days and gently mixed to ensure uniform samples. The samples are then moved to a sealed container with a temperature and humidity sensor. After equilibrium is reached, the sample is placed in the drying unit.
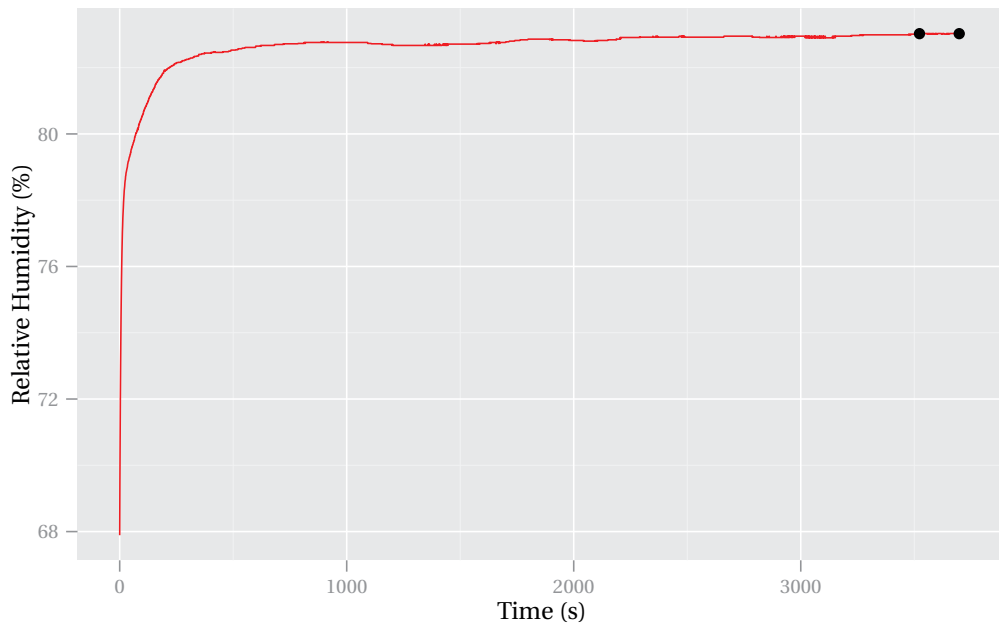
(a) Measurement taken while silica gel sample reaches equilibrium with the humidity sensor.
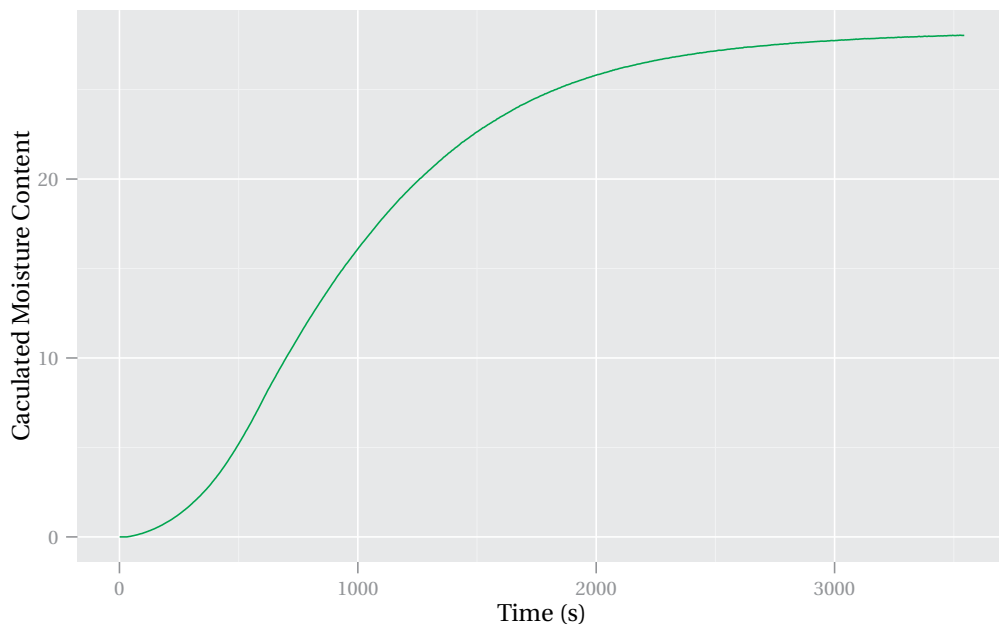
(b) Measurement taken during one run with the moisture analyzer.

Figure 3.17 – Above is a raw set of data which was used to find a point on the isotherm curve. The red lines, which show the sensor reaching equilibrium with the sample, are from step b in Figure 3.16b. The two points on this curve represent the beginning and end of the sample points which were used to find the average relative humidity of the sample. The green curve is the moisture content change as a function of time in seconds. It is found at step c in Figure 3.16c, using the program in Table 3.4. In this graph the moisture content is taken to be the last value on the curve.

METTLER TOLEDO Halogen Moisture Analyzer	
Type H204	
SNR(Drying Unit)	
SNR(Terminal)	
SW(Drying Unit) 1.1	
SW(Terminal) 1.2	
Method Name	SILICA WATER STUDY
Drying Program	Gentle
Drying Temp	105 °C
Ramp Time	10:00 min
Switch Off	$\frac{1}{140}$ mg s^{-1}
Display Mode	%MC
Start Weight	5.000 g
Start Weight Tolerance	10%
Weigh-in Aid	Active
Control Limits	OFF
Resolution	High
Start Mode	Manual
Preheating	Manual
Temperature	40 °C

Table 3.4 – Moisture analyzer product information and settings used to find the isotherm for water.

water in air ($mol\,m^{-3}$). This curve can be seen in Figure 3.19a.

For the heat and mass transport model the equation was:

$$W = \frac{0.46 \cdot RH^{2.4}}{0.12 + RH^{2.4}} \tag{3.26}$$

Where W is the $kgSiO_2/kgSiO_2$ and RH is the relative humidity of the air in the system. It is shown in Figure 3.19b. The best fit curve for rubingel was also found, but was not used in further studies because the isotherms were similar and it was unclear if the indicator in rubingel could react with analytes.

Mass Transport Only Model

Using these isotherms, computational models of the system could be made. The first model focuses on mass transport, and neglects the heat of adsorption. This method is commonly used in liquid chromatography applications [Guiochon and Lin, 2003; DeVault, 1943; COMSOL].
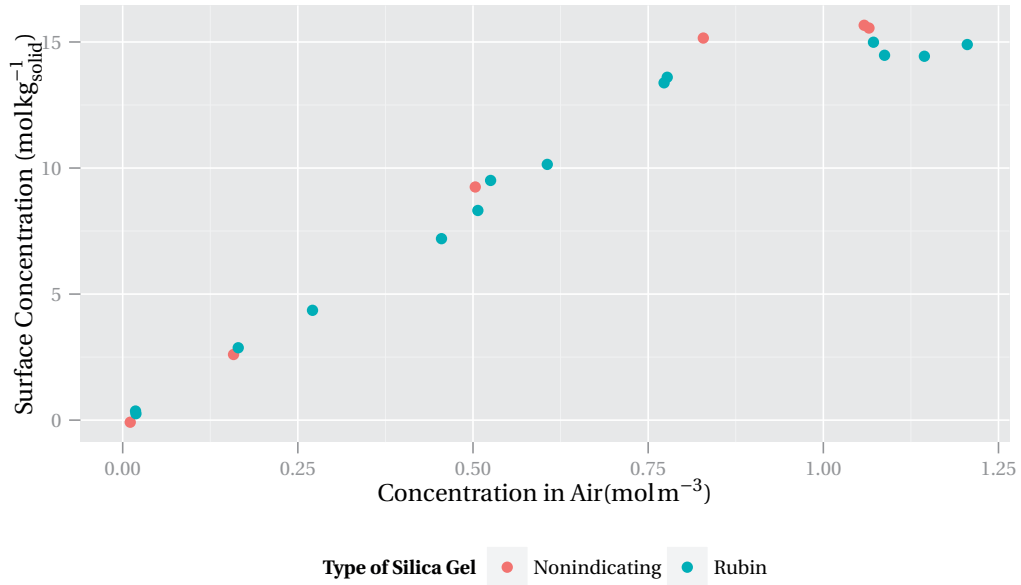
Figure 3.18 – Adsorption isotherm curves for water on nonindicating silica gel and rubingel (silica gel with an indicator).

The general equation for transport of a liquid through a stationary porous media which contains immobile gas bubbles is:

$$\frac{\partial(\theta c_i)}{\partial t} + \frac{\partial(\rho_b c_{Pi})}{\partial t} + \frac{\partial(a_v c_{G,i})}{\partial t} + \nabla(c_i u) = \nabla \cdot [(D_{D,i} + D_{e,i})\nabla c_i]) + R_i + S_i \tag{3.27}$$

Where θ is the liquid volume fraction, c_i is the concentration of species i in the mobile phase, ρ_b is the bulk density of the immobile solid, c_{Pi} is the amount of adsorbed species i, a_v is the gas volume fraction, c_{Gi} is the concentration of species i in the immobile gas phase, **u** is the velocity vector for the entire liquid phase, $D_{D,I}$ is dispersion, $D_{e,i}$ is diffusion, R_i accounts for species generation due to reaction and S_i accounts for species being added from a source.

This equation can be simplified by assuming that there are no trapped gas bubbles (i.e. a condition also known as saturated). In this case the liquid volume fraction (θ) is equal to the porosity (ϵ) and the gas terms can be removed. The resulting equation becomes:

$$\frac{\partial(\epsilon c_i)}{\partial t} + \frac{\partial(\rho_b c_{Pi})}{\partial t} + \nabla(c_i u) = \nabla \cdot [(D_{D,i} + D_{e,i})\nabla c_i]) + R_i + S_i \tag{3.28}$$

The second term in this equation can then be expanded using the following relations:

$$\rho_b = \rho_P(1 - \epsilon) \tag{3.29}$$

69
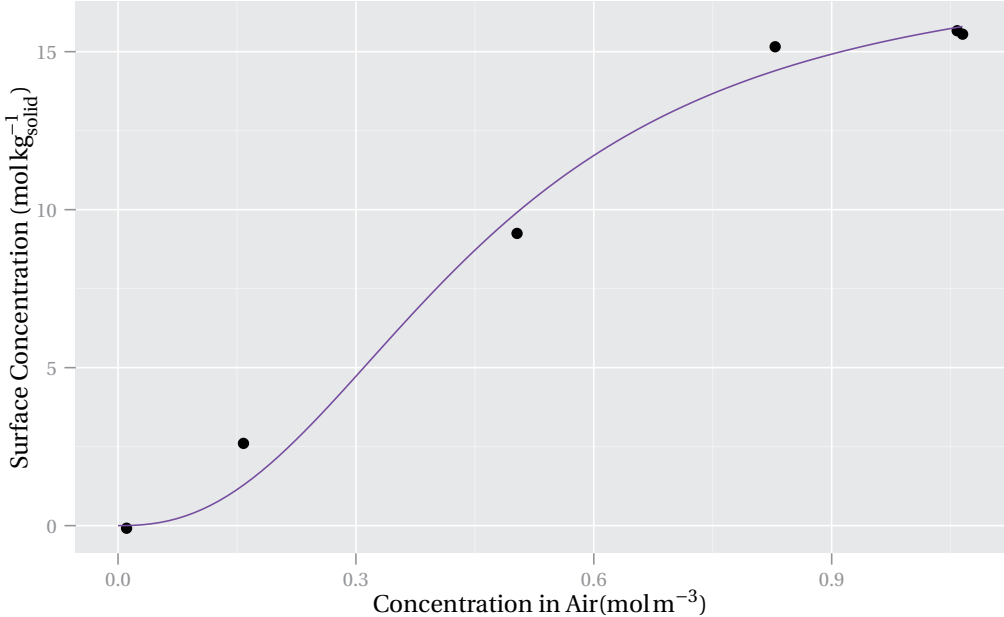
(a) Isotherm used in the Mass Transport Only Model.
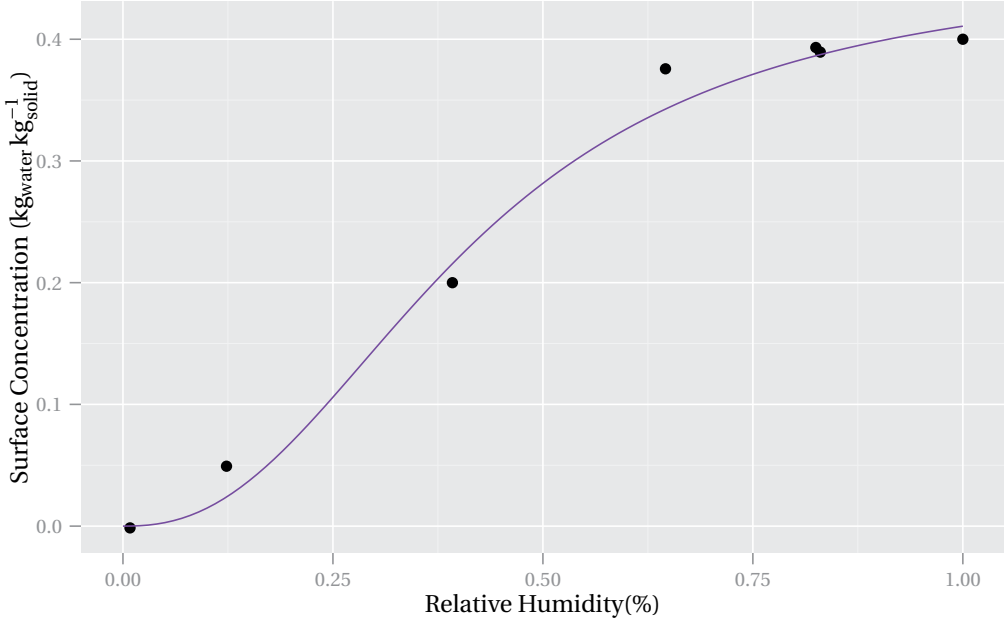
(b) Isotherm used in the Heat and Mass Transport Model.

Figure 3.19 – Isotherms for water used in computational models. Note: the graphs look the same, but the scales and units are different.

Where ρ_p is the solid phase density and

$$\frac{\partial c_{Pi}}{\partial t} = \frac{\partial c_{Pi}}{\partial c_i}\frac{\partial c_i}{\partial t} = k_{P,i}\frac{\partial c_i}{\partial t} \tag{3.30}$$

Where $k_{P,i}$ is the adsorption isotherm. Expansion of the time derivatives gives

$$\frac{\partial(\epsilon c_i)}{\partial t} = c_i\frac{\partial \epsilon}{\partial t} + \epsilon\frac{\partial c_i}{\partial t} \tag{3.31}$$

$$\begin{aligned}\frac{\partial(\rho_b c_{Pi})}{\partial t} &= c_{Pi}\frac{\partial \rho_b}{\partial t} + \rho_b\frac{\partial c_{Pi}}{\partial t}\\ &= c_{Pi}\frac{\partial(\rho_p(1-\epsilon))}{\partial t} + \rho_b k_{P,i}\frac{\partial c_i}{\partial t}\\ &= \rho_b k_{P,i}\frac{\partial c_{Pi}}{\partial t} - c_i\rho_p\frac{\partial \epsilon}{\partial t}\end{aligned} \tag{3.32}$$

Finally, the effective diffusion constant for transport in porous media is

$$D_e = \frac{\epsilon}{\tau_F}D_F \tag{3.33}$$

Where τ_F is the tortuosity factor which accounts for impedance in Brownian motion due to the solid particles and D_F is the diffusion coefficient of the species in the mobile phase.

Applying the Millington quark model, where $\tau_F = \epsilon^{-1/3}$, the diffusion term becomes:

$$D_e = \frac{\epsilon}{\tau_F}D_F = \epsilon^{4/3}D_F \tag{3.34}$$

Additionally, the dispersivity equation for transport through porous beads is:

$$D_D = 2.5ud \tag{3.35}$$

where u is the velocity of the mobile phase and d is the diameter of the adsorbent particles.

Therefore the general equation can be rewritten:

$$(\epsilon + \rho_b k_{P,i})\frac{\partial c_i}{\partial t} + (c_i - c_{Pi}\rho_P)\frac{\partial \epsilon}{\partial t} + \nabla(c_i u) = \nabla\cdot[(2.5ud + \epsilon^{4/3}D_F)\nabla c_i] + R_i + S_i \tag{3.36}$$

The above equation can be further simplified for a mixture of gases going through a silica gel bed. In this case there is no reaction (just adsorption and desorption) and there is no internal source so the generation terms can be neglected (Ri and S_i). Additionally, assuming that the solid phase allows flow in the system to be considered uniform along the width of the column, a 1D model of the system can be generated. The equation for a given species in the system

then becomes:

$$(\epsilon + \rho_b k_{P,i})\frac{\partial c_i}{\partial t} + (c_i - c_{Pi}\rho_P)\frac{\partial \epsilon}{\partial t} + u\frac{\partial c_i}{\partial x} = \frac{\partial}{\partial x}\left((2.5ud + \epsilon^{4/3}D_F)\frac{\partial c_i}{\partial x}\right) \tag{3.37}$$

This expands to:

$$(\epsilon + \rho_b k_{P,i})\frac{\partial c_i}{\partial t} + (c_i - c_{Pi}\rho_P)\frac{\partial \epsilon}{\partial t} + u\frac{\partial c_i}{\partial x} = \frac{\partial}{\partial x}\left((2.5ud)\frac{\partial c_i}{\partial x} + (\epsilon^{4/3}D_F)\frac{\partial c_i}{\partial x}\right) \tag{3.38}$$

And then by the product rule to:

$$(\epsilon + \rho_b k_{P,i})\frac{\partial c_i}{\partial t} + (c_i - c_{Pi}\rho_P)\frac{\partial \epsilon}{\partial t} + u\frac{\partial c_i}{\partial x}$$
$$= \frac{\partial(2.5ud)}{\partial x}\frac{\partial c_i}{\partial x} + (2.5ud)\frac{\partial^2 c_i}{\partial x^2} + \frac{\partial(\epsilon^{4/3}D_F)}{\partial x}\frac{\partial c_i}{\partial x} + (\epsilon^{4/3}D_F)\frac{\partial^2 c_i}{\partial x^2} \tag{3.39}$$

Because the velocity of the fluid phase, the particle diameter, the volume fraction and the effective diffusion coefficient for a gas in another gas (i.e. benzene in air) are independent from location in the length of the column, their values are constants in the x direction and their derivatives in the x direction are zero. This causes their terms to drop out, which yields the simplified equation:

$$(\epsilon + \rho_b k_{P,i})\frac{\partial c_i}{\partial t} + (c_i - c_{Pi}\rho_P)\frac{\partial \epsilon}{\partial t} + u\frac{\partial c_i}{\partial x} = (2.5ud + \epsilon^{4/3}D_F)\frac{\partial^2 c_i}{\partial x^2} \tag{3.40}$$

This gives us a simplified version of the right side of the equation. The next step is to find a relationship between the amount of analyte on the surface of the adsorbent and the amount in the gas. Assuming that adsorption is so fast that its time scale is negligible—which is generally true for physical adsorption of gases onto solid surfaces—an adsorption isotherm curve can be used. Doing this adds the assumption that local equilibrium between the concentrations of analyte in the gas and on the surface of the adsorbent is instantaneous.

The adsorption of many chemical species onto silica gel can be described by the Langmuir equation. Therefore the following relations can be applied:

$$c_{Pi} = \frac{K_{Li}c_{Pi,max}c_i}{1 + K_{Li}c_1} \tag{3.41}$$

$$k_{Pi} = \frac{\partial c_{pi}}{\partial c_i} = \frac{K_{Li}c_{Pi,max}}{(1 + K_{Li}c_i)^2} \tag{3.42}$$

where K_{Li} is the Langmuir constant for species i on the solid of interest and $c_{Pi,max}$ is the maximum amount of species i which can be adsorbed onto a given mass of solid (it is also equal to the monolayer capacity n times the particle specific surface area). Substituting these

relations into equation 3.40 yields:

$$(\epsilon + \rho_b \frac{K_{Li} c_{Pi,max}}{(1 + K_{Li} c_1)^2}) \frac{\partial c_i}{\partial t} + (c_i - \frac{K_{Li} c_{Pi,max} c_i}{1 + K_{Li} c_1} \rho_P) \frac{\partial \epsilon}{\partial t} + u \frac{\partial c_i}{\partial x} = (2.5 u d + \epsilon^{4/3} D_F) \frac{\partial^2 c_i}{\partial x^2} \quad (3.43)$$

Similarly, in the case where the Hill Equation approximates the isotherm equation better than the Langmuir equation the following relations can be used for $k_p i$ and $c_p i$:

$$c_{Pi} = \frac{Q_{sh} c_i^n}{K_d + c_i^n} \quad (3.44)$$

$$k_{Pi} = \frac{\partial c_{pi}}{\partial ci} = \frac{K_d n Q_{sh} c_i^{n-1}}{(K_d + c_i^n)^2} \quad (3.45)$$

giving the following variant of equation 3.40

$$(\epsilon + \rho_b \frac{K_d n Q_{sh} c_i^{n-1}}{(K_d + c_i^n)^2}) \frac{\partial c_i}{\partial t} + (c_i - \frac{Q_{sh} c_i^n}{K_d + c_i^n} \rho_P) \frac{\partial \epsilon}{\partial t} + u \frac{\partial c_i}{\partial x} = (2.5 u d + \epsilon^{4/3} D_F) \frac{\partial^2 c_i}{\partial x^2} \quad (3.46)$$

Lastly, sometimes polynomials are used instead of models based on the chemistry of the system. Using a best fit polynomial results in the following relations:

$$c_{Pi} = p_1 c_i^4 + p_2 c_i^3 + p_3 c_i^2 + p_4 c_i + p_5 \quad (3.47)$$

$$k_{P,i} = \frac{\partial c_{pi}}{\partial ci} = 4 p_1 c_i^3 + 3 p_2 c_i^2 + 2 p_3 c_i + p_4 \quad (3.48)$$

Giving the following form to equation 3.40

$$(\epsilon + \rho_b (4 p_1 c_i^3 + 3 p_2 c_i^2 + 2 p_3 c_i + p_4)) \frac{\partial c_i}{\partial t} + (c_i - (p_1 c_i^4 + p_2 c_i^3 + p_3 c_i^2 + p_4 c_i + p_5) \rho_P) \frac{\partial \epsilon}{\partial t} + u \frac{\partial c_i}{\partial x}$$
$$= (2.5 u d + \epsilon^{4/3} D_F) \frac{\partial^2 c_i}{\partial x^2} \quad (3.49)$$

Isotherm Equations and Variable Values In order to use the mathematical equations above to create a model of the system, parameter values for the isotherm adsorption curves in Section 3.3.1 summarized in Table 3.5 must be incorporated into the model. The resulting equations become:

Variable	Value	Source
$n_{\mathrm{H_2O}}$	2.4	Experimentally determined
$Q_{\mathrm{H_2O}}$	$17.9\,\mathrm{mol\,kg^{-1}}$	Experimentally determined
$K_{\mathrm{H_2O}}$	$0.155\,\mathrm{mol^2\,m^{-6}}$	Experimentally determined
$c_{p,\mathrm{CO},max}$	$0.7437\,\mathrm{mol\,kg}$	Best fit curve of literature data
$k_{p,\mathrm{CO}}$	$0.004\,312\,\mathrm{m^3\,mol^{-1}}$	Best fit curve of literature data
$c_{p,\mathrm{C_6H_6},max}$	$1.755\,\mathrm{mol\,kg^{-1}}$	Best fit curve of literature data
$k_{p,\mathrm{C_6H_6}}$	$0.9168\,\mathrm{m^3\,mol^{-1}}$	Best fit curve of literature data
$c_{p,\mathrm{NO_2}\,max}$	$54.8\,\mathrm{mol\,kg^{-1}}$	Best fit curve of literature data
$k_{p,\mathrm{NO_2}}$	$0.046\,99\,\mathrm{m^3\,mol^{-1}}$	Best fit curve of literature data

Table 3.5 – Isotherm values used in the mass transport only model.

For water:

$$(\epsilon + \rho_b \frac{.155 \cdot 2.4 \cdot 17.9 \cdot c_i^{1.4}}{(.155 + c_i^{2.4})^2}) \frac{\partial c_i}{\partial t} + (c_i - \frac{17.9 \cdot c_i^{2.4}}{.155 + c_i^{2.4}} \rho_P) \frac{\partial \epsilon}{\partial t} + u \frac{\partial c_i}{\partial x}$$
$$= (2.5ud + \epsilon^{4/3} D_F) \frac{\partial^2 c_i}{\partial x^2} \quad (3.50)$$

For benzene:

$$(\epsilon + \rho_b \frac{0.92 \cdot 1.8}{(1 + 0.92 \cdot c_i)^2}) \frac{\partial c_i}{\partial t} + (c_i - \frac{0.92 \cdot 1.8 \cdot c_i}{1 + 0.92 \cdot c_i} \rho_P) \frac{\partial \epsilon}{\partial t} + u \frac{\partial c_i}{\partial x}$$
$$= (2.5ud + \epsilon^{4/3} D_F) \frac{\partial^2 c_i}{\partial x^2} \quad (3.51)$$

For carbon monoxide:

$$(\epsilon + \rho_b \frac{0.0043 \cdot 0.74}{(1 + 0.043 \cdot c_i)^2}) \frac{\partial c_i}{\partial t} + (c_i - \frac{0.043 \cdot 0.74 \cdot c_i}{1 + 0.043 \cdot c_i} \rho_P) \frac{\partial \epsilon}{\partial t} + u \frac{\partial c_i}{\partial x}$$
$$= (2.5ud + \epsilon^{4/3} D_F) \frac{\partial^2 c_i}{\partial x^2} \quad (3.52)$$

For nitrogen dioxide:

$$(\epsilon + \rho_b \frac{0.047 \cdot 55}{(1 + 0.047 \cdot c_i)^2}) \frac{\partial c_i}{\partial t} + (c_i - \frac{0.047 \cdot 55 \cdot c_i}{1 + 0.047 \cdot c_i} \rho_P) \frac{\partial \epsilon}{\partial t} + u \frac{\partial c_i}{\partial x}$$
$$= (2.5ud + \epsilon^{4/3} D_F) \frac{\partial^2 c_i}{\partial x^2} \quad (3.53)$$

These are put into the equations along with the other system specific parameter values in Table 3.6 to create a system of equations which can be solved using software such as Comsol.

The model was solved using the mean inlet sensor values from the calibrated experiments

Variable	Value	Source
Inlet velocity (u)	$0.034213\,\mathrm{m\,s^{-1}}$	Parameter
Solid Material Density (ρ)	$662.5\,\mathrm{kg\,m^{-3}}$	Measured
Fraction of column volume which is air (ϵ)	.5	Measured
Diffusion coefficient of H_2O in air ($D_{eff,H_{20}}$)	$2.82 \times 10^{-5}\,\mathrm{m^2\,s^{-1}}$	[Cussler, 1997]
Diffusion coefficient of CO in air ($D_{eff,CO}$)	$1.925 \times 10^{-5}\,\mathrm{m^2\,s^{-1}}$	[Yaws, 2009]
Diffusion coefficient of C_6H_6 in air (D_{eff,C_6H_6})	$9.35 \times 10^{-6}\,\mathrm{m^2\,s^{-1}}$	[Yaws, 2009]
Diffusion coefficient of NO_2 in air (D_{eff,NO_2})	$1.56 \times 10^{-5}\,\mathrm{m^2\,s^{-1}}$	[Yaws, 2009]
Bead Diameter (d)	3.5 mm	Data Sheet
Length of the column (L)	6.5 mm	Measured

Table 3.6 – Simulation variables used in the mass transport only model.
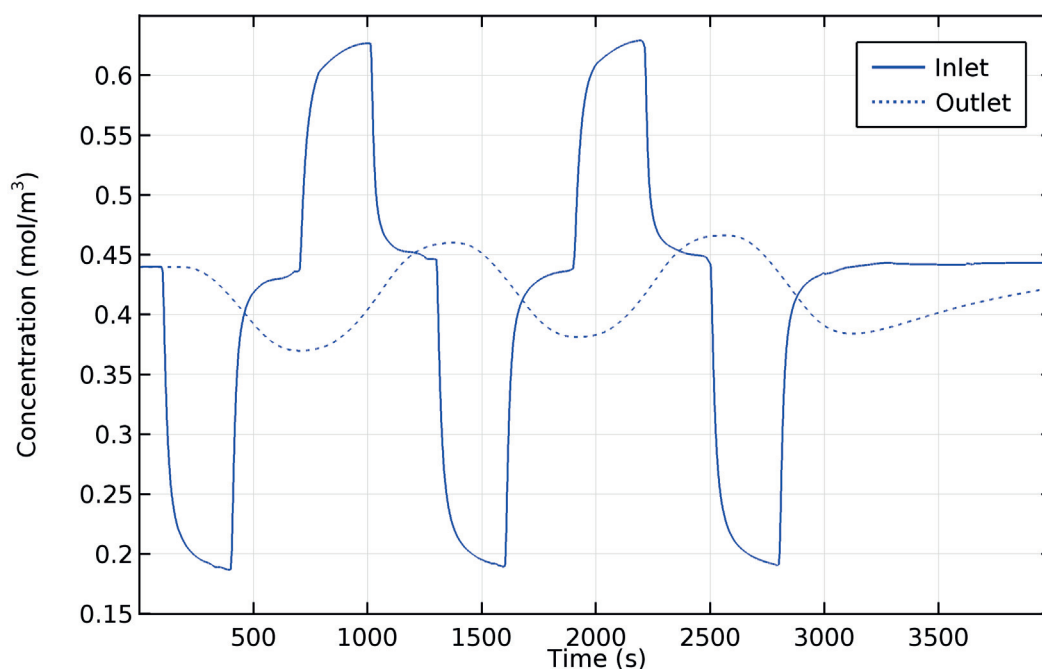
Figure 3.20 – Results of water adsorption model.

as the inlet boundary condition. This makes it possible to compare the experimental output values of the model to the experimentally measured values. For the same reason, the length of the column was taken from the experimental system. However, this length is only a rough estimate because the length of the column is very short and bead packing is not uniform. Therefore, a few different lengths were used in the computational model. The results for water and target gases are in Figures 3.20 and 3.21, respectively. These results were then plotted alongside the experimental results to give the following curves for water (Figure 3.25) and gases (Figures 3.23, 3.24 and 3.22).

Overall, the models for toxic gases fit the data well. In the carbon monoxide simulation the
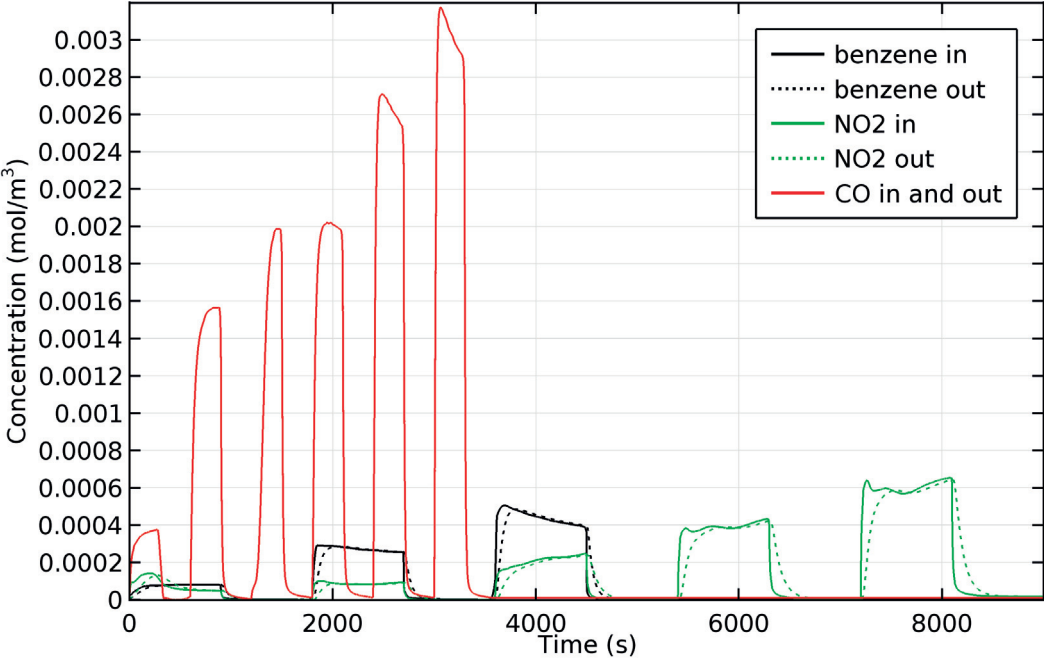
Figure 3.21 – Results of toxic gas adsorption models.
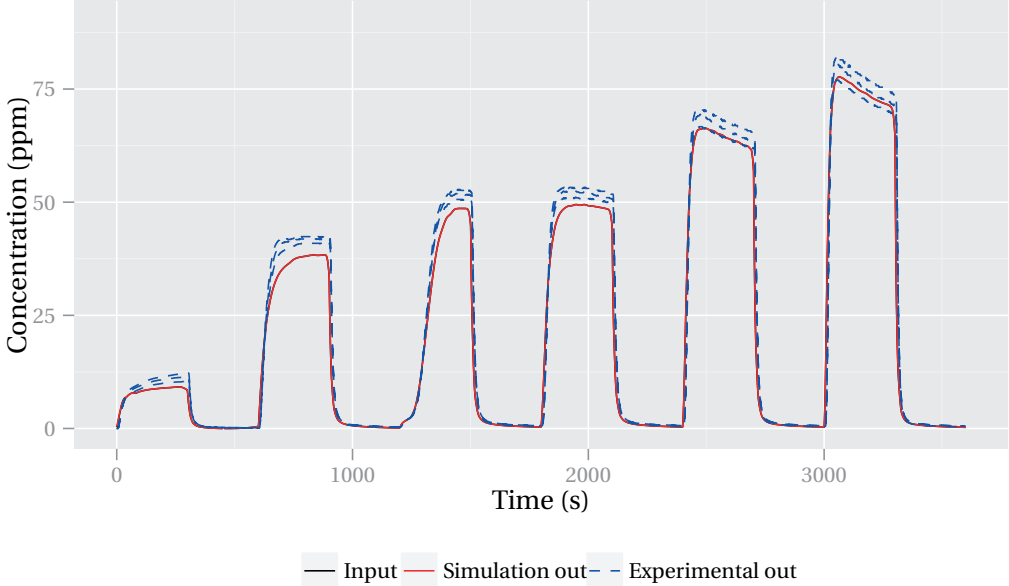
Figure 3.22 – Comparison of simulated and experimental values for carbon monoxide (CO). Note: the black inlet curve is difficult to see because it is almost identical to the red simulation curve.
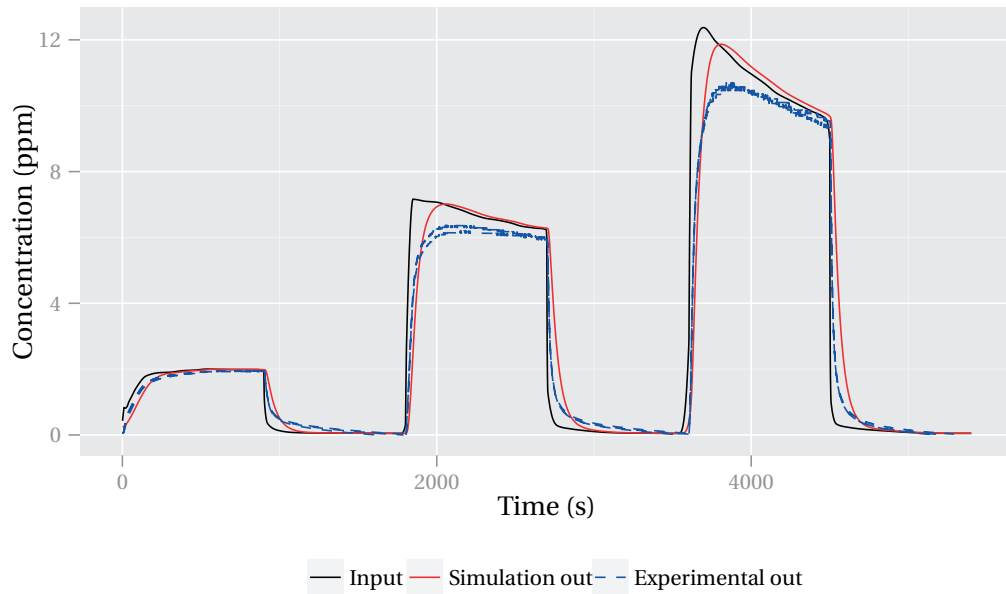
Figure 3.23 – Comparison of simulated and experimental values for benzene (C_6H_6).
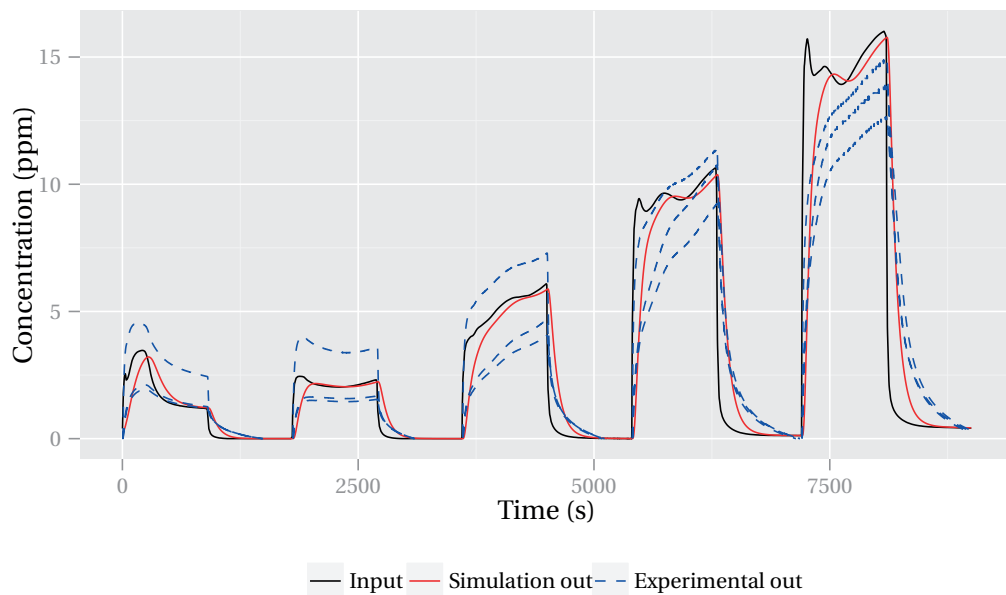
Figure 3.24 – Comparison of simulated and experimental values for nitrogen dioxide (NO_2).

inlet and outlet values of the computational model are so similar that the black inlet line is obscured by the red outlet line. This red outlet value reaches approximately the same peak heights as the blue outlet sensor data, however it is slightly lower. This was also true in the experimental data: during experiments the inlet sensors had slightly lower values than the outlet sensors after calibration. Baseline recovery is the same for both the computational model and the experiments.

Simulation results for benzene show delays in sensor response and base line recovery, which are mirrored in the experimental data. However, there are slight differences. Initially, experimental data responds to either toxic gas or clean air more rapidly than the simulation. Then, after a few seconds the response of the simulation overtakes the experimental values. This discrepancy is negligible for our purposes. The peak heights are also different. However, this is likely a result of the sensors themselves. Specifically, the inlet sensors always show a much more dramatic overshoot than the outlet sensors, even during the experiments without silica gel. Therefore, this overshoot is probably a function of the sensor data which is used as the model inlet value, and not the computational model itself.

The simulation for nitrogen dioxide is also a good fit. Peak heights and sensor responses are similar to experimental data. The only notable difference is the recovery time. The first 90% is similar for the model and experiments. However, the last 10% takes much longer for the experiments. This is at least partly due to the slow baseline recovery for the outlet side sensors because it is present for both experiments with and without silica gel.

Although this modeling technique provides satisfactory results for toxic gases, it is a poor fit for water. The results of the water simulation give outlet humidity fluctuations whose amplitude and frequency compare well with experimental results (Figure 3.25). However, there are two notable differences. First, the outlet curve of the experimental system is less smooth than the corresponding simulated system. Second, the outlet of the experimental system responds immediately to changes in inlet humidity, whereas the simulated system has a delay. To explain this, two adsorbent packing problems were considered. First, a bypass, which could be the result of gas passing through the system without coming into close enough contact with the adsorbent to reach equilibrium, was considered. Second, a column with more than one length was investigated. Either of these could be a potential problem because the length of the column is shorter than its width.

To create the bypass model, a simulation was run where the silica gel was treated as non-adsorbing. The results of this simulation were then combined in various proportions with the simulation from Figure 3.25. The results for 0, 5 and 10 percent of the gas bypassing the silica gel can be seen in Figure 3.26. From these results, it is clear that although the presence of a bypass causes an almost immediate change in outlet humidity when the inlet humidity is changed, it does not cause the smooth transitions which appear in the experimental data. Therefore, the variable column length model was considered.

To generate the variable column length model, the length of the column was changed from
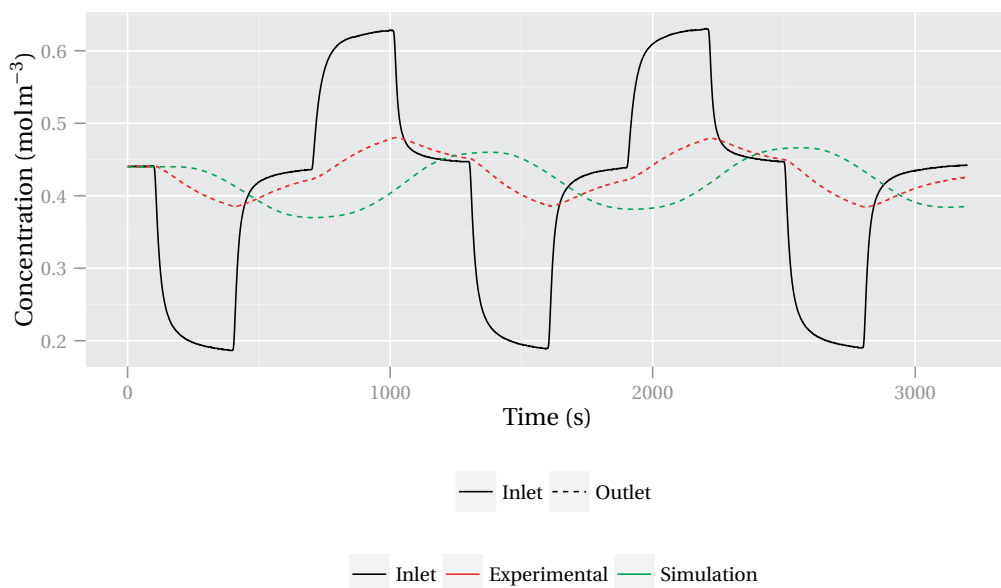
Figure 3.25 – Comparison of experiments and simulation for water, showing that the model alone gives a poor fit.
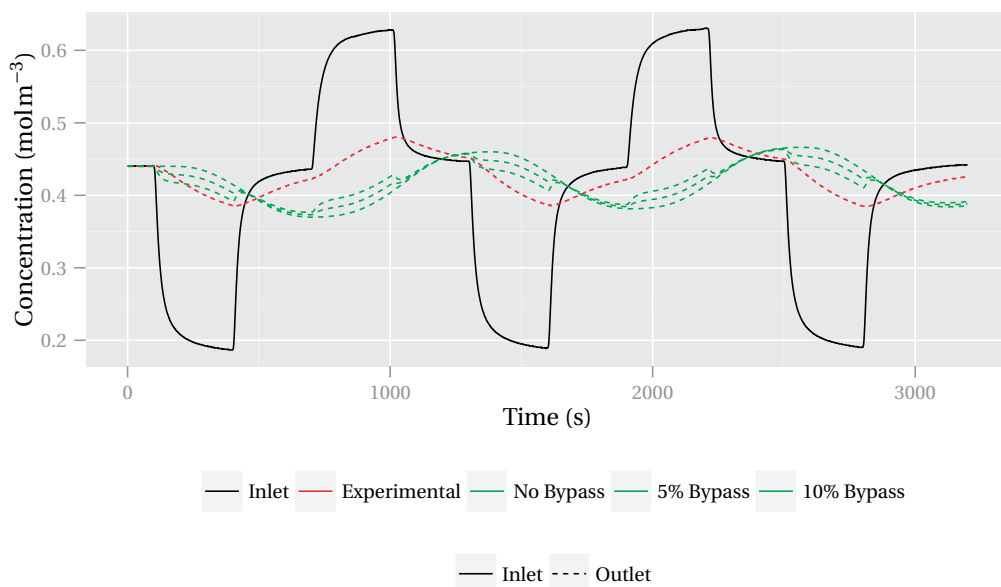
Figure 3.26 – Comparison of experiments and simulation for water including a small bypass which causes a portion of the gas to not be in contact with silica gel. This could occur if the space between the beads is large.
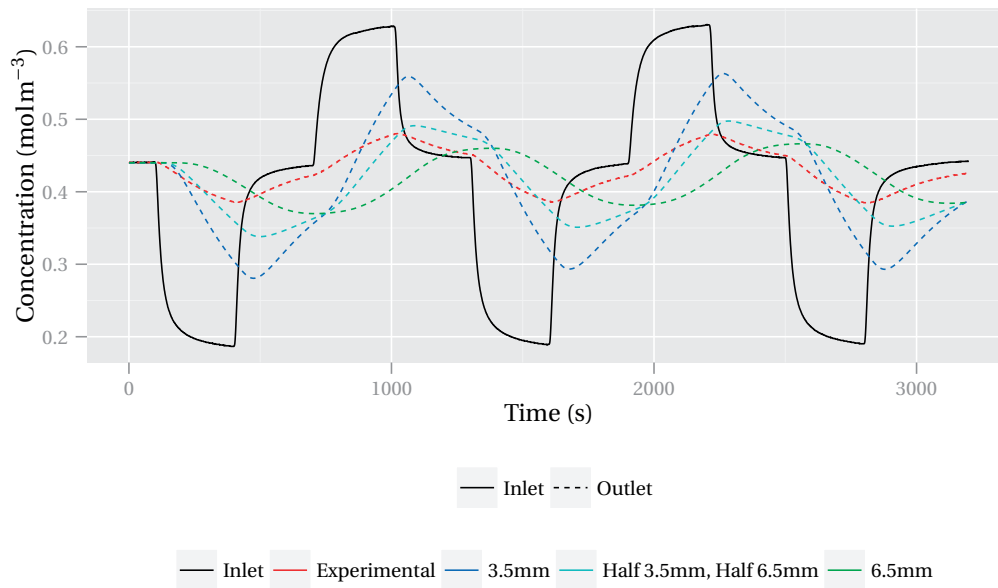
Figure 3.27 – Comparison of experiments and simulations for water including mixed heights in the packed bed. This can occur if the bed is not ideally packed.
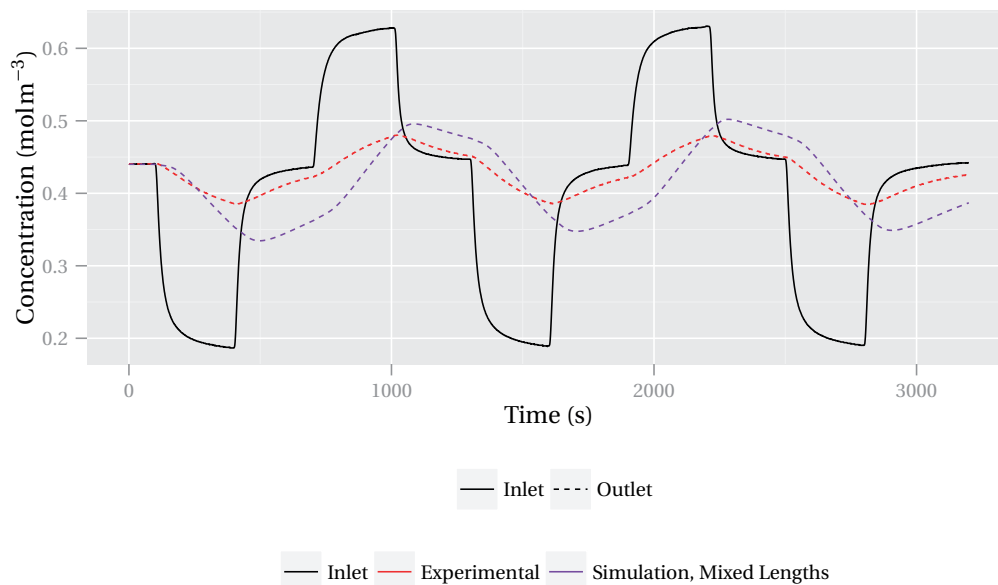
Figure 3.28 – Comparison of experiments and an example simulation for water including a small bypass and non-ideal bed packing. Ultimately, the poor agreement between the experiment and simulation shows that bed packing is not the problem with the model.

6.5 mm to 5.5 mm, 4.5 mm and 3.5 mm and the simulation was rerun. The results of these four simulations were then recombined in various proportions. An example of these results can be seen in Figure 3.27. These results indicated that incorporating short column lengths gives rise to abrupt transitions, similar to those in the experimental data.

In the last set of models all three previously described models were combined in varying proportions (Figure 3.28). The result is a model which shows abrupt changes in outlet humidity concentration when the inlet humidity is changed and jagged transitions which are characteristic of the experimental data. However, these results still did not satisfactorily reproduce the data. Therefore, models used to describe desiccant dryers were investigated.

3.3.2 Heat and Mass Transport Model

The above model works well when thermodynamics do not need to be considered. However, when sorption is sufficient to cause a temperature change in the system, the above model no longer holds because the adsorptive capacity of both silica gel and air change as a function of temperature. This is the case with water. Therefore, when modeling water sorption, the thermodynamics of the system must be considered. The easiest way to do this is using the following set of coupled equations developed to describe both adsorption and desorption in desiccant dryers. Detailed information on model derivation ([Pesaran and Mills, 1987b]), experimental validation([Pesaran and Mills, 1987a]) and implementation ([Jain et al., 2013; Bau et al., 2014; Pesaran, 1983]) can be found in the literature. It is composed of five main equations, whose terms are defined in Table 3.7.

Species conservation in the gas phase:

$$\dot{m}_G \frac{\partial m_{l,e}}{\partial z} = K_{G,eff}(m_{l,s} - m_{l,e})p \tag{3.54}$$

Species conservation in the solid phase:

$$A\rho_b \frac{\partial W_{ave}}{\partial t} = -K_{G,eff}(m_{l,s} - m_{l,e})p \tag{3.55}$$

An equilibrium relation which relates the mass of water at the surface of the silica gel to the mass in air:

$$m_{l,s} = \frac{0.622 P_{water}}{P_{dry\,air} + 0.622 P_{water}} = \frac{0.622 \cdot RH \cdot P_{sat}(T)}{P_{total} + 0.378 \cdot RH \cdot P_{sat}(T)} \tag{3.56}$$

where the .622 value is the molar mass of water divided by the molar mass of dry air and $RH \cdot P_{sat}(T)$ gives the partial pressure of water in humid air. Energy conservation in the solid phase, written in temperature terms:

$$A\rho_b c_{solid} \frac{\partial T_s}{\partial t} = p[h_c(T_e - T_s) - H_{ads}K_{G,eff}(m_{l,s} - m_{l,e})] \tag{3.57}$$

Term	Definition	Further Information
A	Cross-sectional area	$\sqrt{3} \cdot \frac{1}{2} L_s^2 \, \text{m}^2$
$c_{dry\,air}$	Specific heat of dry air	$1005 \, \text{J}\,\text{kg}^{-1}\,\text{K}^{-1}$
c_{gas}	Specific heat of gas mixture	(eq: 3.61)
$c_{H_2O,gas}$	Specific heat of gaseous air	$1884 \, \text{J}\,\text{kg}^{-1}\,\text{K}^{-1}$
c_{SiO_2}	Specific heat of silica gel	$921 \, \text{J}\,\text{kg}^{-1}\,\text{K}^{-1}$
c_{solid}	Specific heat of the immobile phase	(eq: 3.62)
h_c	Convective heat transfer coefficient	(eq: 3.64)
H_{ads}	Heat of adsorption	(eq: 3.67)
$K_{G,eff}$	Gas-side mass transfer coefficient	(eq: 3.63)
L_c	Length of the column	$6.5 \times 10^{-3} \, \text{m}$
L_s	Column side length	$30 \times 10^{-3} \, \text{m}$
$\dot{m}_G$	Mass flow rate of mixture	$\dot{V} \cdot \rho, \, 7.9 \times 10^{-6} \, \text{kg}\,\text{s}^{-1}$
$m_{l,e}$	Water vapor mass fraction in air	$\text{kg}_{H_2O}/\text{kg}_{humid\,air}$
$m_{l,s}$	Water vapor mass fraction near surface	$\text{kg}_{H_2O}/\text{kg}_{humid\,air}$
ν	Kinematic viscosity of air	$1.568 \times 10^{-5} \, \text{m}^2\,\text{s}^{-1}$
p	Perimeter of bed	$3 L_s \, \text{m}$
$P_{dry\,air}$	Partial pressure of dry air in the gas mixture	(eq: 3.56)
$P_{sat}(T)$	Saturation pressure at a given temperature	(eq: 3.59)
P_{water}	Partial pressure of water in the gas mixture	(eq: 3.56)
P_{total}	Total pressure	1.01 bar
r_p	Particle radius	$1.75 \times 10^{-3} \, \text{m}$
Re	Reynolds number	$\frac{2 r_p v_{superficial}}{\nu}$
RH	Relative Humidity	(eq: 3.66
ρ	Density of humid air	$1.18 \, \text{kg}\,\text{m}^3$
ρ_b	Bulk density of silica gel	$662.5 \, \text{kg}\,\text{m}^{-3}$
t	Time	s
T_0	Temperature of inlet gas and system at $t = 0$	296.85 K
T_e	Temperature of the gas	K
T_s	Temperature of the solid	K
$\dot{V}_g$	Volumetric flow rate of gas	$0.4 \, \text{L}\,\text{min}^{-1}, \, 6.7 \times 10^{-6} \, \text{m}^3\,\text{s}^{-1}$
$v_{superficial}$	Superficial velocity	$\frac{\dot{V}_g}{A} \, \text{m}\,\text{s}$
W_{ave}	Water content of silica gel	$\text{kg}_{H_2O}/\text{kg}_{SiO_2}$
z	Axial distance	m

Table 3.7 – Variable and parameter definitions for the heat and mass transport model. Many names are consistant with [Pesaran and Mills, 1987b] and [Pesaran and Mills, 1987a].

Energy conservation in the gas phase, written in temperature terms:

$$c_{gas}\dot{m}_G\frac{\partial T_e}{\partial z} = -p[h_c + c_{H_2O,gas}K_{G,eff}(m_{l,s} - m_{l,e})](T_e - T_s) \qquad (3.58)$$

In addition to the 5 main equations, initial conditions, boundary conditions, relationships for the specific heats, the isotherm equation, heat transfer coefficient, gas-side mass transfer coefficient and the heat of adsorption must also be known. The latter four are system specific and can be different for different types of silica gel. The equations which could be taken directly from literature are:

The Antoine equation which describes the relationship between vapor pressure and temperature ([Antoine, 1888; Bank]):

$$P_{sat}(T) = \begin{cases} 10^{8.07131 - \frac{1730.63}{233.426+T}} & 0 < T \le 100 \\ 10^{8.14019 - \frac{1810.94}{244.485+T}} & 100 < T < 374 \end{cases} \qquad (3.59)$$

where $P_{sat}(T)$ is in mmHg and T is in °C.

The specific heat for gaseous water is:

$$c_{H_2O,gas} = 1884\,\mathrm{J\,kg^{-1}\,K^{-1}} \qquad (3.60)$$

The specific heat for the gas mixture at any humidity is:

$$\begin{aligned} c_{gas} &= c_{H_2O,gas}m_{l,e} + c_{dry\,air}(1 - m_{l,e}) \\ &= 1884\,\mathrm{J\,kg^{-1}\,K^{-1}} \cdot m_{l,e} + 1005\,\mathrm{J\,kg^{-1}\,K^{-1}}(1 - m_{l,e}) \end{aligned} \qquad (3.61)$$

and the specific heat for the solid phase of the system is:

$$\begin{aligned} c_{solid} &= c_{H_2O,liquid}W_{ave} + c_{SiO_2} \\ &= 4178\,\mathrm{J\,kg^{-1}\,K^{-1}} \cdot W_{ave} + 921\,\mathrm{J\,kg^{-1}\,K^{-1}} \end{aligned} \qquad (3.62)$$

The gas side mass transfer coefficient:

$$K_{G,eff} = 1.7\rho v_{superficial}Re^{-0.42}\mathrm{kg\,m^{-2}\,s^{-1}} \qquad (3.63)$$

The convective heat transfer coefficient:

$$h_c = 1.6\rho v_{superficial}Re^{-0.42}c_{gas}\mathrm{W\,m^{-2}\,K^{-1}} \qquad (3.64)$$

The other equations needed to be changed to fit this specific system. The measured isotherm equation in the correct units for this system is:

$$W = \frac{0.46 \cdot RH^{2.4}}{0.12 + RH^{2.4}} \qquad (3.65)$$

which is rearranged to the form useful when solving the system of equations:

$$RH = \sqrt[2.4]{\frac{0.12 \cdot W_{ave}}{0.46 - W_{ave}}} \tag{3.66}$$

The equation for heat of adsorption must be modified to compensate for heat loss to the environment. This is not necessary in desiccant dryer models because these dryers are usually an order of magnitude larger in all dimensions. Therefore, the heat loss at the edge of the column is negligible. To quantify the heat loss to PMMA in terms of air temperature, a simple thermodynamic COMSOL simulation was conducted. The result is that the change in the temperature of the air is about 40 percent of what the desiccant dryer model predicts. Therefore, we simply multiply the published heat of adsorption by 0.4 to get:

$$H_{ads} = 0.4 \cdot (2950 - 1400 W_{ave}) \text{kJ kg}^{-1} \tag{3.67}$$

Lastly, the initial temperatures for both the surface of the silica gel and the air are set to room temperature and the initial values for water contents of the system are found using the experimental starting equilibrium humidity value. The inlet humidity concentration is continuously reevaluated at every time step to mimic the experimental values. It is then solved using the methods outlined in Pesaran's doctoral thesis [Pesaran, 1983]. Specifically, time derivatives are solved using Euler method and the length derivatives are solved using Rung-Kutta 4 method. The results of the simulation and experiments are shown in Figure 3.29.

According to the data sheet, it takes the Sensirion SHT 75 sensor 8 s to reach 63% of a humidity pulse reading, on average. It also takes up to 30 s to have a 63% temperature response. Additionally, the error is ± 1.8 percent relative humidity and ± 0.3 °C. Therefore, the sensor data should respond more slowly than the computational model, which it does.

When comparing the inlet data of the simulation–which mimics the experimental output of the mass flow controllers and not the sensor response–it is clear that the sensor responds as quickly as its data sheet suggests, until it reaches the error range. The last 2% relative humidity takes more than fifteen minutes to reach on the inlet side of the experimental system. The range of outlet humidities predicted by the simulation is about twice the error range. Therefore, the difference in humidity change delays between experiments and simulations on the outlet side are largely a function of the sensor signal delay and error, and not computational inaccuracies. The simulation results for temperature change seem to fit the model quite well: the curves have similar slopes after humidity decreases or increases and the computational model is always within the summed error range of the sensors. This demonstrates, that despite being small, the temperature changes caused by adsorption have a significant effect on humidity sorption in the preconditioning unit.
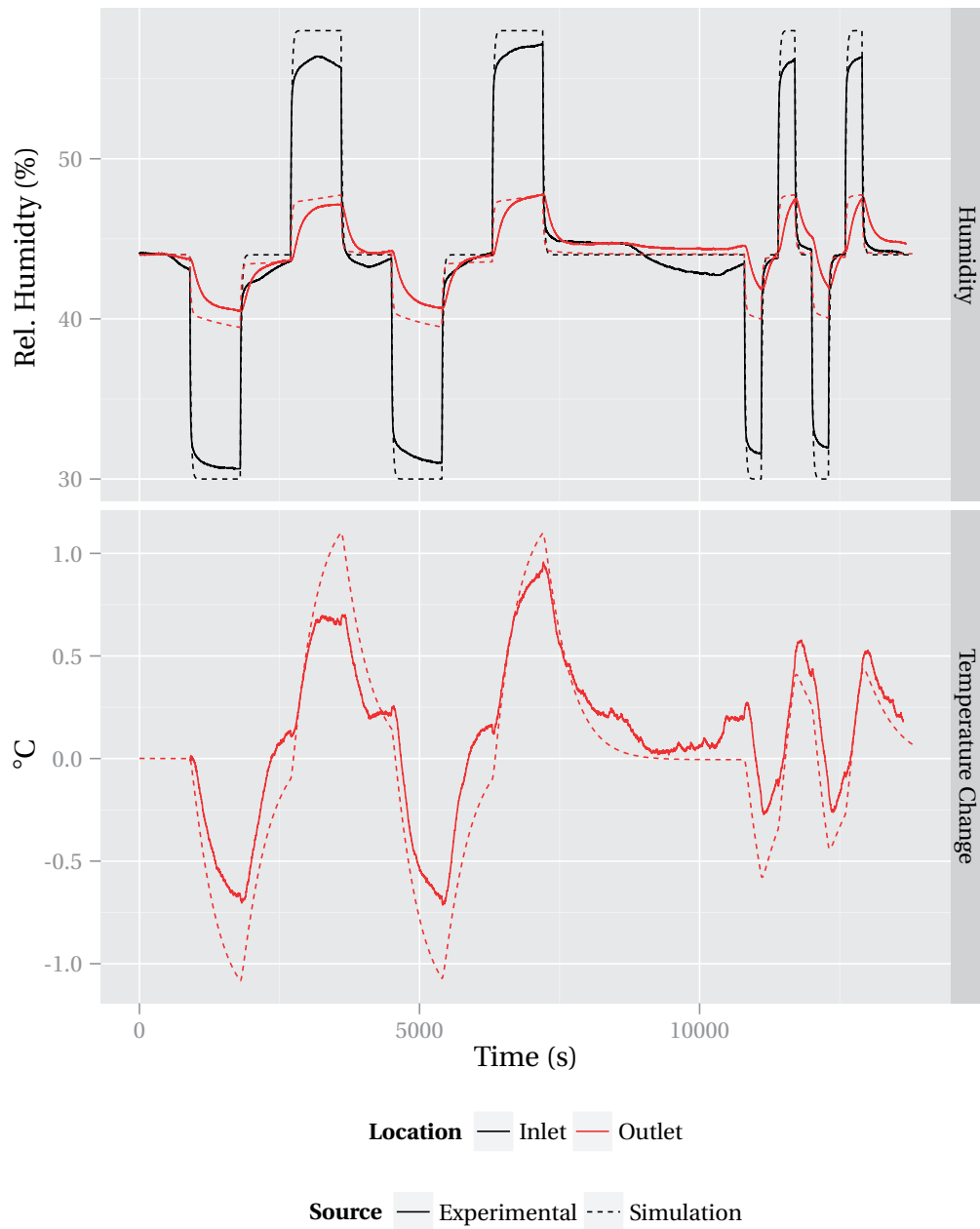
Figure 3.29 – Plot of the experimental and simulated results. In the upper image, red lines represent the outlet data. Black lines are the inlet data. For both, solid lines are experimental results and dashed lines are simulated results.

3.3.3   Conclusion

This application is quite unusual: while most gas adsorption studies focus on removing toxic gases, water or a combination of the two, this application required humidity buffering without toxic gas removal. Literature searches on optimal adsorbents therefore became a study of what was not published as much as what was. This is because negative results are rarely published. For example, even though there are many published statements indicating that silica gel and carbon were both tested for use in gas masks during World War I and II [Allen and O'Shea, 2014], scientific documents from this time period on toxic gas removal [Pearce, 1946] only cover carbon, but not silica gel. This lack of data indicated that silica gel might not sufficiently remove the toxic gases. Combining this gap in the scientific literature with the fact that silica gel is frequently used in liquid chromatography because it is relatively inert, indicated that it would minimally adsorb the toxic gases. Furthermore, its use in desiccant dryers, as well as its low regeneration temperature indicated that it would be both reversible and retain a large volume of water at room temperature.

Upon testing, this hypothesis was confirmed. Silica gel buffers humidity fluctuations while allowing the accurate measurement of toxic gases such as CO, benzene and NO_2. Adsorption of toxic gases onto silica gel can be modeled using porous media models whereas water must be modeled using a method which accounts for thermodynamics. This is because the amount of heat generated by water adsorbing onto the silica gel was large enough to change the temperature of the system, which in turn changes the saturation pressure of air and thus the local relative humidity. This has an effect on the adsorptive capacity of the silica gel. The quantities of toxic gases, on the other hand, are so small that the temperature of the system is not effected. Thus, a simpler model can be used.

These methods are well established and are commonly used to computationally model packed bed reactors, columns used in liquid chromatography, and desiccant dryer systems. However, the volume of columns and desiccant dryers is typically two orders of magnitude larger than the preconditioning unit, and are measured in liters rather than milliliters. In the laboratory packed bed reactors can be the size of a large column, but in industry they are often measured in square meters and require a ladder to fill. Thus, this is possibly the smallest silica gel column published in literature.

4 Overview of Integration and Use Outside of CSEM and EPFL

The previous work described in this thesis was exclusively the work of the author. All non-commercially available components including gaskets, milled device and PCBs etc. were designed and assembled by the author. Additionally, all components were made by the author with the exception of the PCBs, which were manufactured by EPFL. All gaskets were laser cut by the author for the single sensor platform, but a few were cut by a Stefan Berchtold, an engineer at CSEM, in the multisensor platform. Computational simulations, data analyses and chemical experiments with toxic gases were conducted solely by the author.

However, throughout this project advice and direction was given by research mentors and collaborators. This section outlines this collaborative work and incorporates other's contributions. Additionally, it showcases research and development which was conducted using the fluidic platforms described in previous sections.

4.1 Overview of the INTASENSE Project and Consortium

INTASENSE was a European Commission funded 7th Framework Project. It was composed of seven research groups from academia and industry, who came together to create an indoor air quality monitoring system. This air quality monitor was originally planned to include a small particle monitor, a large particle monitor, UV activated metal oxide sensors and thermally activated metal oxide sensors. These sensors would be housed in a single package which would communicate wirelessly with a main control system.

The major research task breakdown of each group was as follows: the particle sensors were to be designed and fabricated at the Technical University at Ilmenau in Germany, the UV activated sensors were to be designed and built by C-Tech innovation in Chester U.K. and the thermally activated sensors were created at CEIT in San Sebastian, Spain. The fluidic platform and gas preconditioning system, and commercial electronics selection were the responsibility of the author at CSEM. The wireless electronics board and user interface for the integrated system was done by Advanticsys in Madrid, Spain. Final packaging was conducted

by Gooch and Housego in Torquay, England. The packaged system was then to be tested in real world environments by UC Technologies in Amsterdam. Air quality testing using gas chromatography was conducted by the University of Lancaster.

Major leadership roles were held by C-tech, who led the entire research project, CSEM, who organized the integration of the single sensor prototype, and Gooch and Housego, who took this prototype and created a final demonstrator.

4.2   Project Planning Phase

After the grant proposal was accepted, the creation of the multisensor demonstrator occurred in three phases. First, the INTASENSE consortium met to discuss the properties and requirements of each sensor and create a list of target gases. Decisions made at this meeting were used to design a single sensor testing platform, which was the second phase. Information gathered from using the single sensor testing platform was then used to create the multisensor demonstrator in the third phase.

The project began with discussions about the electrical, preconditioning and gas delivery systems required for each air quality sensor. From this information flow diagrams were generated. It was determined that a single sensor testing platform, including an optional preconditioning unit, fluidics, commercial electronics, wireless interface and software should be created so that all three sensor designers could have a uniform testing platform. This also allowed all five groups—the 3 sensor designers (CEIT, C-tech, and the Technical University of Ilmenau), CSEM, and the electronics and software developer (Advanticsys) to work simultaneously, with minimal dependencies on each other. It was also decided that the information gathered from this single sensor testing platform, would be used to design and construct the multisensor testing platform.

An overview of the preliminary design plans are given below:

Housing/Packaging Material Requirements

- Must withstand temperatures up to 300 °C (depending on thermal isolation of CEIT sensor, or the temperature of the air out of the system).
- Must be UV light resistant while allowing UV light to reach the UV activated gas sensor.
- Components in contact with sample gas must not react with analyte or exhaust chemicals.
- Must not adversely interact with the electromagnetic field.
- Must be easily machined using a laser cutter or mill.
- Must be a low cost material.

Air Preconditioning Requirements

- Must be capable of buffering humidity and filtering air down to 10 PM and 2.5 PM.
- Must not remove chemicals of interest.
- Components must work for 1 year.
- Must provide enough air flow.
- Airflow must be continuous.
- Energy consumption must be minimized so that the whole platform can run on a battery.

Sensor Requirements

- Air into this system should be pumped at $1\,\mathrm{mL\,min^{-1}}$ to $500\,\mathrm{mL\,min^{-1}}$ and should be confirmed with a sensor and flow rates should be easily changed.
- The pump should be after the particle or gas sensor.
- Air should be supplied continuously (non-pulsing).
- Air entering the sensor should be at room temperature.
- Air exiting the sensor should not heat up other sensors.
- Humidity should be buffered before contact with the gas sensor.
- Dust larger than either 10, 2.5 or 1 PM should be removed before entry into the sensor chamber.
- There must be space for electrical connections.
- The sensor can be housed in any standard commercial gas sensor packaging.

Possible Adverse Sensor Initiated Interactions

For the integrated platform there were the following concerns:

- The housing needs to be heat resistant (possibly up to 300°C) to be compatible with the CEIT sensor and may need to thermodynamically insulate this sensor from the others. Specifically, the catalyst in the C-Tech sensor is thermodynamically activated, so measurements may be inaccurate if the CEIT sensor is improperly insulated.
- Similar to the thermodynamic isolation issue, UV light could damage other sensors. Most obviously, it could cause the CEIT sensor to give false readings, but it could also react with housing materials or initiate reactions between organic analytes before they are sensed. The end user should also not be exposed to a UV light source.
- Reactive species, given off during sensor cleaning cycles could react with the exhaust housing material.
- Water, which might be used to clean the TUIL sensor, must be kept isolated from the other systems.
- Finally, The TUIL sensor uses an electromagnetic source and this may interfere with the other electronics within the device.

However, two years into the project it was decided to only incorporate the CEIT sensors into

(a) Single sensor platform

(b) Multisensor platform
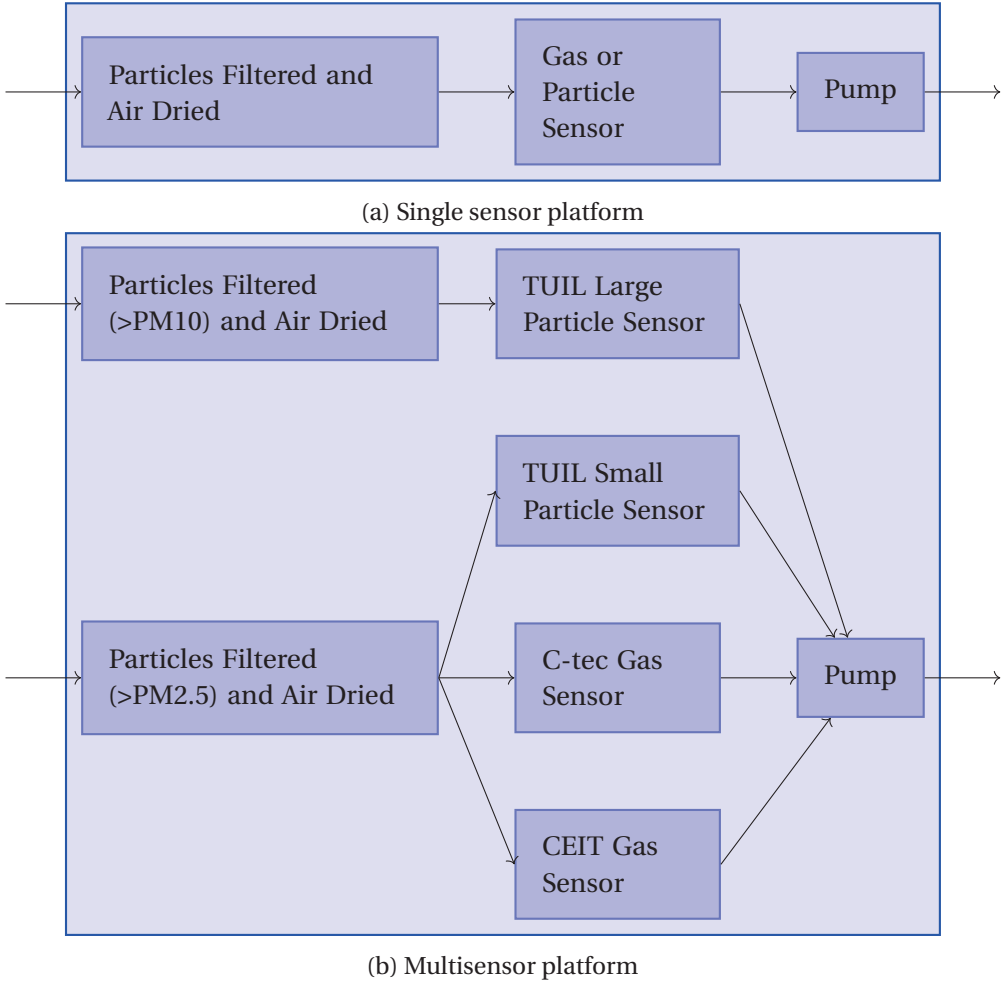
Figure 4.1 – Early block diagrams of INTASENSE platforms.
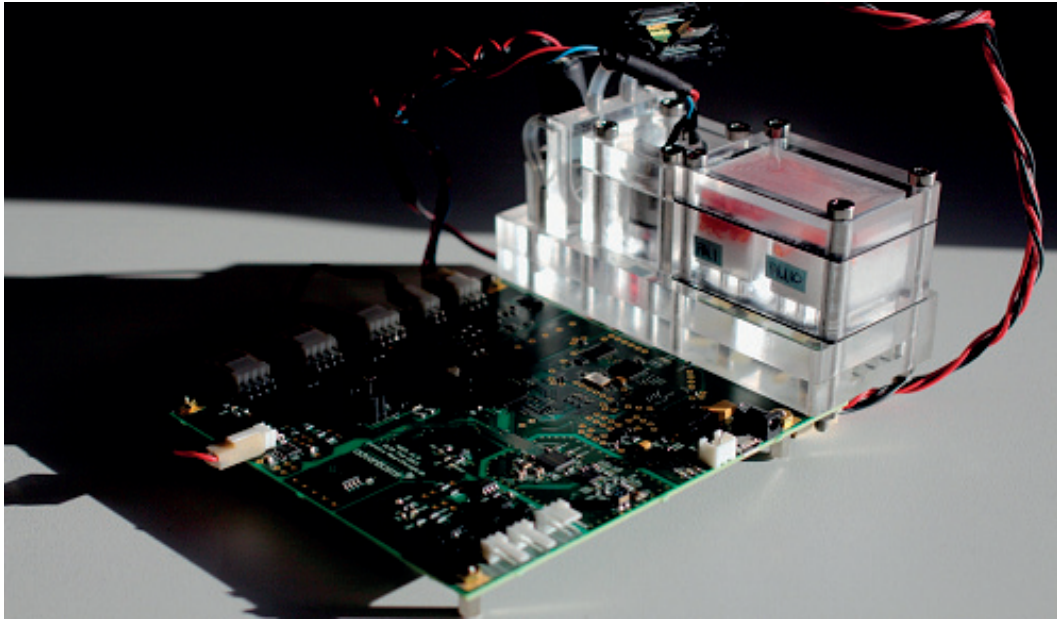
Figure 4.2 – Image of the integrated single sensor platform and electronics platform developed at Advanticsys.

the platform. Therefore, the temperature concerns were the only adverse interactions which needed to be addressed.

4.3 Integrated Single Sensor Testing Platform

Seven copies of the single sensor testing platform developed and described previously were delivered to collaborators. At Advanticsys this platform was used to test the electronics design and software. At C-tech and CEIT it was used to test gas sensors. Lastly, at Gooch and Housego the single sensor platform was used as a guide for the multi-sensor integration.

4.3.1 Product Prototype Using a Commercial Sensor

Electronics integration was conducted by Advanticsys. This involved developing a PCB which would power and receive signals from two Sensirion SHT75 temperature and humidity sensors (which use a data format similar to I2C), a Sensirion SDP610 differential pressure sensor (I2C), a Schwartzer precision microvane pump and an LED to activate the C-Tech sensor surface. It also included a demo-sensor which could be used to measure oxygen levels (SGX EC410) (Figure 4.2). Signals from these sensors, were then sent wirelessly to a computer. The computer ran specially designed software which converted the output of the sensors into numerical values so that a person could observe changes in humidity, temperature, flow rate or oxygen concentration in real time. Additionally, this software could be used to change the voltage delivered to the pump (and thus the pump speed) and turn the LED on or off (image 4.3).
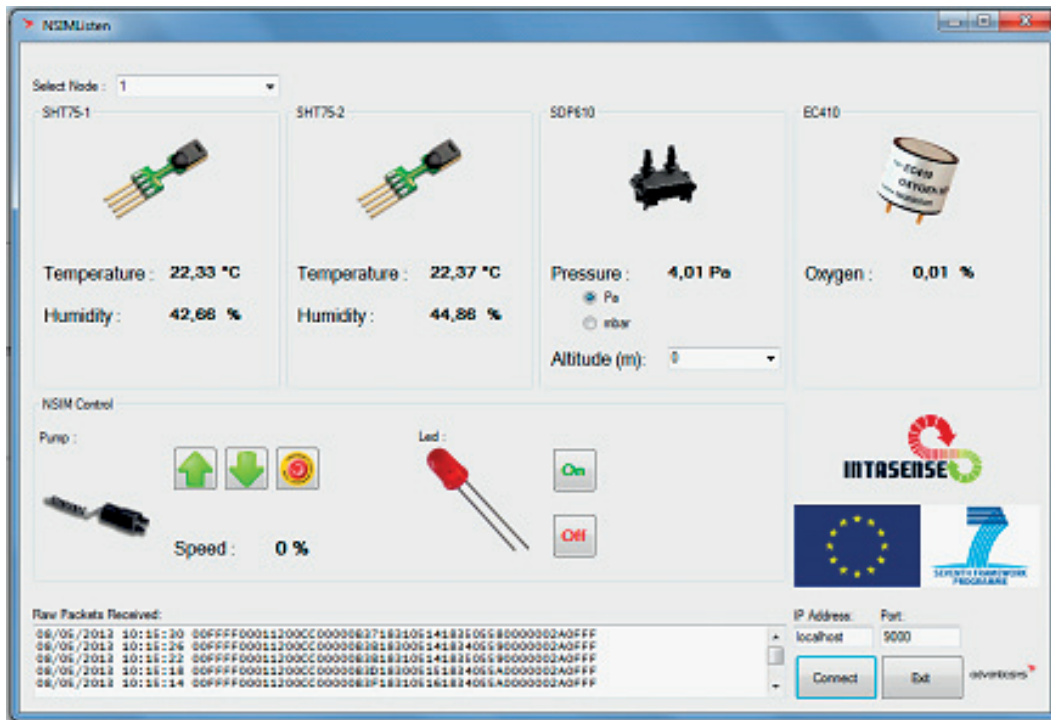
Figure 4.3 – Screen capture of the Advanticsys software.

This software was optimized for an end user as a tool in developing the final integrated prototype, not sensor research. As such it is very user friendly, easy to install and understand. However, the gas sensor type and the power supplied to the LED are fixed. Additionally, the data read interval cannot be controlled by the user, nor could the data be recorded. There was thus a need to design a similar device targeted at researchers.

4.3.2 Researcher Electronics Design and Integration

To collect data at a user defined rate and adjust variables such as the voltage supplied to the prototype metal oxide sensor, two commercially available platforms were combined and new software was developed as part of a master's thesis at CEIT. This student used an Arduino Uno to gather data from the differential pressure sensor and control the pump. To collect data from the temperature and humidity sensors and prototype gas sensors he used a Stellaris Launchpad LM4F120. It was important to use both platforms because the Stellaris Launchpad has greater data resolution (12 bits), which allows the temperature and humidity sensor to operate in 12 bit rather than 8 bit mode, giving a more accurate signal. Similarly, this higher resolution also allows smaller changes in resistance across gas sensor surfaces to be measured. The pump and the differential pressure sensor did not need this level of resolution; however, they need digital inputs. Therefore, an Arduino Uno, which includes a digital I/O port which can be used in PWM mode was included. A Labview program was then used to generate a GUI which allowed the system to be easily controlled by the user (Figure 4.5). This program allows
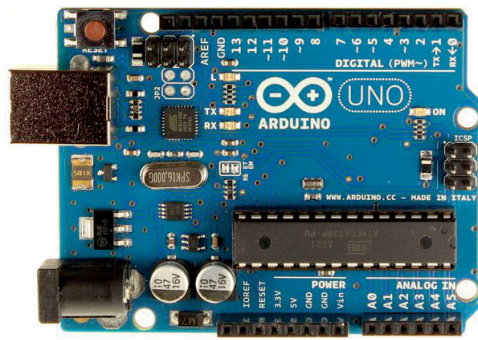
(a) Arduino Uno
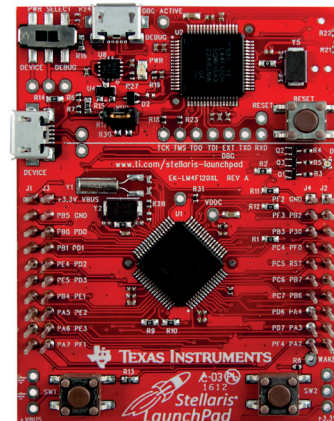
(b) Stellaris Launchpad LM4F120

Figure 4.4 – Commercial electronics boards used in the electronics platform developed at CEIT.
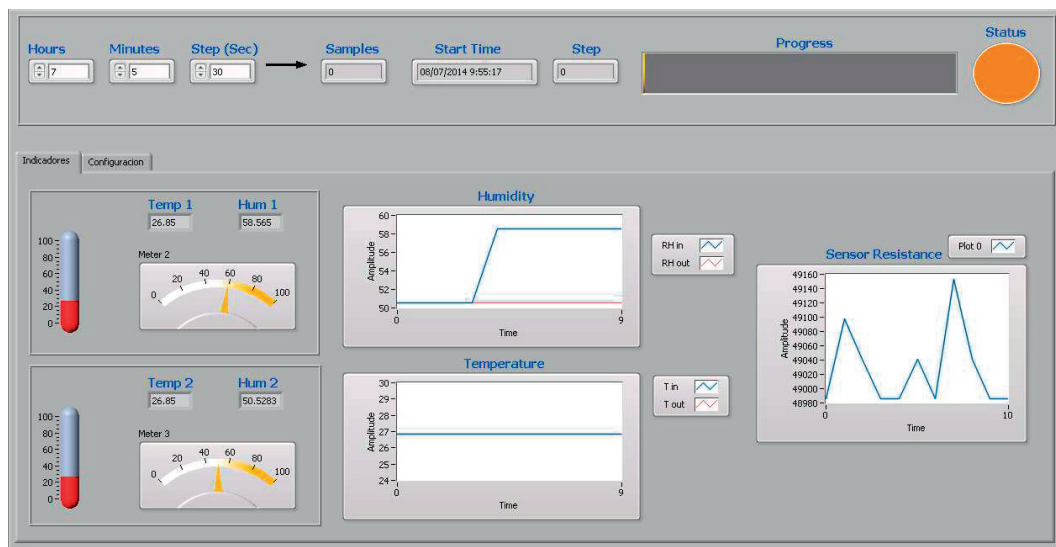
Figure 4.5 – User interface of the program developed by CEIT to collect data using the single sensor platform. Image source [Alday, 2014]

the user to set various communication parameters, read data from the sensors, convert this data to a decimal value and display and record these values in a text file.

4.3.3 Totally Commercial Data Acquisition Option

As an alternative to the methods above, it was possible to collect data from all commercial sensors using corresponding evaluation kits. When this method was used, data from each sensor would be recorded in a .csv file which could later be concatenated using Microsoft Excel, Matlab or other software. The pump would need to be run using a power supply. This method is described in the previous two chapters, and was used by CSEM for experiments with electrochemical sensors.

4.4 Multisensor Devices

Using feedback from CEIT, Advanticsys and Gooch and Housgo a multisensor demonstrator was designed. This platform includes three gas sensors which can be a combination of commercial and CEIT prototype sensors. Each of these sensors is housed in a TO8 package, so from a fluidics design perspective, they are interchangeable.

Aside from the experiments conducted by the author in previous sections of this thesis, this platform was used by CEIT C-Tec and Gooch and Housego to conduct sensor experiments. For some of these experiments, the researchers designed their own programs and electronic setups. Additionally, Advanticsys designed an electonic platform and computer software for use with both prototype and commercial sensors. The electronics platform and the multisensor device were then packaged at Gooch and Housego. These demonstrators were tested at and UC Technologies.

4.4.1 Lessons Learned for the Next Stage of Development

In addition to the sensor studies done by CEIT using the single sensor platform, and the electronics integration work done by Advanticsys, both Gooch and Housego and UC Technologies set up the system and used it as a demonstrator. Based on my personal experience manufacturing and assembling the device and their experiences using it, it was determined that the following additions or alterations should be made in the final demonstrator:

- For a ceiling mountable system, the platform needs to be smaller, lighter and house three sensors (maximum fluidic platform dimensions of: 75 by 145 by 60 mm).
- Data needs to be recordable.
- Work needs to be done to make the humidity sensor penetration point air tight.
- 3 sensors using TO8 packages will be used so large plug and play sensor chambers are not needed.
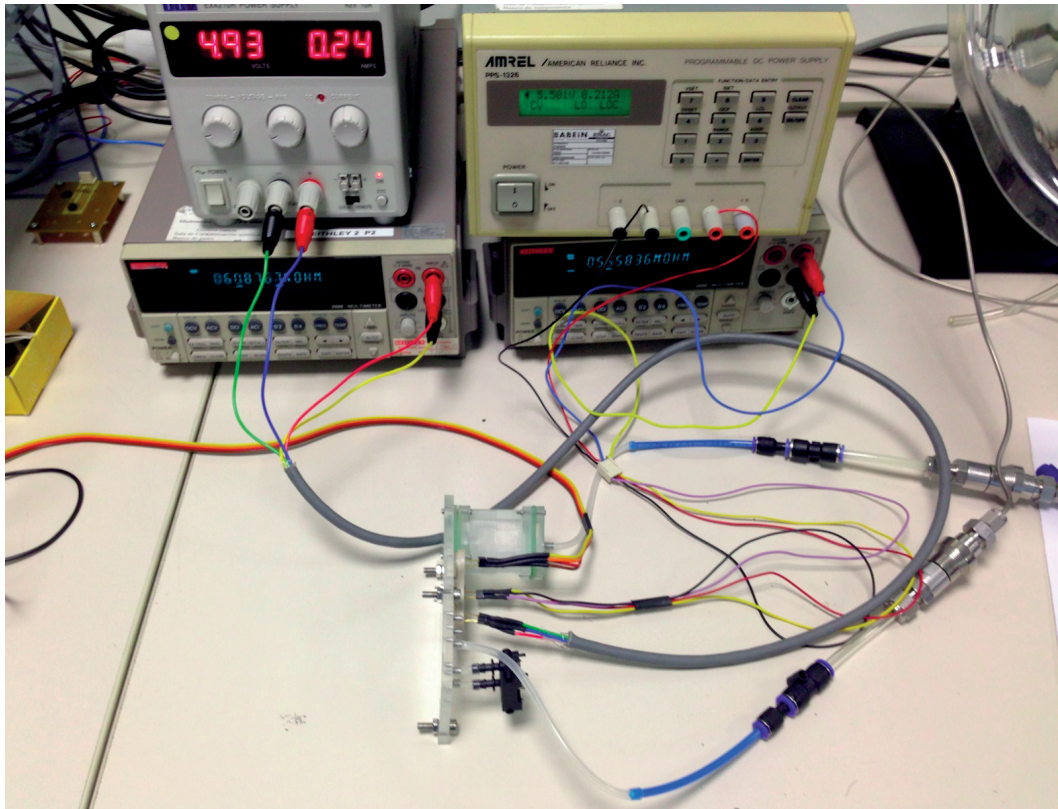
Figure 4.6 – Electrical equipment used to run sensors at CEIT during experiments with the metal oxide sensor platform.

- System should not be damaged by a user forgetting to use a gasket (it should not provide thermal insulation rather this should be done by the plastics).

4.4.2   Researcher Electronics Design, Integration and Use

My collaborators at CEIT used this platform in combination with commercial electronics and custom programs to test the insulation and the sensitivity of their sensors. During the thermal insulation studies 3 packaging approaches were tested. In the first version, the sensor was suspended above the package by the 4 electrical connections. This method was well insulated, but difficult to manufacture and very fragile. Therefore, two methods of directly attaching the sensor to the sensor holder were tested. Specifically, small plates of Aerogel, Delomonopox GE785 and Wurth High Temperature Sealer attached with silicone were used. Additionally, a micro machined u-shaped plate of alumina was tested. Of these options, aerogel was the best insulator, but too brittle to machine reliably. Therefore, Wurth High Temperature Sealer was selected because it is robust, easy to work with and provides sufficient insulation for long term use in the fluidic platform.

In addition to the thermal insulation studies, the calibration curves for the CEIT sensors were
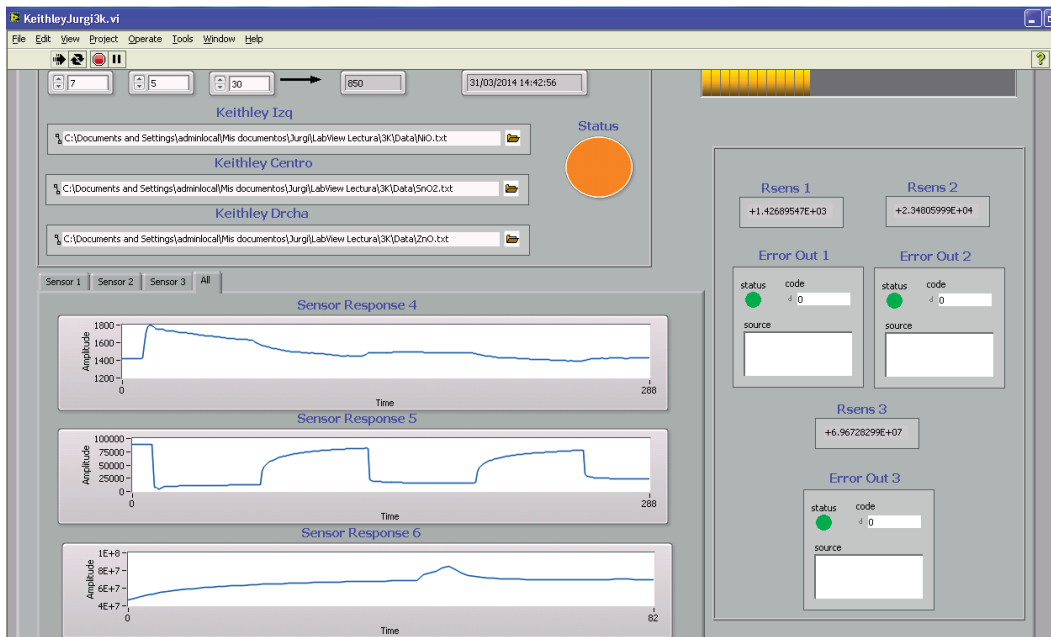
Figure 4.7 – User interface of the program used by CEIT to collect data using the metal oxide sensor platform.

found using the multisensor microfluidics platform. For these experiments, the inlet of the fluidic platform was attached to a gas delivery system which uses 3 mass flow controllers to regulate humidity, air and analyte gas concentrations. Clean air was sent through the system until equilibrium was reached. The resistance across the sensor was recorded. This is known as the base line or Ro. Then synthetic air doped with a small quantity of toxin was sent through. Once a steady resistance could be measured across the sensor surface, the value of the resistance was recorded and clean air was again sent through. This process was repeated using various concentrations of toxic gas until a calibration curve could be made. An example of the experimental setup and data acquisition during a multisensor experiment are presented in images 4.6 and 4.7, respectively.

4.4.3 Multisensor Demonstrator

In addition to the experimental electronics and data acquisition setups, shown previously, this fluidics platfom was integrated into the final demonstrator shown in Figure 4.8. This includes housing, wireless communication and an electronics platform which runs either commercial or CEIT sensors. However, because each sensor requires a different amount of power to operate at the correct temperature, the electronics and software are not interchangeable for each sensor. The unpopulated PCBs however, were identical.

The electronics and software (Figure 4.9) created for the multisensor demonstrator were very similar to the single sensor platform except that the electrochemical oxygen sensor cannot
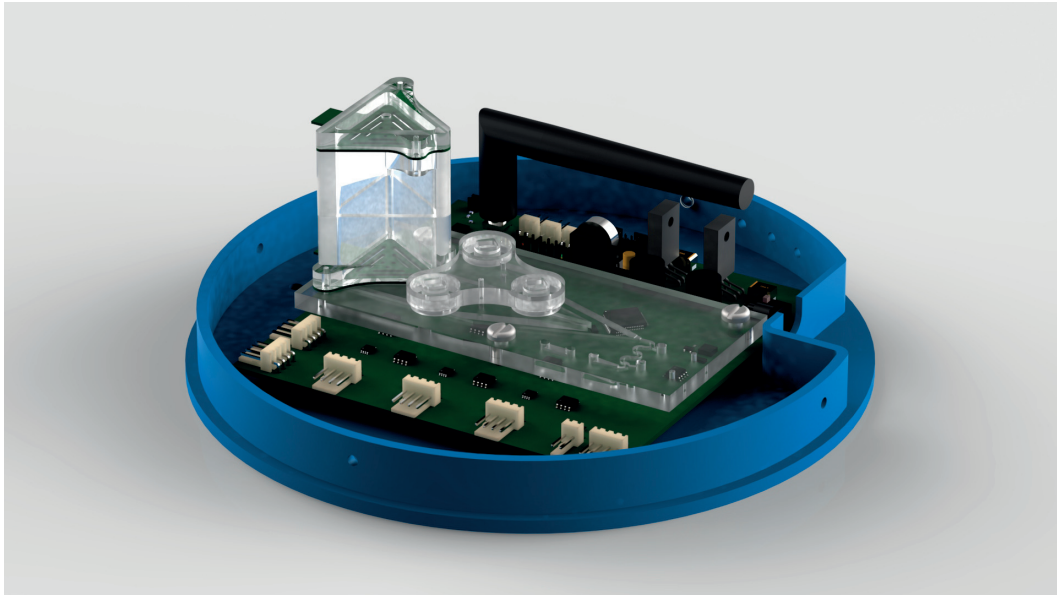
Figure 4.8 – Rendering of the final demonstrator without lid.
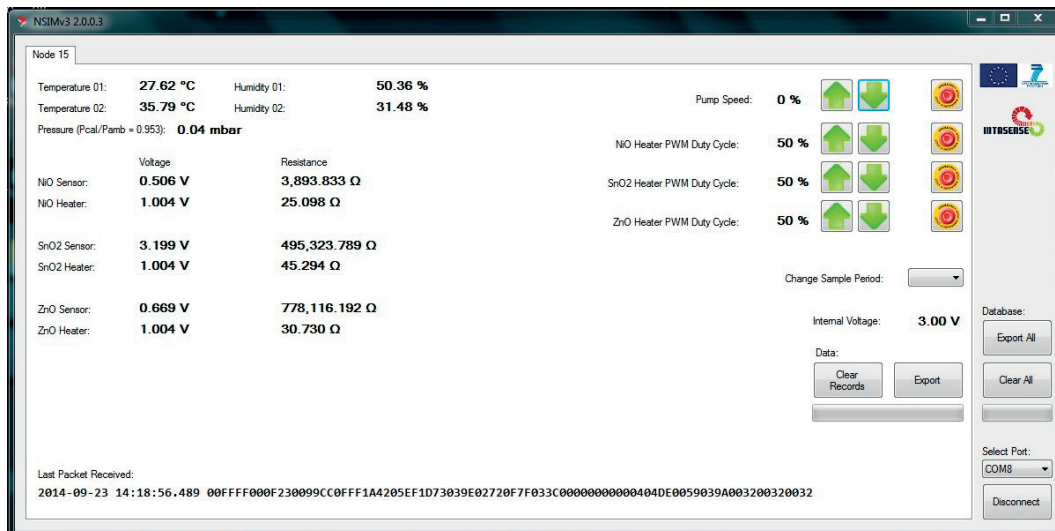
Figure 4.9 – User interface for the demonstrator.
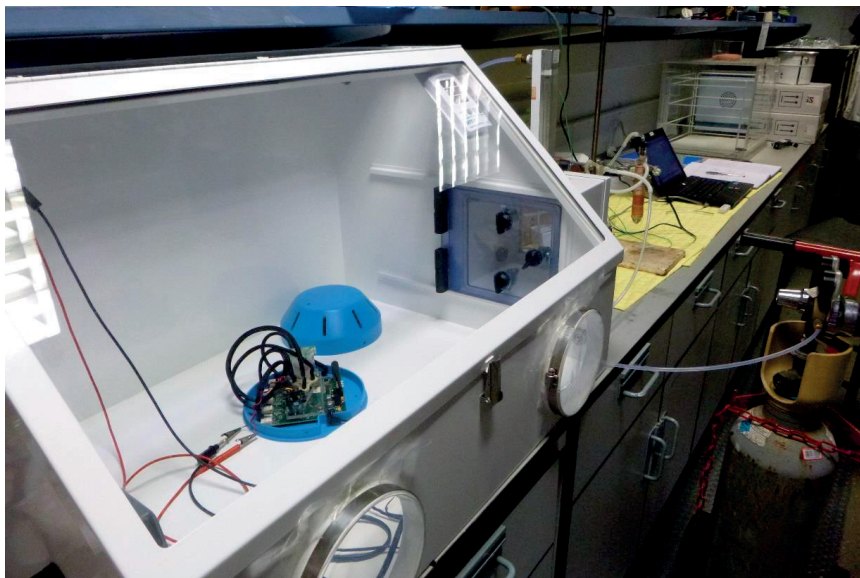
Figure 4.10 – Image of experiments conducted using the Intasense platform in a gas-tight chamber at C-tech Innovation.

be used on the multisensor platform. Rather this platform is designed to run three different metal oxide sensors. Correspondingly, the software was updated to include information about the resistance and voltages of both the heating element and sensor surface for each sensor. Additionally, the ability to save recorded data was added. The user was also given the ability to change the heating cycle for each sensor. These new features allowed researchers at C-Tech Innovation to use the demonstrator to test prototype sensors in air tight gas sensor chambers which mimic real world environments (Figure 4.10). An additional web-based user interface was also created for this platform . This interface allows the user to remotely review live data. It is also compatible with the commercial monitoring system sold under the name Concordia and can be easily modified to communicate with any SCADA or PLC compatible device which uses the Modbus protocol. An example of the Intasense Demonstrator integrating with commercial monitoring systems can be seen in Figures 4.12 and 4.11. The final product demonstrator can be seen in Figures 4.13 and 4.14. Figure 4.13 shows the demonstrator with the housing opened, while Figure 4.14 shows the device fully assembled.

4.5 Use of Fluidic Platform in Published Works

Doctoral Thesis:
J. Gonzales-Chavarri, Development and Optimization of Nanostructure –Based ZnO Conductometric Sensors for Indoor Air Quality, Tecnun Universidad de Navarra, Donostia-San Sebastian, Spain, February 2015

Masters Thesis:
Aizpea Eceiza Alday, Implementación de Sistema Compacto de Medida Para Sensors de Gas
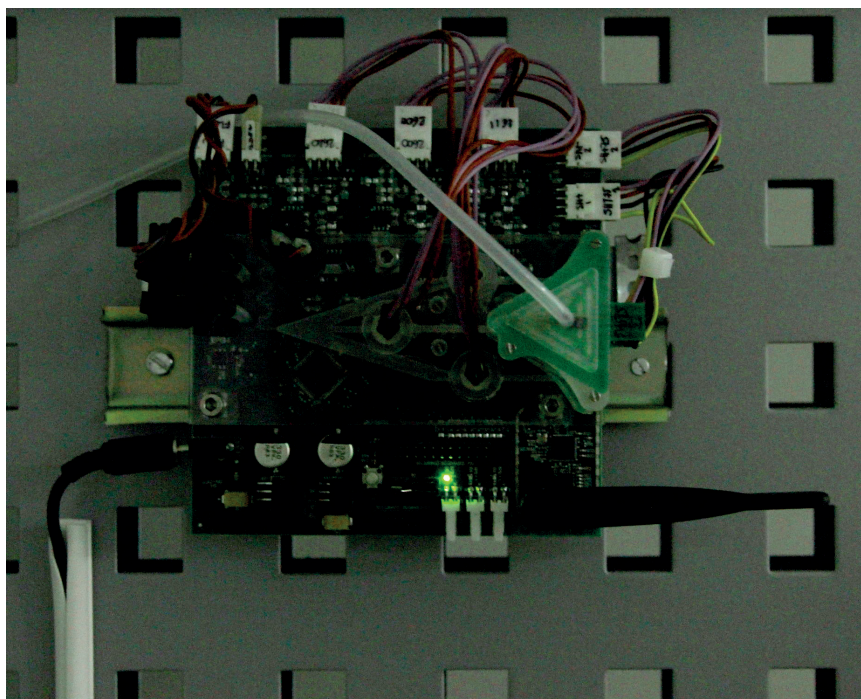
Figure 4.11 – A close up of the Intasense system at Advanticsys.

Conductométricos, Tecnun Universidad de Navarra, Donostia-San Sebastian, Spain, July 2014
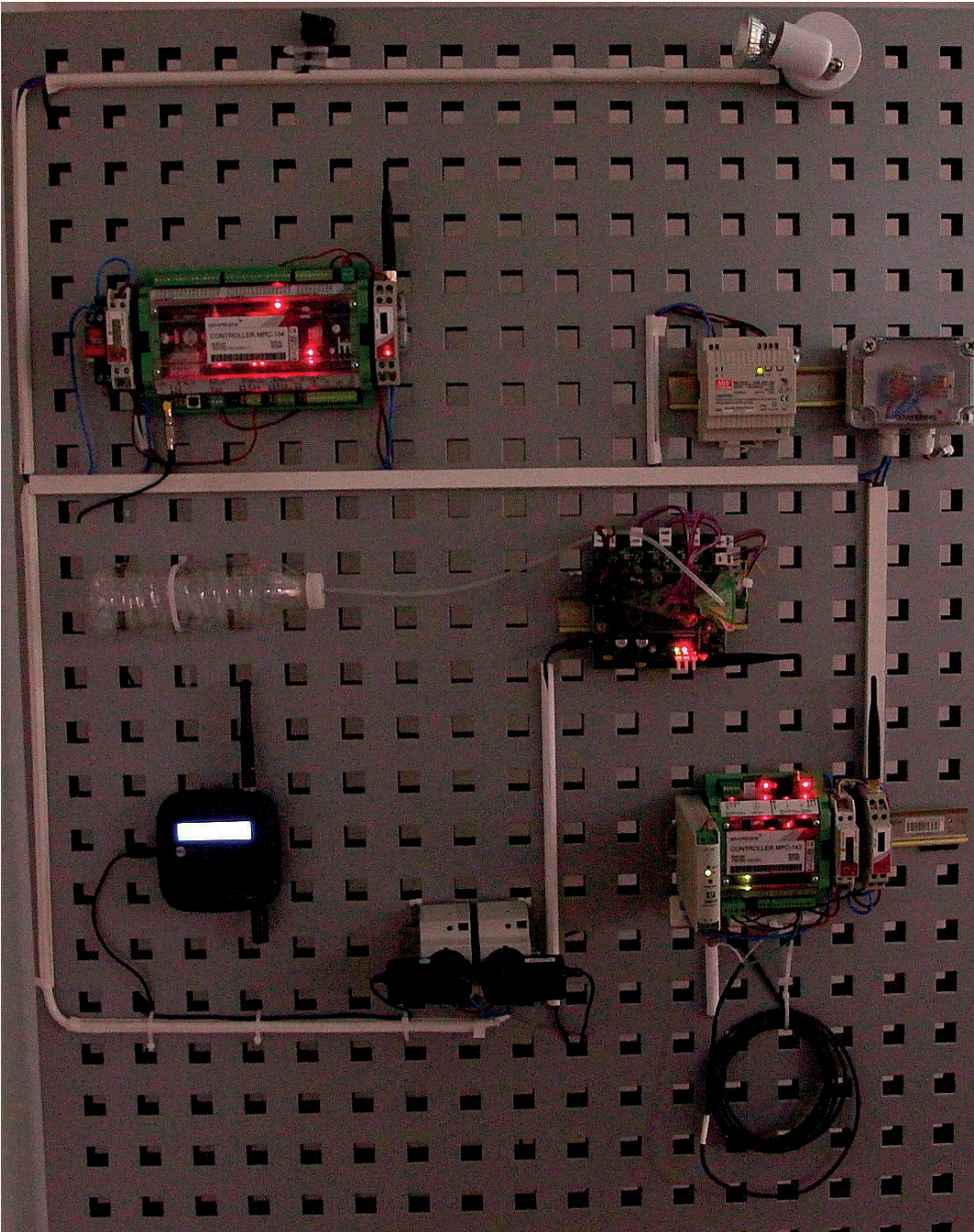
Figure 4.12 – Use of an unhoused Intasense demonstrator at Advanticsys, showing integration with other commercial monitoring systems.
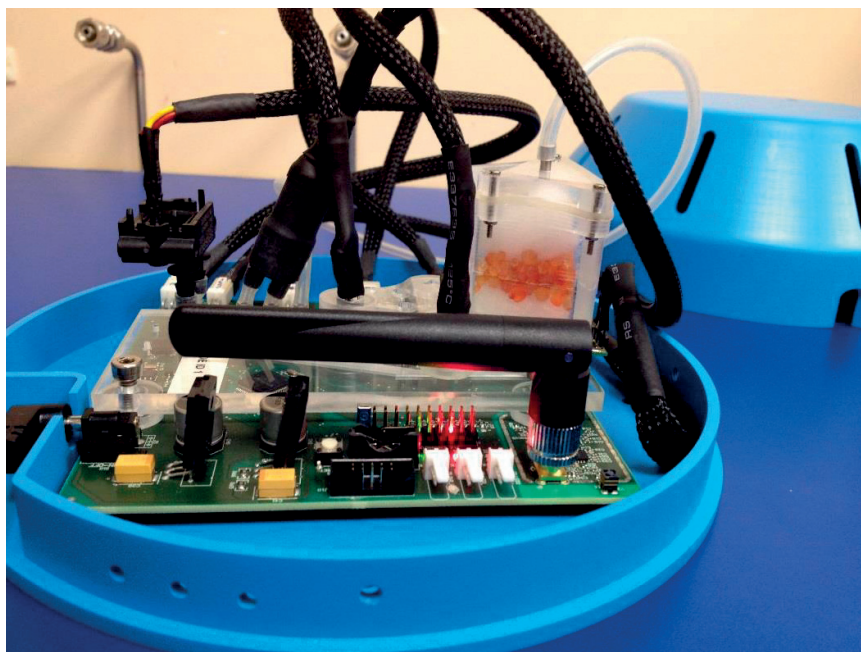
Figure 4.13 – A close up of the Intasense demonstrator at UC Technologies, with the case open.

Figure 4.14 – A close up of the Intasense demonstrator at UC Technologies, fully assembled.

4.6 Future of the Integrated System: Manufacturing Plan for the Device

At the end of the project, the following agreement was made regarding transfer of intellectual properties and manufacturing of the platform, should it go to market.

HEADS OF AGREEMENT

This heads of agreement was made on 15th September 2014 between the following parties:

1. Centro de Estudios e Investigaciones Tecnicas, hereafter referred to as **CEIT**

2. Centre Suisse d'Electronique et de Microtechnique S.A., hereafter referred to as **CSEM**

Background:

A. The parties have agreed to form a partnership in a venture to be known as INTASENSE technology.
B. The partners CEIT and CSEM have agreed that relevant roles and responsibilities will be distributed amongst the partners as outlined within this agreement, but such arrangements may change from time to time dependent on market conditions, cashflow, skill base and the like.

For the final exploitation of the INTASENSE project results, CEIT will ask for a patent with the potential title "Conductometric metal oxide sensor to measure low concentrations of volatile organic compounds and toxic gases and its fabrication procedure". The patent will protect the sensor structure together with the fabrication process of the three metal oxide materials: tin oxide, nickel oxide and zinc oxide, as a whole. CEIT has previous patents of the same nature.

In a next step in the value chain, a sensor manufacturer will be necessary, as CEIT cannot assume this role. The suggested profiles of companies to manufacture the INTASENSE conductometric sensors are for example SGX Sensortech in Switzerland or Hybtronics Microsystems in Spain.

The next step in the chain requires a system integrator profile, the role played by G&H in the INTASENSE consortium.

Finally, the system will be commercialized by companies such as UC Technologies, which should reach an agreement with the manufacturer.

CEIT will manage their relationship with the rest of the members of the chain as follows:

1. A contract about know-how transfer will be signed with the manufacturer.
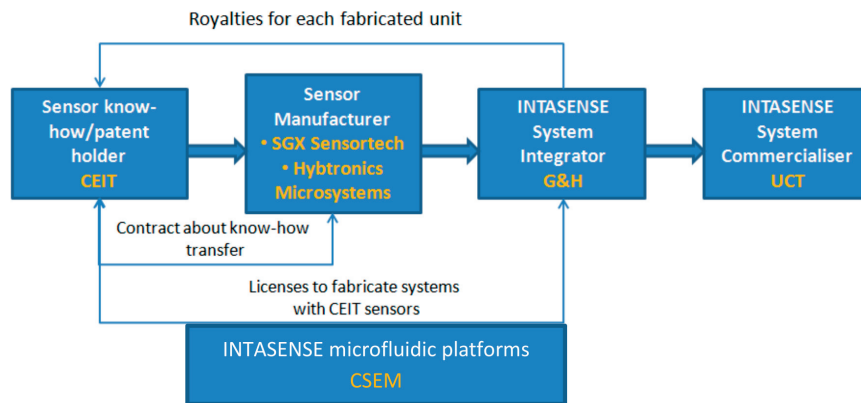
Figure 4.15 – Fabrication plan for the Intasense Air Quality Monitor.

2. CEIT will license the fabrication of systems including their sensors to the system integrator.
3. CEIT will receive royalties for each manufactured INTASENSE system.

The general terms for access rights for use of technology (for commercialization) developed by CSEM within the project INTASENSE are defined in the consortium agreement. Specifically, the fluidic platform for sensor integration and humidity stabilization as developed by CSEM has not been explicitly protected by IP, but rather is protected by the specific know-how and equipment needed for making the individual components and assembly technologies involved for the assembly of fluidic platform units.

After the end of INTASENSE, fluidic platform units can be provided by CSEM on a contractual basis for numbers up to 100 units/year. Prices per unit would be based on the material costs for the bought-in components involved (e.g. humidity/temperature sensor, flowsensor, air pump) and the labor costs for making the remaining components and assembly of the units and adding a fair and reasonable margin. If the numbers of units exceeds 100 units/year, CSEM would either subcontract the manufacture and assembly of the units and remain the provider of the units or alternatively perform a complete technology transfer (CAD drawings and manufacturing and assembly details) to a manufacturer, so that this manufacturer could then directly supply the fluidic platform. The efforts for the technology transfer from CSEM would then be covered by the manufacturer.

5 Conclusions and Outlook

The purpose of this project was to design, build, test and distribute gas sensor platforms to seven research groups in academia and industry, throughout Europe. These platforms were used to test prototype gas sensors and calibrate commercial sensors. Nine single sensor platforms were used in the early phases of integration, when sensor requirements were not fixed. This platform includes a prototype electronic platform, used to run commercial sensors. Additionally, six multisensor platforms were integrated into the Intasense product demonstrators. These demonstrators and single sensor prototypes include electronics to run and record data from the pump, flow sensor, humidity sensors, temperature sensors, air filters and either one commercial oxygen sensor or three metal oxide semiconductor sensors.

Gas sensors which measure ambient air frequently require particle filtration because particles can damage the sensor surfaces, prevent accurate measurements and limit the lifespan of the sensor. Therefore, particle filters were included in all of the fluidic platforms. In order to maximize the lifespan of the particle filters, for real world applications, the amount of gas passing through the system needs to be minimized, and thus, the transport of the gas through the system needs to be optimized. Gas transport optimizations were conducted to ensure efficient transport of the gas to the sensor surface for all platforms. Additionally, in the multisensor platforms, the fluidic paths were also optimized to ensure that equal quantities of gas were delivered to each sensor simultaneously. These optimizations are fully discussed in Chapter 2.

Heat transport can also be a problem when working with metal oxide sensors because they have a surface operating temperature which usually ranges from $250\,°C$ to $450\,°C$. This is not a problem when using commercial sensors, because the insulation between this surface and the packaging has been optimized to prevent the package from becoming too hot to be handled by a technician without protective clothing immediately after the sensor is turned off. However, part of sensor development is perfecting this insulation. Therefore, heat transport from the sensor insulation layer needed to be computationally modeled and experimentally tested to confirm that the fluidic platform would not be damaged during insulation studies. This process is described at the end of Chapter 2.

Lastly, humidity fluctuations needed to be controlled in order for the gas sensors to give an accurate reading. This is because humidity acts as a reducing gas, and thus causes a change in sensor resistance. This change is interpreted as a change in toxic gas concentration, and thus, causes the sensor to give a false reading. To prevent these false readings, gas transport through the preconditioning unit was buffered using 2 g of silica gel which acts as a reversible adsorbent. Because silica gel has a greater affinity for water than the toxic gasses of interest, these gasses could pass through the gel with a delay in the seconds or minute range while equilibrium with humidity fluctuations took hours. Results of experimental tests and computational models of this transport process are covered in Chapter 3.

Once each fludic platform design was manufactured and tested, they were distributed throughout the Insasense consortium. These platforms were used to test and calibrate commercial and prototype sensors. Additionally, they were integrated into the Intasense prototype and the Intasense Demonstrator. Experimental tests using these platforms included calibration of commercial electrochemical and metal oxide sensors as discussed in Chapter 3; prototype sensor insulation studies, discussed in Chapter 2 and and gas sensor tests as shown in Chapter 4. The benefit of using the multisensor platform, instead of a traditional sensor chamber, is that three sensor readings can be acquired simultaneously. This reduces the number of experiments required for reliability testing for a batch of sensors, optimization of the surface operating temperature of a metal oxide sensor or calibration of multiple types of sensors. Additionally, many data acquisition programs and electronics platforms were developed for use with these platforms (Chapter 4). The metal oxide sensor platform was used to create the Intasense demonstrator, a device which is ready for integration into a building.

All of this work lays the foundation for a product which measures the current air quality of a room and sends feedback to the ventilation system, thereby optimizing the trade off between energy efficiency and occupant health. However, before this can happen, a few steps must be taken. First, commercially available gas sensors must be selected and tested for cross sensitivity to other target gasses, using gas standards. Additionally, sensor baseline shifts and noise must be quantified. The longevity of the particle filters should also be quantified so that an optimal replacement schedule can be established. Simultaneously, a redesign of the plastic components should be done so that the platform and housing are optimized for low cost manufacturing techniques such as injection molding.

Once the system has been fully studied in a controlled setting, actions need to be assigned to the gas sensor readings. This could include an alarm in the case of carbon monoxide, altering the ratio of fresh to recycled air or opening or closing air vents. Then a series of real world experiments would need to be done to confirm that the appropriate action had been selected by the Intasense system.

For these experiments measurements should be taken in many energy efficient buildings with the Intasense demonstrator and compared to gas samples taken at the same time from the same location and analyzed using gas chromatography. Then safety of the combined

concentrations of all gasses, as determined by the chromatographic measurements, should be quantified using an equation such as eq.1.1, which is used by OSHA, to determine the overall acceptable limit of the combination of all toxic gasses. This value should then be compared to the action prescribed by the Intasense system. Once all errors which cause building occupants to be exposed to hazardous concentrations of chemicals have been resolved, and the errors which cause excess ventilation have been minimized, the product will be ready to go to market, from an engineering perspective.

6 Appendix

6.1 Inconclusive Experiments and Model: Formaldehyde

Attempts were made to include formaldehyde in the studies outlined in Chapter 3 but there were issues with both the experiments and the computational model. First, there was no applicable isotherm data. Second, it is likely that chemical reactions are occurring in the system, and it is not possible to quantify them with the equipment available. Finally, it is not clear if the experimental methods used in this thesis for the other gases reflect real world scenarios for formaldehyde.

6.1.1 Formaldehyde Experiments

Experiments were conducted using the same methods outlined in Section 3.2 without electrochemical sensors. Pulses of 2, 8 and 20 PPMs were sent through the system at 45% relative humidity. Additionally, humidity fluctuation studies were conducted by changing the relative humidity to 30 or 60% while sending a pulse of formaldehyde through the system. The results of this experiment are plotted in Figure 6.1. Just like in the experiments with NO_2, CO and C_6H_6, experimental values found during experiments without silica gel in the preconditioning unit were used to calibrate the silica gel experiments.

6.1.2 Isotherm

The only isotherm data available for formaldehyde was determined by [Yang et al., 2005], who measured it for two different types of silica gel. These are reported as type 1 and type 2. Their best fit curves followed the Langmuir equation:

$$[\text{SiOH} \cdots \text{CH}_2\text{O}] = \frac{K_{CH2O} \cdot [\text{SiOH} \cdots \text{CH}_2\text{O}]_{max} \cdot [\text{CH}_2\text{O}]}{1 + K_{CH2O} \cdot [\text{CH}_2\text{O}]} \qquad (6.1)$$
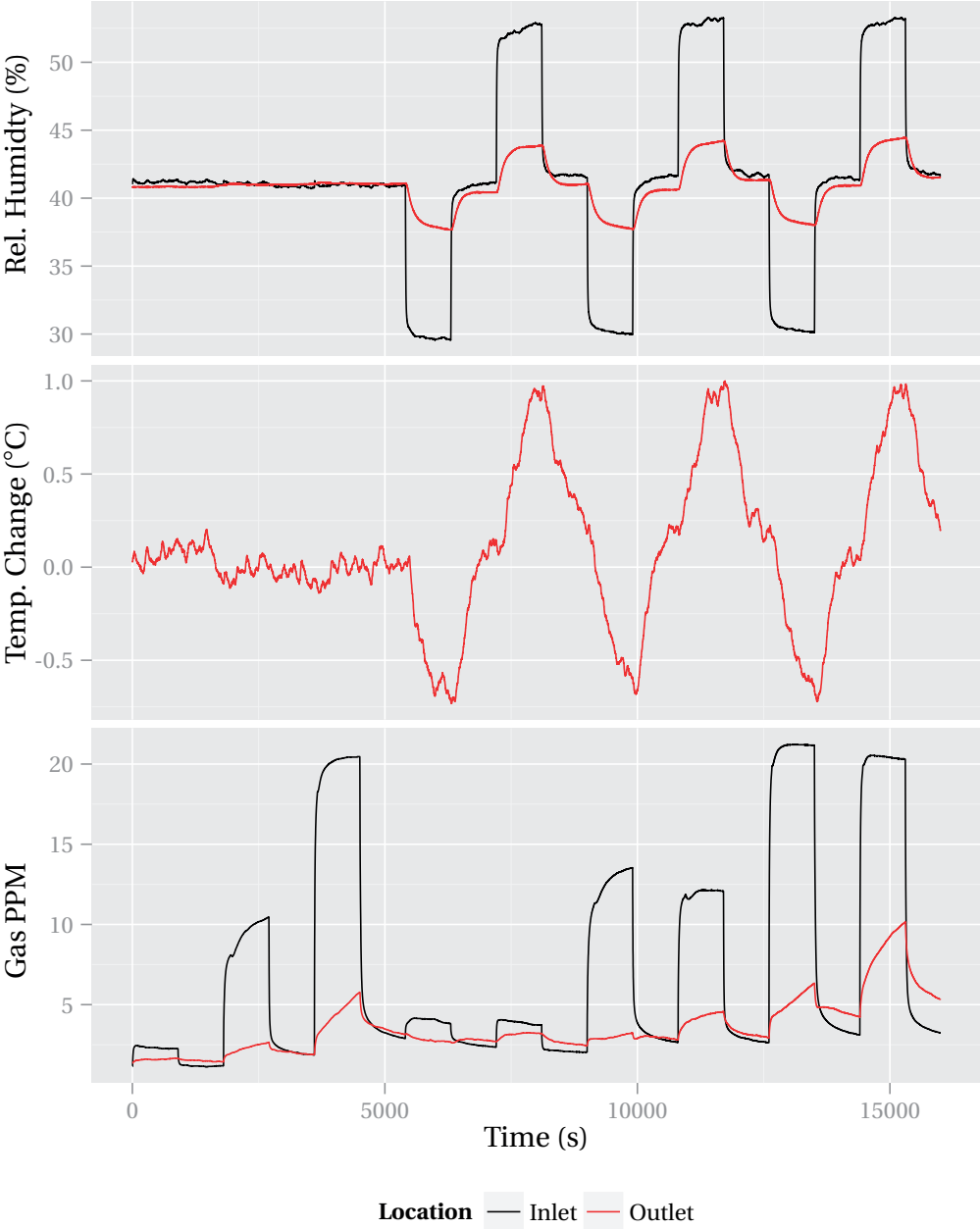
Figure 6.1 – Results of formaldehyde experiments.

Figure 6.2 – Chemical Structure of an aldehyde.

When their best fit Langmuir curves are converted to the correct units for equation 3.40 the values reported in Table 6.1 are found. This means that the the maximum quantity of formaldehyde adsorbed onto silica gel is about $0.00001\,\mathrm{molCH_2O/kgSiO_2}$, which is five orders of magnitude less than carbon monoxide. This is unlikely, because formaldehyde can hydrogen bond with silica gel, while carbon monoxide cannot. Thus, the value for the maximum concentration of formaldehyde on silica gel should be greater than the maximum concentration for carbon monoxide. This error could be methodological, because the researchers only measured up to 4 Torr formaldehyde, or numerical, because there are other numerical typos in the paper.

Although no other isotherm for formaldehyde on silica gel could be found, Gosh et al. conducted experiments using acetalaldehyde, propionaldehyde and butyraldehyde, which are all chemically similar to formaldehyde [Ghosh and Hines, 1990]. Specifically, they vary only in their R group which is a hydrogen atom for formaldehyde, a methyl group for acetylaldehde, an ethyl group for propionaldehyde, and a propyl group for butryaldehyde (Figure 6.2). The length of the carbon chain in the R group should not have a large effect on the aldehyde's ability to hydrogen bond with the OH group on the surface of the silica gel or adsorbed water molecules. However, the longer the carbon chain on the R group, the more likely it is to block neighboring OH groups on the silica gel. Therefore, there should be slight differences between each chemical's isotherm curve.

To compare the Gosh isotherm to the Yang isotherms, the best fit curve for acetylaldehyde, propionaldehyde and butrylaldehyde, as published by Gosh, were plotted in the $0\,\mathrm{mol\,m^{-3}}$ to $0.1\,\mathrm{mol\,m^{-3}}$ range. In this range, the best fit curves are almost identical to the Langmuir isotherm. These best fit Langmuir isotherms could then be directly compared to the Langmuir isotherms found by Yang et al.. All of the parameter values can be found in Table 6.1. The data for acetylaldehyde in this table confirms the hypothesis that the values for the maximum bound concentration are very low. The values for the kinetic constants for all aldehydes vary within one order of magnitude. Thus, this value is probably close to the real value, and the differences between reported values could just be a function of the type of the silica gel used.

Author	Chemical (X)	Formula (X)	$[\text{SiOH}\cdots\text{X}]_{max}$ $(\text{mol}\,\text{kg}^{-1})$	$K_{eq} = \frac{k_f}{kr}\,\text{m}^3\,\text{mol}$
Yang	(1) formaldehyde	CH_2O	.0000138	171
	(2) formaldehyde	CH_2O	.0000136	92
	(1) acetylaldehyde	C_2H_4O	.0000515	156
	(2) acetylaldehyde	C_2H_4O	.0000299	171
Gosh	acetylaldehyde	C_2H_4O	2.58	18
	propionaldehyde	C_3H_6O	2.37	78
	butyraldehyde	C_4H_8O	2.39	71

Table 6.1 – Isotherm parameters for aldehydes derived from Yang et al and Gosh et al. The labels (1) and (2) refer to the types of silica gel used by Yang et al.

6.1.3 Model Building

In order to model the transport of formaldehyde through the preconditioning unit, the mass transport only model in the following form was used:

$$(\epsilon + \rho_b \frac{K_{Li}c_{Pi,max}}{(1 + K_{Li}c_1)^2})\frac{\partial c_i}{\partial t} + (c_i - \frac{K_{Li}c_{Pi,max}c_i}{1 + K_{Li}c_1}\rho_P)\frac{\partial \epsilon}{\partial t} + u\frac{\partial c_i}{\partial x} = (2.5ud + \epsilon^{4/3}D_F)\frac{\partial^2 c_i}{\partial x^2} \quad (6.2)$$

which is just a reprint of equation 3.43. Each of the values for K_eq and $[\text{SiOH}\cdots\text{X}]_{max}$ were substituted for K_{Li} and $c_{Pi,max}$, respectively to create 7 equations. These were solved using the same parameter and variable values used for other toxic gases (Table 3.6). The diffusion coefficient was $1.6 \times 10^{-5}\,\text{m}^2\,\text{s}^{-1}$ for all isotherms. The system was solved using Comsol, and the results can be seen in Figure 6.3.

In this simulation, the formaldehyde (CH_2O) and the acetylaldehyde (C_2H_4O) using the isotherms reported by Yang et al. are labeled 1 or 2 depending on which silica gel was used in Yang's experiments. These do not appear clearly because they overlap the inlet data which shows up as a thick black and green dotted line. The isotherms found by Gosh are clearly visible. The Gosh isotherms mimic the experimental data better than the Yang isotherms. However, because the Gosh isotherms are not for formaldehyde, a perfect fit is not expected.

6.1.4 Discussion

During the experiments, formaldehyde was detectable after exposure to silica gel. However, the outlet side peak heights were smaller, and the baseline was not recovered after 15 minute time intervals. If the Yang isotherm data is correct, formaldehyde should essentially not adsorb onto the silica gel. Alternatively, if the trends observed in the Gosh data continue, formaldehyde should have a larger peak height than acetylaldehyde. However, the peak height from the experimental data is much too low for either the trend from the Gosh data or the Yang isotherm to be correct. This indicates that there is a reaction or much stronger adsorption than predicted by the model, or both. This chemical reaction or interaction is not sufficient to
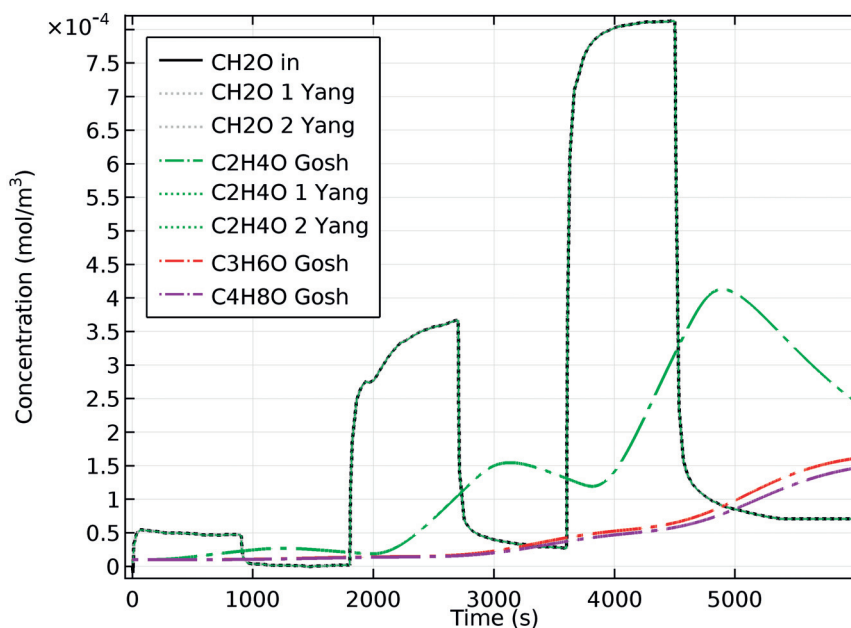
Figure 6.3 – Results of computational simulations using formaldehyde experimental data as the inlet data. All of the Yang lines are indistinguishable from the inlet data. The Gosh curves, however are visible.

change the temperature of the system, so the discrepancy is not a result of thermodynamics. However, stronger adsorption is possible because formaldehyde is smaller, so it is possible that it blocks fewer of the neighboring binding cites, allowing more molecules to bond to the same surface area of silica gel. However, if this were true, then the chain length should have a much stronger influence on the other isotherms for aldehydes. That is unless there are pores on the silica gel which are so small that only formaldehyde is small enough to reach these sites. Alternatively, chemical reactions could be happening in the air or in the liquid water on the surface of the gel.

It is unlikely that the silica gel is acting as a catalyst: [Cheng, 1996] showed that formaldehyde in air flowing through a packed bed filled with SiO_2 at 190 °C did not form CO, CO_2, dimethyl ether, methanol, methyl formate or methylal. However, there were small conversions at higher temperatures. Although formaldehyde is probabily not reacting with silica gel, it is probaibly reacting with air and humidity. Specifically, in humid air, formaldehyde monomers are at equilibrium with paraformadehyde and trioxane [Safriet, 1991]. In air formaldehyde can also be oxidized to formic acid [OSHA, 2013]. Additionally, in liquid water formadehyde reacts to form methylene glycol [Safriet, 1991]. Because of the longer retention times through the silica gel bed, it is likely that the formaldehyde is being more completely converted to all of these products. It is also possible that there is some methalyene glycol in solution with the water on the surface of the silica gel, causing longer retention times than predicted by adsorption alone. Thus, chemical reaction or formation of a solution could be causing the difference in inlet and outlet signal.

Although the experiments show delays caused by the preconditioning unit when pure formaldehyde is run through the system, it is unclear if these experiments show that silica gel would not work in a real world application. This is because formaldehyde must be stored in dry nitrogen in order to be stable. Upon exposure to oxygen, humidity and light it converts to the chemicals listed above. In the real world, formaldehyde in the air would be in equilibrium with, or at least partially converted to, these other chemical species. However, the formaldehyde in these experiments was not in equilibrium. Therefore, because the inlet gas mixture is reactive with itself, it is not clear which parts of the signal change are caused by adsorption alone and which parts are caused by adsorption allowing longer retention times and thus, more time to reach equilibrium. In other words, it is unclear if inlet sensor responses would be the same if formaldehyde in equilibrium with its polymerized, oxidized and hydrated forms in humid air was used instead of a pure formaldehyde source.

Thus, if the preconditioning unit is used before a formaldehyde sensor, more experiments need to be done. Specifically, the isotherm for formaldehyde should be measured experimentally. Additionally, the chemical species present in the outlet gas should be quantified. Lastly, the optimal properties of the inlet gas should be determined.

6.2 Failed Experiments

There is a German saying: "Wer misst misst Mist" which translates to "he who measures, measures shit", implying that unless you are very careful to control your experiments, you are probably measuring something completely different than you think you are. In the main body of this thesis, successfully controlled measurements have been explained. Here measurements, which for one reason or another, look good, but are not accurate are included. These highlight why it is so important to measure not only the specific parameter you are interested in, but also parameters which can cause your experiments to be inaccurate.

6.2.1 Humidity Leak Using Tedlar Bags

Tedlar gas sample bags are commonly used in air quality monitoring to transport a gas sample from an environment of interest, such as factories, refineries and wastewater treatment plants, to a laboratory where the chemicals in the air sample can be analyzed. Additionally, they are used to create and transport gas calibration standards [Coyne et al., 2011]. As such, each bag contains a valve which can be opened or closed to allow gases to enter or exit. Additionally, there is an injection port which can be used to introduce contaminants or remove small quantities of gas for analysis.

Although these bags are very user friendly, it is important to think about the chemicals which are being stored and measured, and use them only when appropriate. This is because not all chemical compounds are stable in the bags. For example, it has been reported that 45.5% of nitrogen dioxide will be lost during 24 hours of storage in the bag and 63.6% will be lost over 2
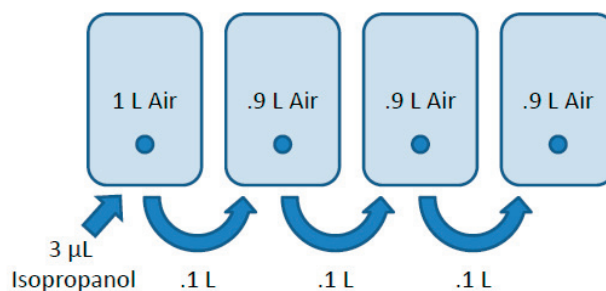
Figure 6.4 – Dilution scheme for gas samples in Tedlar bags.

Sample Number	Amount of Isopropanol in µL	Approximate ppms of Isopropanol
1	3	1000
2	0.3	100
3	0.03	10
4	0.003	1

Table 6.2 – Gas dilution concentrations.

days of storage [Coyne et al., 2011]. However, other chemicals, such as isopropanol appear to be completely retained over the same time period [Coyne et al., 2011].

With this in mind, it was decided not to use this setup for gases which will be lost over the time period of the experiment. Additionally, it was not possible to use benzene, formaldehyde, nitrogen dioxide or carbon monoxide due to SUVA (Swiss Occupational Safety Regulator) regulations. This is because CSEM does not have the facilities to work with toxic gases, and building up such a lab is economically prohibitive. Therefore, isopropanol was chosen as a first candidate for the experiments because it is not dangerous in low concentrations and alcohols have a better ability to bind to polar adsorbents than most other functional groups (Figure 3.6).

In order to create gas standards which could be used to calibrate three types of metal oxide sensors, a serial dilution was conducted (Figure 6.4 and Table 6.2). First, four labeled gas bags were filled with synthetic air (20% O_2 and 80% N_2 by weight) using a red-y mass flow controller. Three of these received 0.9 L and one received 1 L. Then, using a 5 µL Syringe (Model: 75 RN part number: 87930 by Hamilton), 3 µL of isopropanol was injected into the bag containing 1L of synthetic air. The result was a bag with approximately 1000 PPM of isopropanol in clean, dry air. This sample was then connected to a syringe pump and 0.1 L of the gas mixture was transferred to one of the bags containing 0.9 L of clean air. The result is a bag with 1 L of air containing approximately 100 PPM isopropanol. This procedure was repeated 2 more times to generate samples with 10 PPM and 1 PPM isopropanol in air.

Using these standards, calibration studies could be done. To do these studies 3 L of synthetic air was pumped though the multisensor platform and data from three different e2v metal oxide
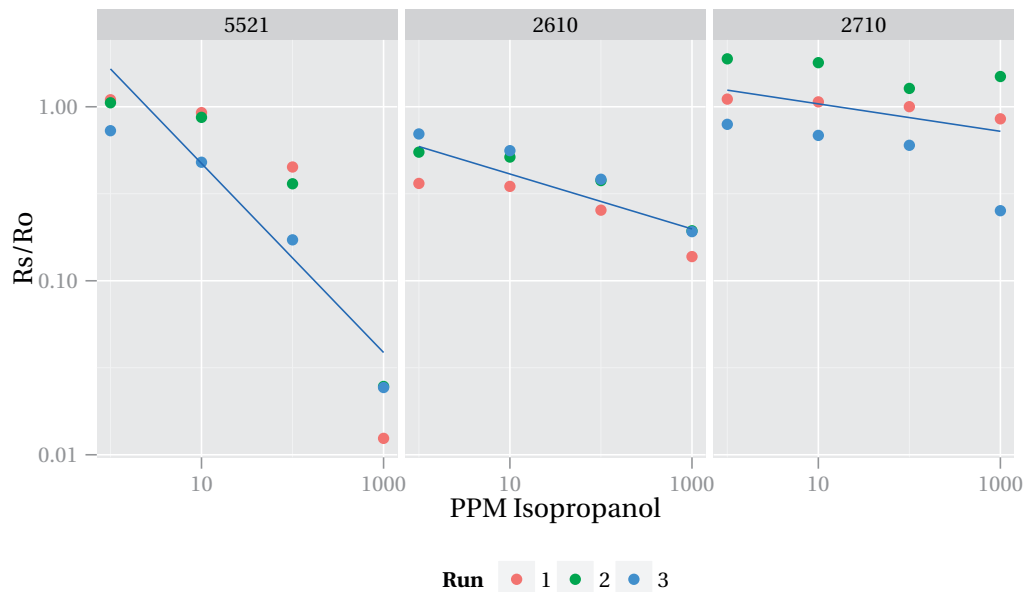
Figure 6.5 – Calibration curves for three metal oxide semiconductor sensors manufactured by e2v.

sensors were recorded. In this way the sensor base line resistance (Ro) was found for a MiCS 5521, a MiCS 2610 and a MiCS 2710. Then air with analyte was run through the system and the resistance across the sensors was recorded once equilibrium had been reached (Rs). Clean air was then used to return the sensor resistance to its equilibrium value, which was sometimes not exactly the same value as the original baseline. Then the next isopropanol sample was run through the system until the new equilibrium value was found. This process was continued until the sensor resistances for all isopropanol values were recorded. A calibration curve was then made for each sensor. Then new gas samples were created by serial dilution and the process was repeated two more times. The three calibration curves can be seen in Figure 6.5.

Although the calibration curve for the e2v 5521 sensor is good enough that this sensor might be usable in future experiments, a flaw was discovered which made it impossible to use this method. Specifically, humidity was able to pass into the tedlar bags so quickly that bags filled with dry air would reach equilibrium with laboratory humidity in less than two hours. To try to control the atmospheric humidity, the samples were placed into a container with an overpressure. However, during these studies it was found that our air compressor system was having a mechanical problem. The result was that the inlet air which created the overpressure was fluctuating between 5 and 15% relative humidity. Thus, the calibration curves generated by this method were unusable because there was no way to determine the influence of humidity changes on the sensor baseline.

It was therefore decided that a mass flow controller system must be used. However, it was

not possible to conduct these experiments at CSEM because buying the equipment to build a gas lab that is up to safety regulations is extremely expensive. Additionally, we lacked an appropriate lab space to build such a system. Therefore, it was agreed that the facilities of our partner CEIT in San Sebastian, Spain and Siemens Building Technologies in Zug, Switzerland should be used.

6.2.2 Humidity Leak During Mass Flow Controller Experiments

A humidity leak occurred during the first run of the toxic gas experiments, presented in Chapter 3.2. The experiments used the same setup as the experiments reported in that section, however only 2 toxic gas sensors were used on each side. An example data set from these experiments is reported in Figure 6.6. In this figure, the top graph is the relative humidity of the system and the top middle curve is the sensor response—the resistance of the sensor at a given time divided by the resistance of the sensor in clean air. The middle bottom curve is the absolute value of the difference of the sensor response between the experiment with silica gel and the experiment without. The bottom curve is the calibrated response from all 4 sensors in both experiments. In the bottom two images, the black curves and red dotted curves are not influenced by the presence of silica gel whereas the solid red curves are.

Although this data demonstrates that gas concentration fluctuations are detectable after the preconditioning unit, there are problems. Most notably, the humidity was not stable in any of the experiments. In fact, the humidity was positively coelated to the amount of analyte introduced to the system. Because the sensors are humidity sensitive, this makes it impossible to differentiate between signal changes caused by humidity fluctuations and signal changes caused by the presence of toxic gas. Additionally, this fluctuation in humidity is the result of some problem with the mass flow controllers or the program which runs them. As it was unclear what the problem was, and the experiments were conducted using a borrowed set of mass flow controllers, these experiments were rerun using a different set of the same mass flow controllers. The results of these new experiments are included in the main body of the text.

This leak was only detected because both humidity sensors were used in the experiments, even though this should not have been necessary. Specifically, the experiment shown in Figure 6.6 should have a stable inlet and outlet humidity, which should have been controlled by the mass flow controllers, so the humidity measurements should have been about 35% relative humidity for all time points. However, for security and consistency with the humidity fluctuation experiments, the humidity was measured. If gas sensors alone had been used–which is the standard in published literature–this would have gone undetected and the published data would have contained errors. Similar failures–in this case leaks in the system or loose tubing–were detected using the mass flow meter. The results of these failed experiments show the necessity of redundant measurements in scientific experiments: without the redundant humidity and flow measurements, bad data would have been published.
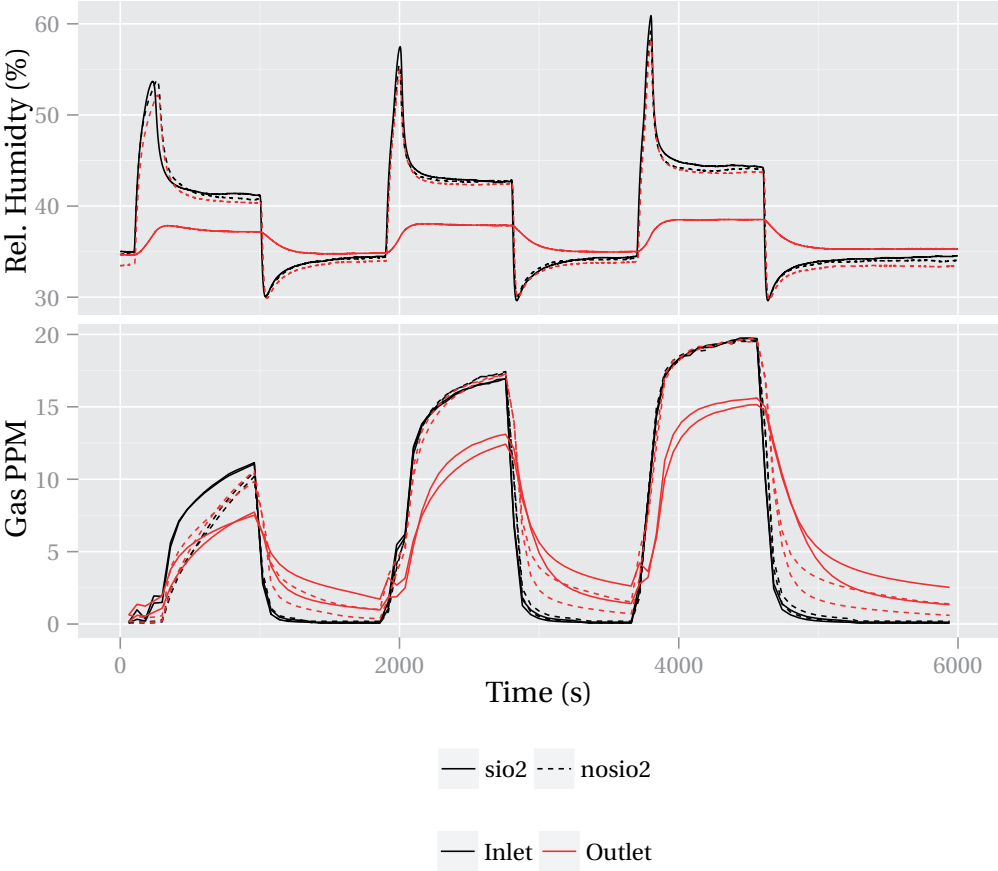
Figure 6.6 – Graph of NO$_2$ experiment
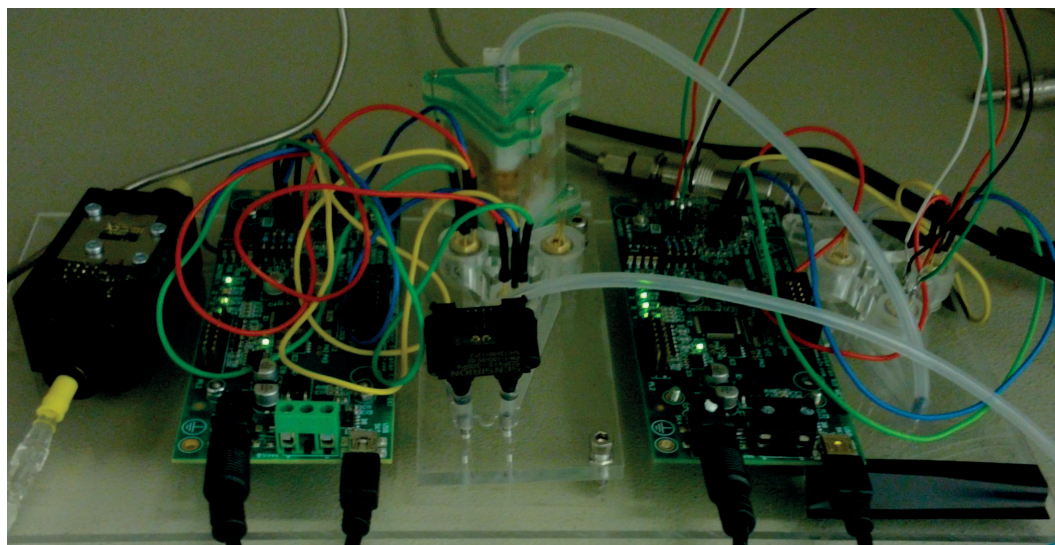
(a) place silica gel in system in wait for sensor equilibrium
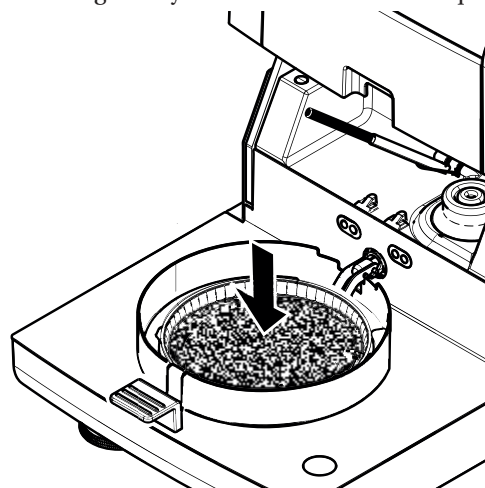
(b) place sample in moisture analyzer

Figure 6.7 – Steps used to create the isotherm data for VOCs and combustion gases

6.2.3   Humidity Leak During Isotherm Experiments with Toxic Gases

In addition to the water experiments, tests were conducted to try to determine the isotherms for the toxic gases. The experimental methods used to determine the VOC concentration were slightly different than those used for water. Specifically, because carbon monoxide, formaldehyde and nitrogen dioxide are gases at room temperature, it was not possible to use a bubbler to generate samples with different adsorbed concentrations. Therefore, air or nitrogen with a known quantity of VOC was created using the platform described in Figure 3.7 in Section 6.2.2. This gas was run through the multisensor device until the metal oxide sensors were at equilibrium. The preconditioning unit was then opened and the silica gel placed into the moisture analyzer (Figure 6.7). The difference in mass before and after desorption was

Chemical	ppm	Humidity	Dry Content
Formaldehyde	2	1.26	978
	8	5.00	970
	14	3.73	976
	20	5.04	962
	50	3.73	965
	100	0.17	979
Carbon Monoxide	20	-1.73	994
	40	0.11	981
	60	-1.95	995
	80	2.80	970
	100	-2.03	997
Benzene	2	1.63	972
	8	-0.013	982
	14		887
	20	4.08	973

Table 6.3 – Results of the equilibrium values for the toxic gas measurements

found. This was used to create isotherm curves for these gases.

Unfortunately, these results, presented in Table 6.3 were unsatisfactory: somewhere in the experimental setup, trace amounts of humidity got into the system. The result was data which correlated more with the trace humidity than the amount of VOC in the system (Figure 6.8). Additionally, the authors of [Baur et al., 2015] were contacted to see if their isotherm measurement equipment could be used. However, the mass spectrometer was broken, and was too expensive to replace without additional funding. Therefore, toxic gas data was taken from literature using the equations in Section 3.3.1.

6.2.4 Humidity Leak During Water Isotherm Experiments

Prior to the moisture analyzer experiments, which determined the isotherm for water on silica gel, a platform was made to sequentially measure the adsorption isotherm of a liquid analyte on an adsorbent. The working principle of this platform is that by starting with no analyte in a closed system with recirculating air, small quantities could be injected at the inlet of the preconditioning unit. Over time, the analyte would evaporate and be adsorbed onto the silica gel in the preconditioning unit. Once the concentration of analyte at the inlet and the outlet sides of the preconditioning unit were the same, and not changing with respect to time, an equilibrium value could be taken. Then another small aliquot of analyte could be added, and the process repeated to find the next value and so on, until the entire curve had been generated.

To do this, a device was created which held two sensors, one placed before the preconditioning
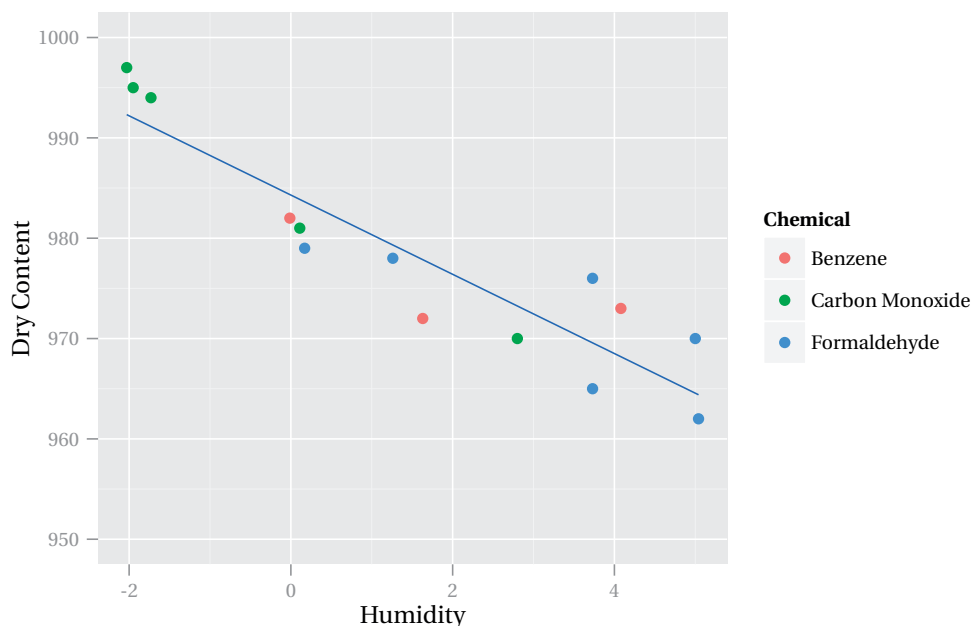
Figure 6.8 – Correlation of relative humidity values and dry content
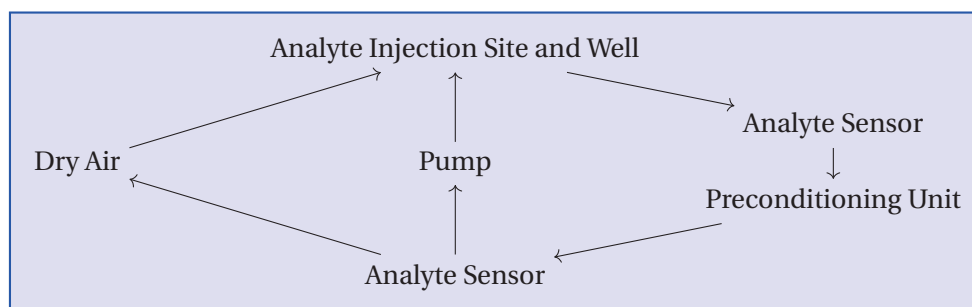
Figure 6.9 – Schematic of the flow through the isotherm measurement device.

unit, one placed after. An injection site and small well were placed before the first sensor. Flow was generated through the system by a Schwarzer Precision 135 FZ miniature vane pump. Additionally, during setup, clean dry air was run through the system to stabilize the sensors and remove any residual humidity from air trapped in the device. The overall schematic of the platform and a drawing of the platform itself can be seen in Figures 6.9 and 6.10, respectively.

After construction, the platform was tested using water. The equilibrium data can be seen in Figure 6.11. Here, the inlet side of the preconditioning unit is red while the outlet side is black. There is a difference in these values because the sensors used do not have perfect calibration curves. Therefore, they contain a maximum error in their reading which ranges from ±1.7%, at normal room humidities to ±4.0% at 0 or 100% relative humidity. The time and inlet values, shown as blue points, were used as the equilibrium value for the isotherm calculations in
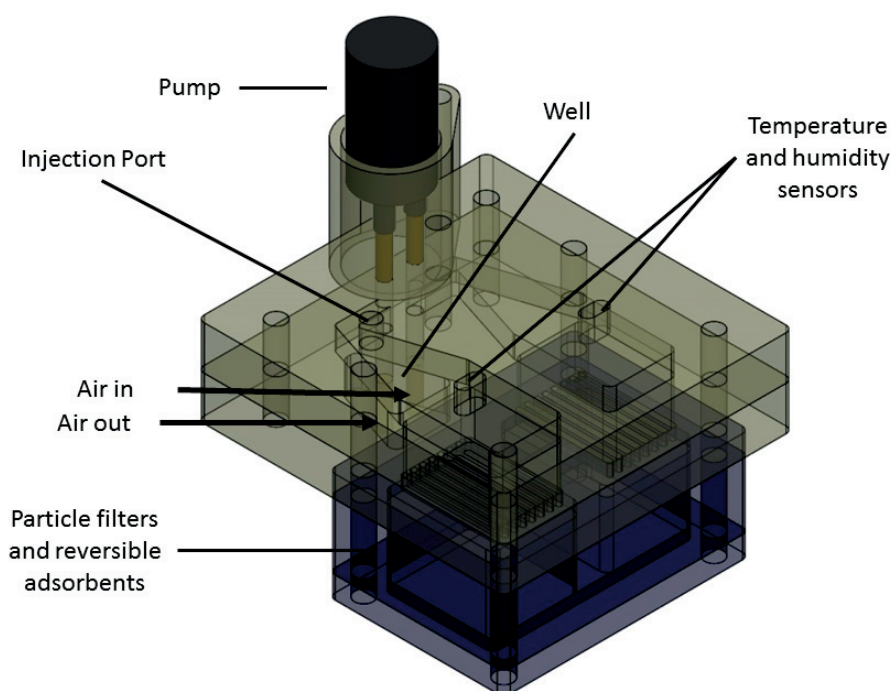
Figure 6.10 – Solidworks rendering of the isotherm measurement device.

Figure 6.12, top, where they appear as red dots. The black dots are the corresponding outlet values.

Additionally, because temperature was not controlled, but has a large effect on the amount of water which can be adsorbed onto a given substrate, this too was measured. The values for each equilibrium point can be seen in Figure 6.12, bottom. As temperature varied randomly with water content, and its range was small, it does not seem that it would contribute significantly to final isotherm curve.

Although it may seem that the final curve is quite good: it is smooth and there is a value for each point which lies within the error range for both sensors, there are two problems with this data. First, because data is collected sequentially, errors accumulate in the system. For example, if the user added more liquid than intended halfway through the experiment, all data after that point would also contain those errors. Alternatively, if too much or too little liquid is consistently added at each step, the overall system can be off by a large quantity. This could happen when a researcher does not know which part of a meniscus to read when measuring a liquid.

The second and more important problem is that the system does not appear to be air tight. It is likely that there was a very small leak in the pump or the metal connections which extend

Figure 6.11 – Continuous sensor readings during the experiment.

out of the device, or both. This can be seen in the concave equilibrium value around 5000 seconds and the convex values at high humidities. This means that when the system has a low humidity, humidity is also being transported into the system. At high humidities water is also being lost to the outside environment. Because of this leak and the fact that the errors accumulate in the system over time, this method was rejected in favor of the moisture analyzer method. However, this does not mean that the the experiments do not contain a valuable lesson: it is not the final solution that determines if a scientific experiment makes sense, but every step taken to that final answer must also be logical and correct. If every step had not been checked, the leak would have never been detected and a bad isotherm would have been used in the body of this thesis.

6.3 Lessons Learned About Research (In This and Other Projects)

6.3.1 Good Collaboration Equals Better Research and more Coauthorships

CSEM is a coauthor on 1 journal article and 2 conference proceedings with CEIT. CEIT is a coauthor on 1 poster, 2 conference proceedings, two Scientific and Technical Reports and (potentially) 1 journal article. CEIT helped CSEM by providing a lab to test the platform, whereas CSEM designed many components of the system to fit CEIT's sensor's needs. This was possible because our research backgrounds are very different, but complementary.
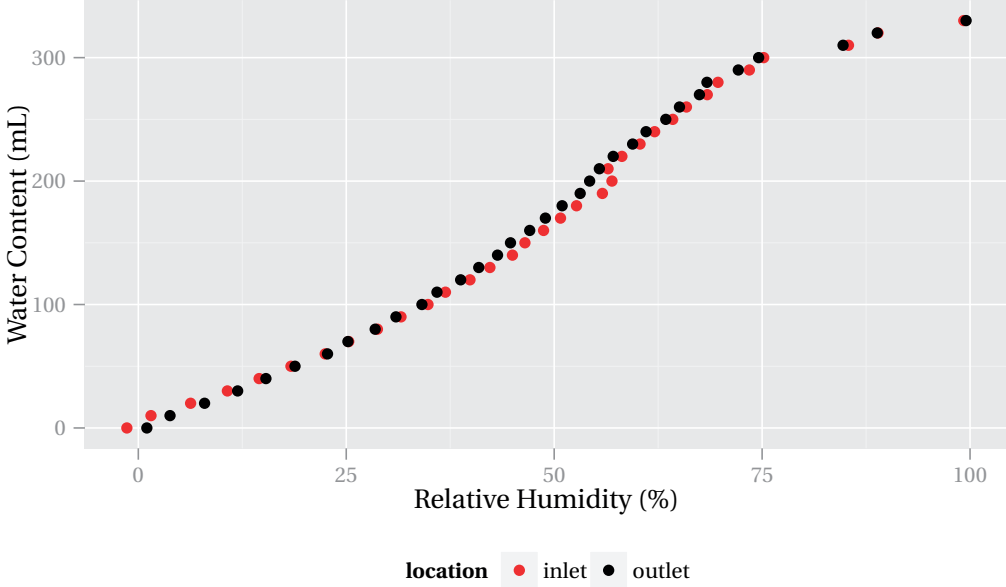
(a) Humidity measurements
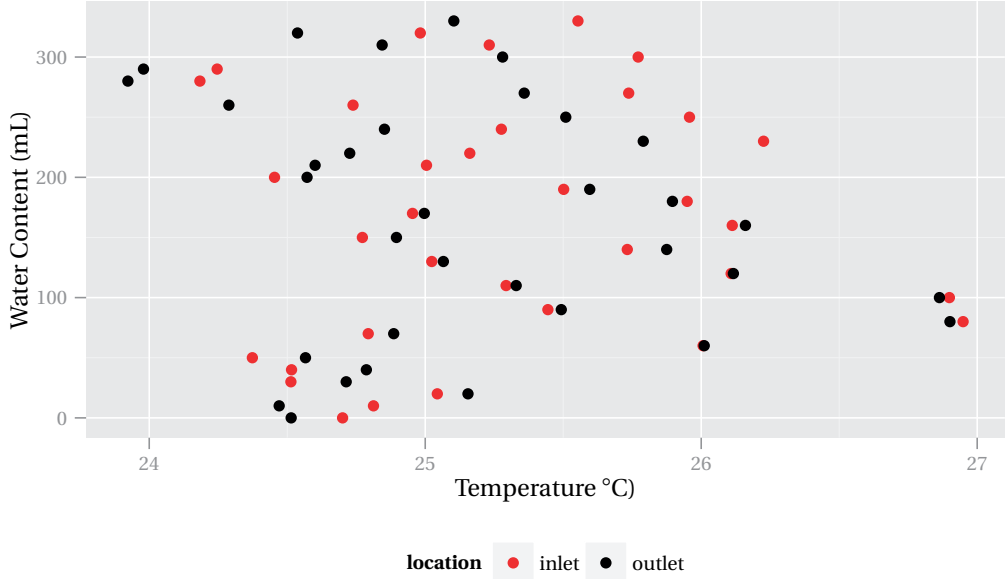
(b) Temperature measurements

Figure 6.12 – Isotherm found using data measured using the isotherm measuring platform.

6.3.2 Do Not Create a Project where your Success Depends on Others

While in the doctoral school at the Max Planck Institute in Magdeburg, my primary research project was to develop a model of mesenchymal stem cell differentiation using proteomic data. Eventually this model was to be validated using the experimental results of three biological researchers in a different laboratory in Western Germany. However, due to complications with working with these cells, no data was generated. Because the model could not be validated, it was not publishable.

A similar, but less severe, situation happened in the INTASENSE project. Specifically, it took much longer to create a working demonstrator of the particle sensor than originally planned. Additionally, although it was possible to make a UV activated metal oxide sensor, it was not as reliable as the heat activated prototypes. Ultimately, time was lost in the learning process, which meant that there were delays in the development of a final microfluidic and electronics platform to house the prototype sensors. In the end, there was not enough time left on the grant for testing in real world environments, such as hospitals or hotels.

6.3.3 Include Funding for Testing Equipment or Facilities Rental in the Original Grant

This was a problem when converting my work on the Intasense project into a Ph.D. thesis. Specifically, laboratory and real world experiments using the integrated system were going to be done by our partners, thus we did not request funding for the equipment to conduct these tests. However, due to a number of delays it was not possible to thoroughly do these experiments before the INTASESNSE grant ended. This meant that I needed to do experiments with the toxic gases and CSEM needed to fund them. Specifically, CSEM lacked the mass low controlers, a gas mixer, a bubbler and tubing which was chemically resistant. It was possible to use CEIT's lab space for free, however, staying in San Sebastian cost almost the same amount as conducting the experiments at Siemens Building Technologies. Ultimately, the price of these experiments was around 1,000 chf per week, which quickly adds up to a large sum of money. It is difficult for a company to come up with these funds if they are not included in the original grant.

6.3.4 Read Up on Safety Regulations and Include Safety Equipment in the Original Grant

The materials required to conduct gas experiments would have cost CSEM around 10,000-14,000 chf. However, this is only a fraction of the actual cost because safety infrastructure is required when working with toxic gases. This includes storing the toxic gases in a location with limited access, fire proofing and an air turnover of 3 to 5 times per hour. Gas mixing needs to be conducted in a location which has a lower pressure than the room pressure. Experiments need to be conducted in the hood, in case of leaks in the system. Finally, alarm

systems which monitor the toxic gases need to be installed in the room or worn by the experimenter. Although CSEM could have purchased the experimental equipment, setting up a lab dedicated to toxic gas experiments was prohibitively expensive. Moreover, there are very few laboratories dedicated to this type of research. Locating a lab space which had this equipment and setting up contracts between companies proved to be one of the most time-consuming and challenging aspects of this project.

6.3.5   Conduct Experiments Remotely Only When Absolutely Necessary

Conducting experiments remotely, in my experience, has meant an additional time constraint on the experiments. Specifically, the researcher must arrive at the new lab, set up equipment, run experiments back to back, often with no time to completely analyze the acquired data before returning home. This means that all possible equipment failures need to be considered before the researcher begins to pack and ship equipment. Duplicates of all components (at a bare minimum) need to be created or acquired so that a failure of one piece of equipment does not cause the entire set of experiments to fail. Additionally, any programs for data analyses (or confirmation of experimental success) need to be written prior to arriving at the remote laboratory. A priority schedule needs to be created in order to assure that the most important experiments are conducted and that time is not wasted at the remote location. Additionally, a backup plan needs to be made so that, when the originally planned experiments do not work as intended, an alternative method can be employed to acquire useful data. Lastly, the researcher should bring any emergency medication (antibiotics, epinephrine etc.) so that experiments do not need to be canceled as a result of infection or allergic reaction and an extra week or two of other medications so that the researcher can easily extend their stay if necessary.

6.3.6   Reaching Statistical Significance Can Require More Experiments Than Originally Planned

This was particularly the case with my neruo-rehabilitation research. When I was an undergraduate, I conducted experiments at the Rehabilitation Institute of Chicago, Marquette University and Northwestern University. In these experiments we tested the nervous system of stroke survivors and healthy controls to determine how humans learn new motion. Specifically, we wanted to see if the spinal cord (responses like knee jerks), the brain or both are involved. At the end of the project we had collected almost a dozen sets of data. This was sufficient to see trends, but not nearly enough to reach statistical significance. Further funding needed to be acquired.

6.3.7 The First Design May have Flaws that Will Require Redesign

A few components in the INTASENSE platform required a redesign at some point in the project. The first example was in the restriction which allows the differential pressure sensor to act as a flow meter. In the original design, I glued components together. However, because the channels were quite small and small qualities of glue entered and dried inside the channel during gluing process, the restrictions were statistically different from each other. This meant that each channel needed to be calibrated. In the next design, I eliminated the need for this calibration by using an adhesive foil to create the restriction. This new design allowed the channels to be identical within statistical bounds.

Another design flaw which we overcame in the INTASENSE project involved thermal insulation of the sensors. Inadequate sensor surface insulation caused part of the housing to melt to the sensors during experiments. To resolve this problem I worked with researchers at CEIT, and Gooch and Housego. They came up with better insulation methods for the sensors, while I conducted heat and mass transport simulations and made replacement components from a material which can get much hotter without being damaged. In the end we had a solution which could work long-term.

6.3.8 Experimental Labs Take More than One Year to Establish

Be it building a new X-ray device, setting up chemical equipment or setting up a laboratory which uses animal models—it takes many months to set up a new lab. While at Illinois Institute of Technology, over the course of 2 years, I helped Dr. Papavasiliou establish her lab. Originally, the plan was to spend a few months conducting experiments, and then use this data to build a computational model of the surface initiated photopolymerization reaction. However, it took far longer than expected to establish the lab. After 2 years of research, we had enough experimental data to publish one paper and no computational model. While at EPFL and CSEM I have seen researchers take similar lengths of time to turn an empty room into a working laboratory.

6.3.9 Plan 18 Months between Submission and Publication of a Journal Article

Both the Urban Climate and the Tissue Engineering Publications took this long.

6.3.10 Do Not Use Funding from a Project to Fund a Researcher Who cannot Work on the Project

While working on a bioengineering project in a previous lab, I was being funded by a project which another student was working on. In turn, the funding for the project I was working on was being used to fund a third student and so on. Each of these grants had different termination dates, which was fine, as long as grants kept being accepted. However, with the

economic crises first in the USA, and then in Europe, the lab ended up short of funds. Contracts were uniformly extended for 6 months, then 3 months. Some students graduated earlier than originally planned. In the end, the lab ended up with funding for multiple biological projects, but no researchers with a biological background.

6.4 Technical Drawings

6.4.1 Single Sensor Platform
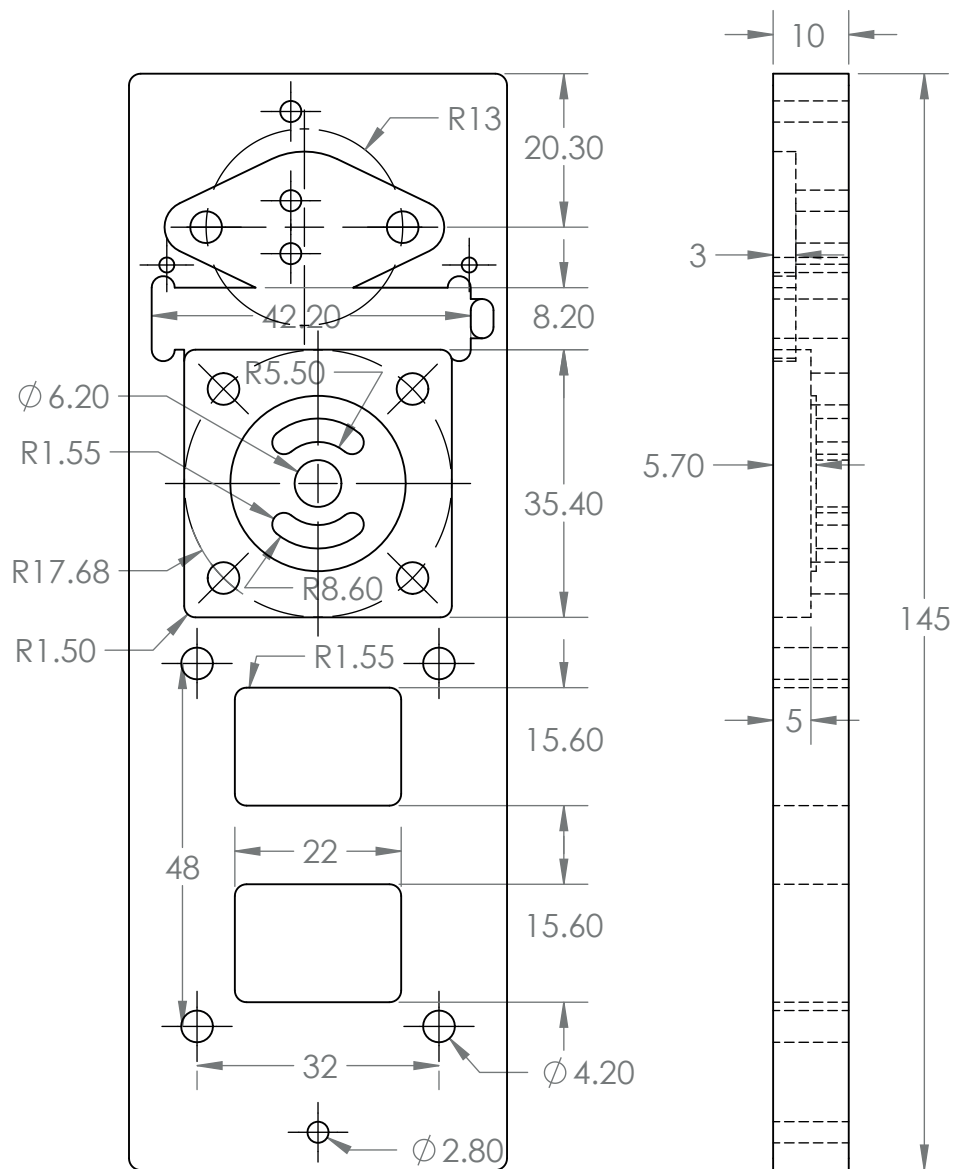
Figure 6.13 – Base top of the single sensor platform for use with the U shaped pressure channel. This component is tan in Figure 2.2. Labels are in millimeters.
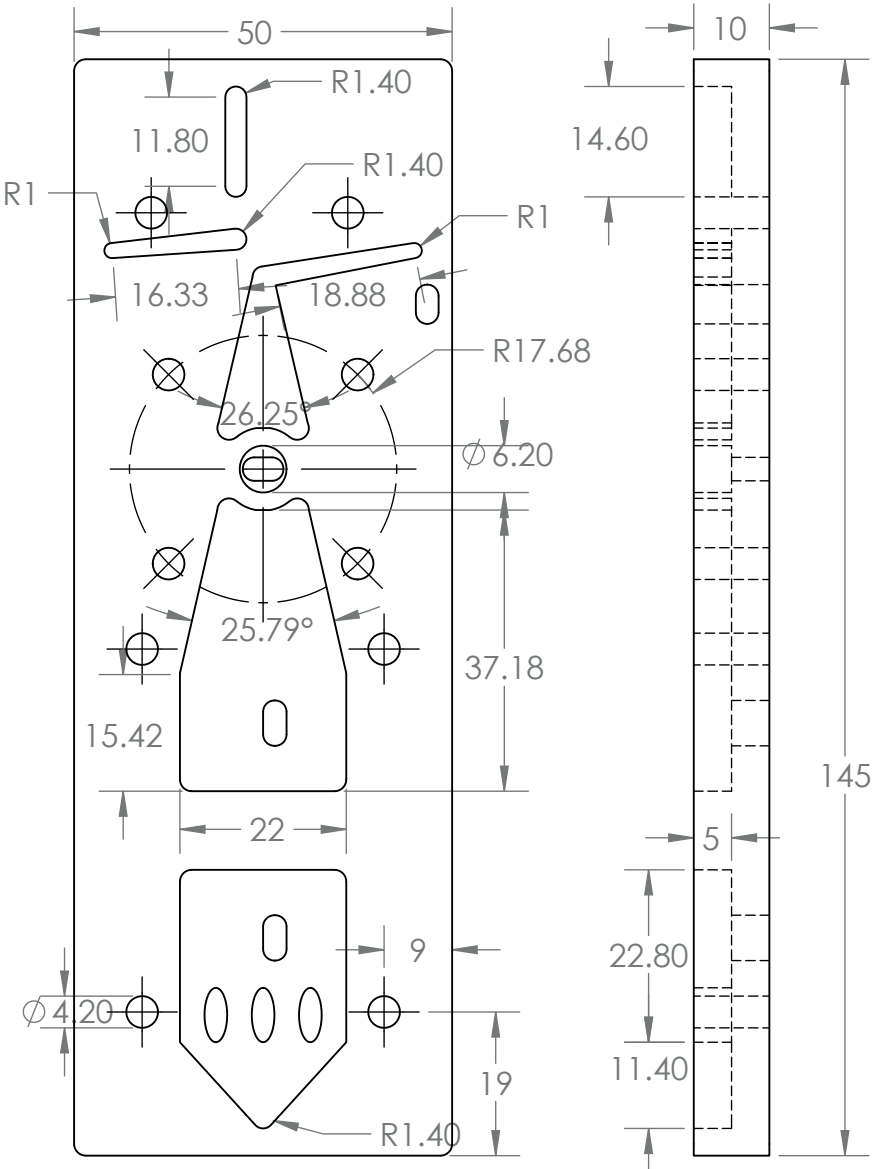
Figure 6.14 – Base bottom of the single sensor platform for use with the U shaped pressure channel. This component is tan in Figure 2.2. Labels are in millimeters.
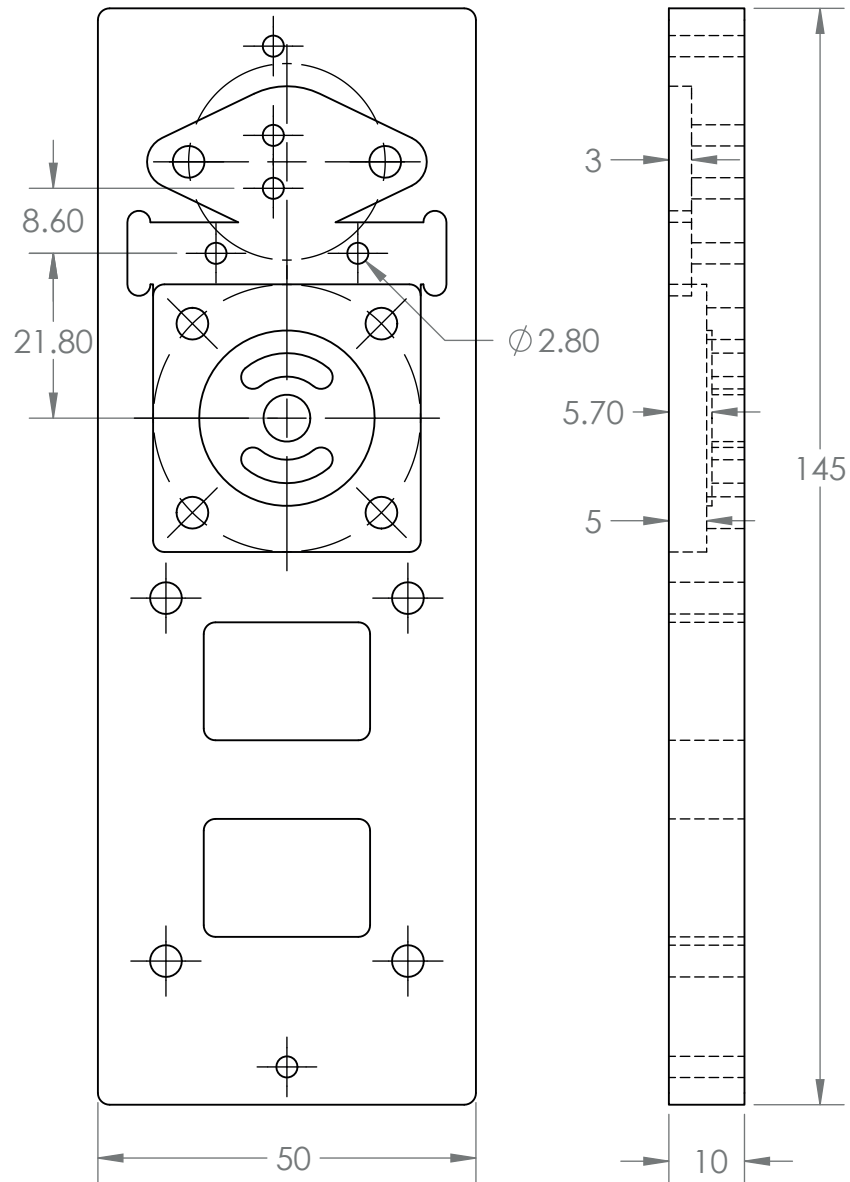
Figure 6.15 – Base top of the single sensor platform for use with the S shaped pressure channel. Unmarked dimensions are the same as the part in Figure 6.13. This component is tan in Figure 2.2. Labels are in millimeters.
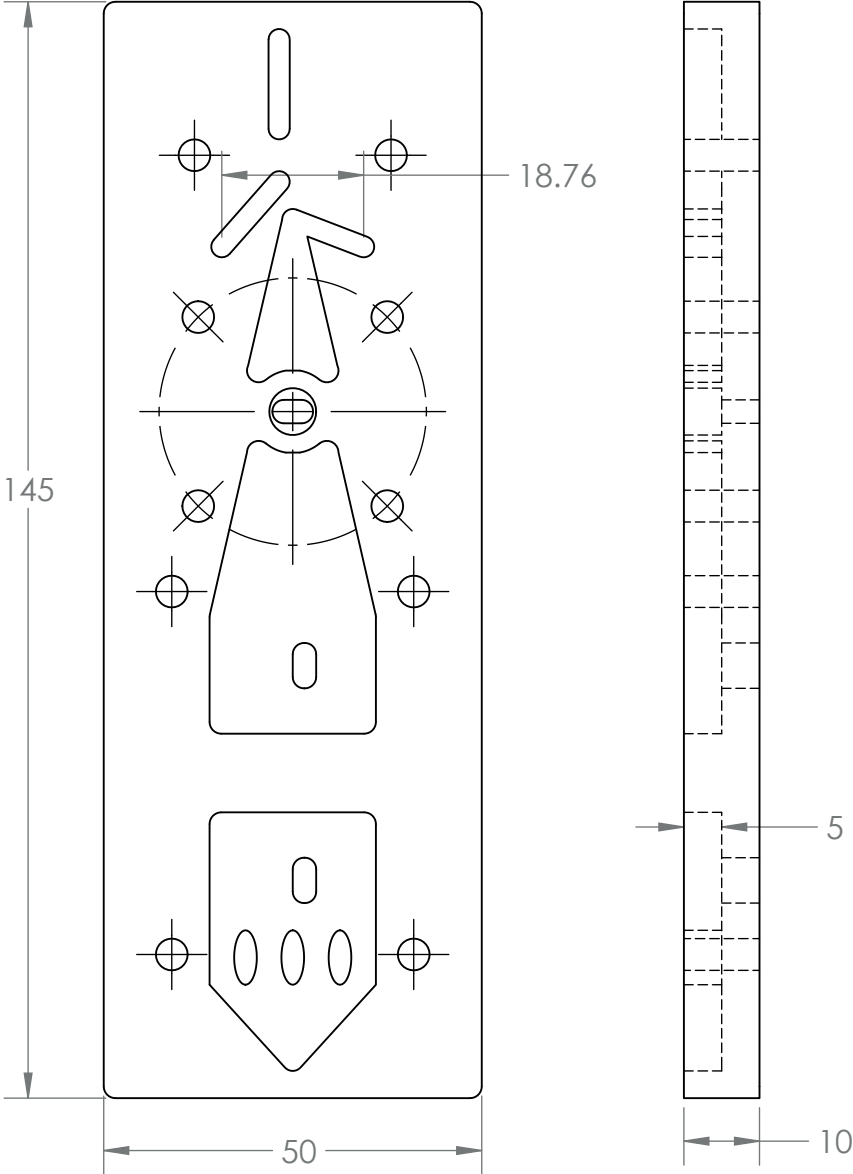
Figure 6.16 – Base bottom of the single sensor platform for use with the S shaped pressure channel. Unmarked dimensions are the same as the part in Figure 6.14. This component is tan in Figure 2.2. Labels are in millimeters.
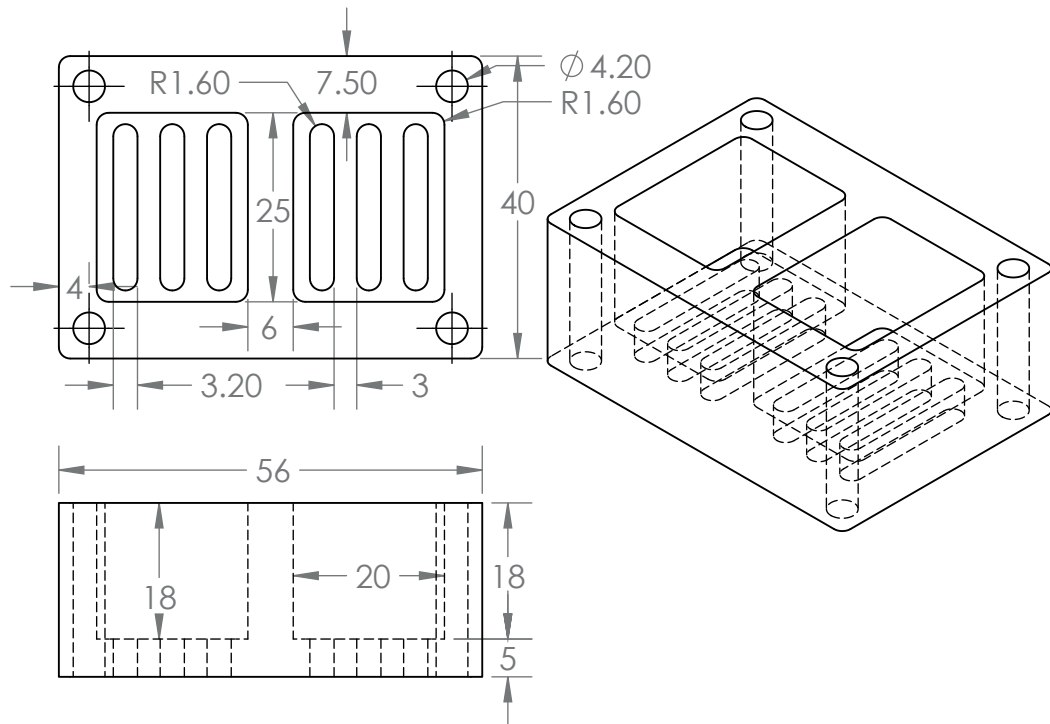
Figure 6.17 – Base of the preconditioning unit used in the single sensor platform. This component is purple in Figure 2.2. Labels are in millimeters.

Figure 6.18 – Lid of the preconditioning unit used in the single sensor platform. This component is purple in Figure 2.2. Labels are in millimeters.
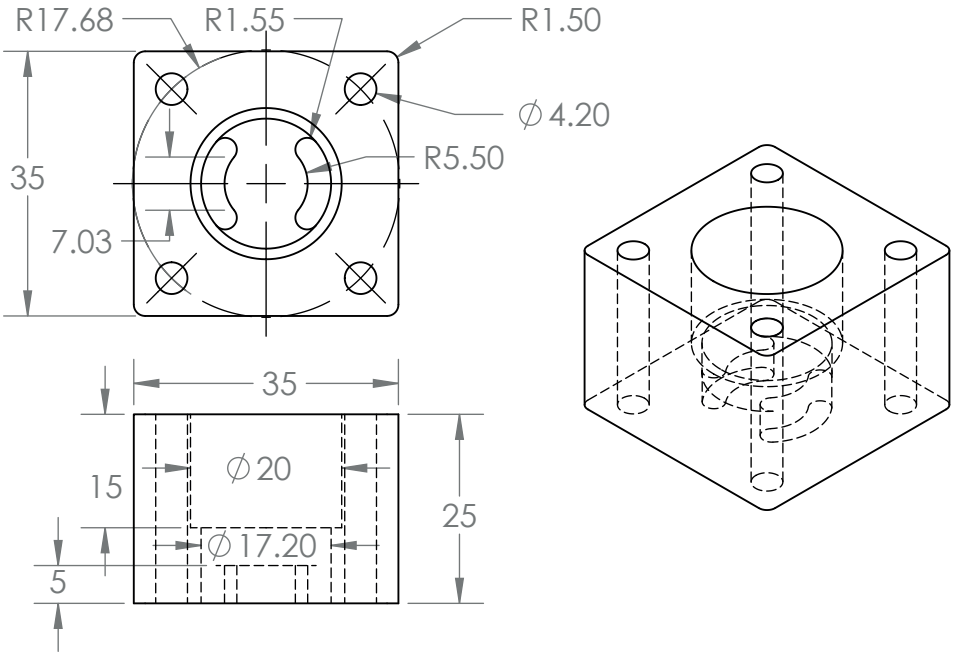
Figure 6.19 – Base of the electrochemical sensor housing. This component is green in Figure 2.2. Labels are in millimeters.
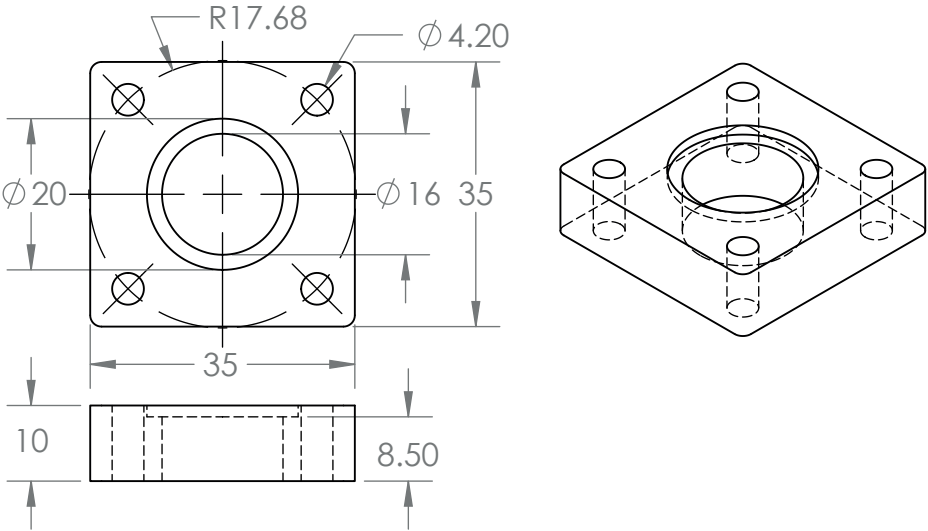
Figure 6.20 – Lid of the electrochemical sensor housing. This component is green in Figure 2.2. Labels are in millimeters.
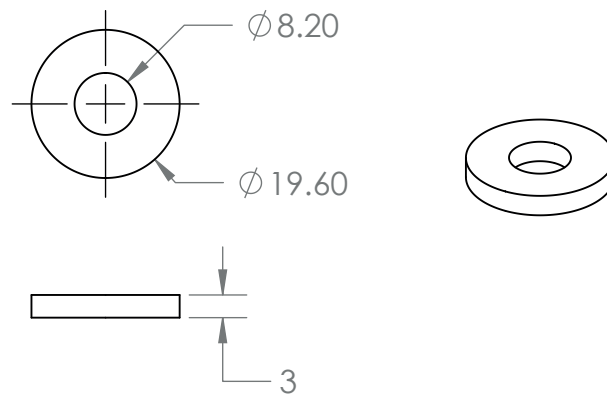
Figure 6.21 – Plastic washer for the metaloxide sensor housing. Labels are in millimeters. The thickness of this washer should be adapted so that thesensor surface is flush with the washer. Additionally, this should be manufactured in conjunction with the component in Figure 6.19, however the sensor cavity depth must be reduced to allow a tight fit with the shorter sensor, while maintaining a 5 mm high fluidic path.
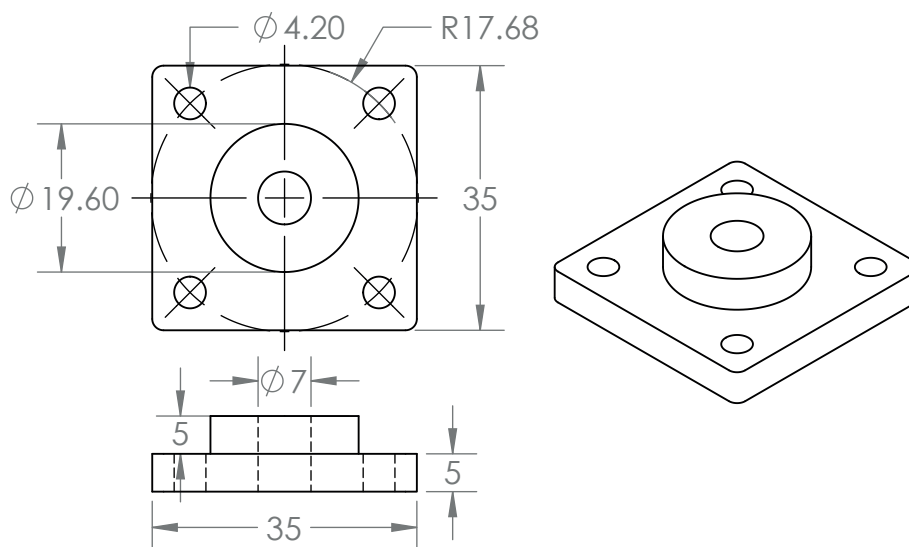
Figure 6.22 – Lid of the metaloxide sensor housing. Labels are in millimeters.
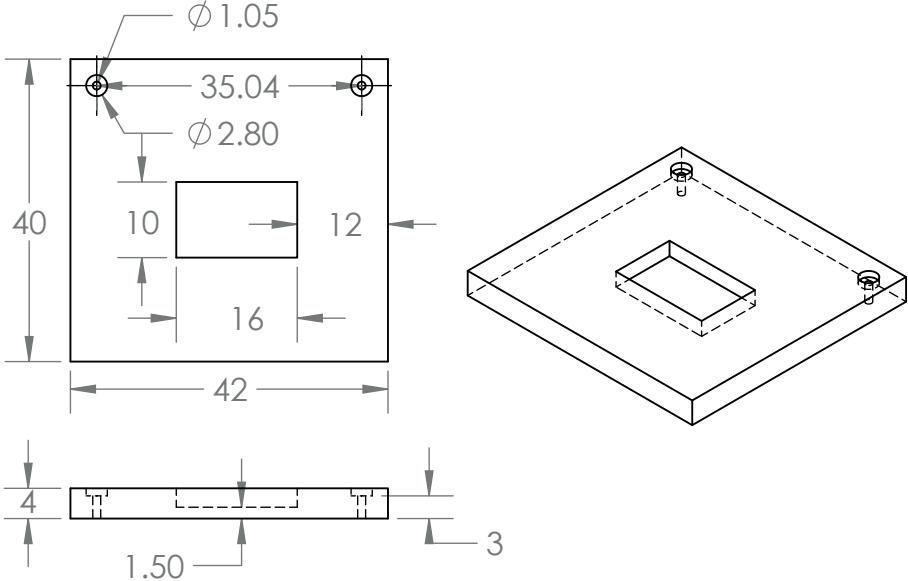
Figure 6.23 – Front of the first (U shaped) version of the differential pressure channel. Labels are in millimeters.
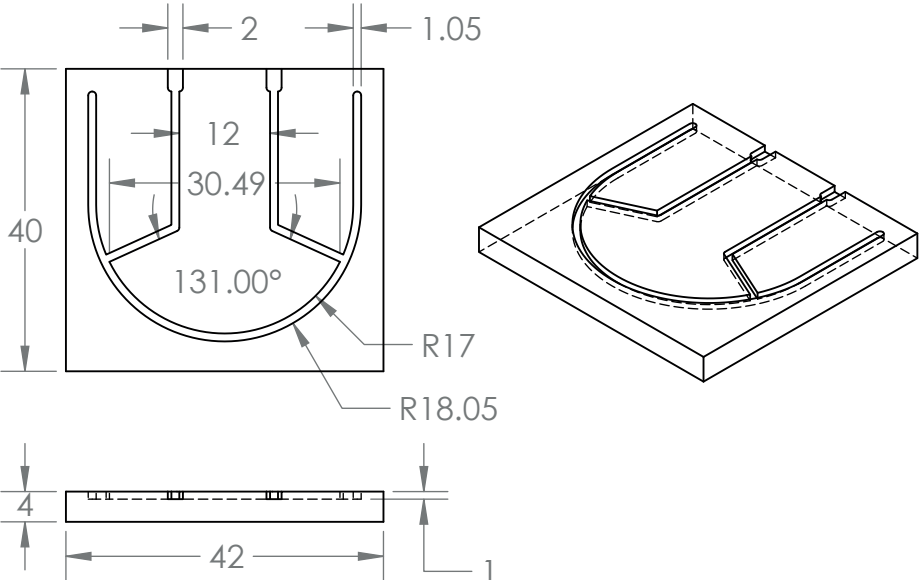
Figure 6.24 – Back of the first (U shaped) version of the differential pressure channel. Labels are in millimeters.
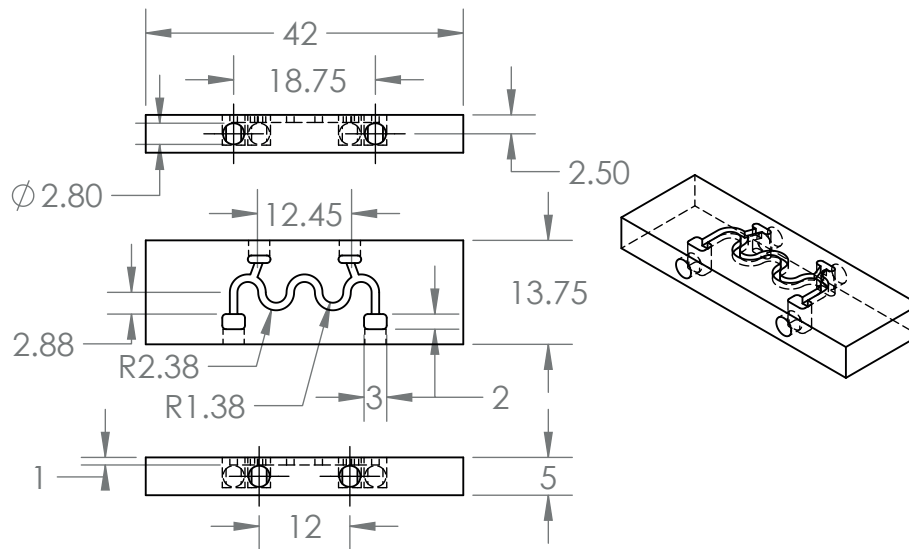
Figure 6.25 – Second version of the differential pressure channel. This component is red in Figure 2.2. Labels are in millimeters.
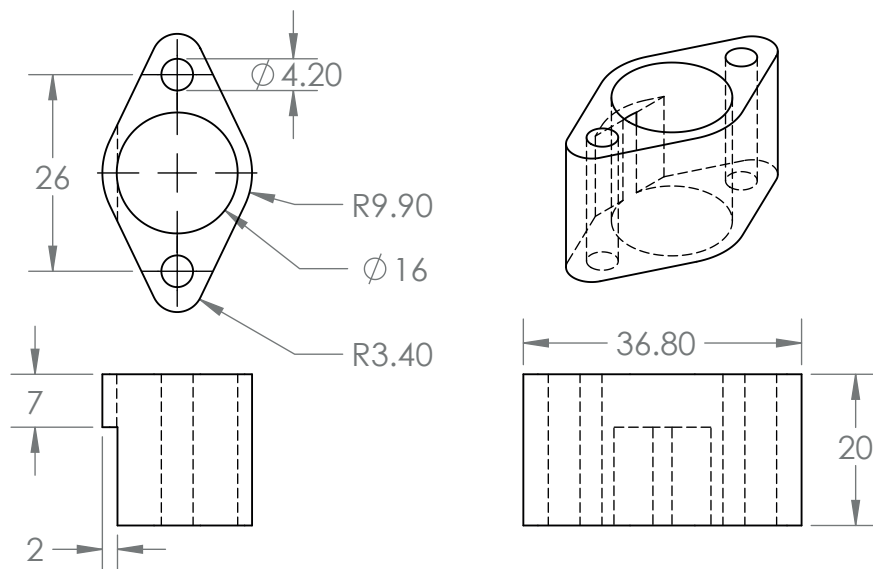
Figure 6.26 – Pump holder used in the single sensor platform. This component is white in Figure 2.2. Labels are in millimeters.

6.4.2 Metaloxide Sensor Platform
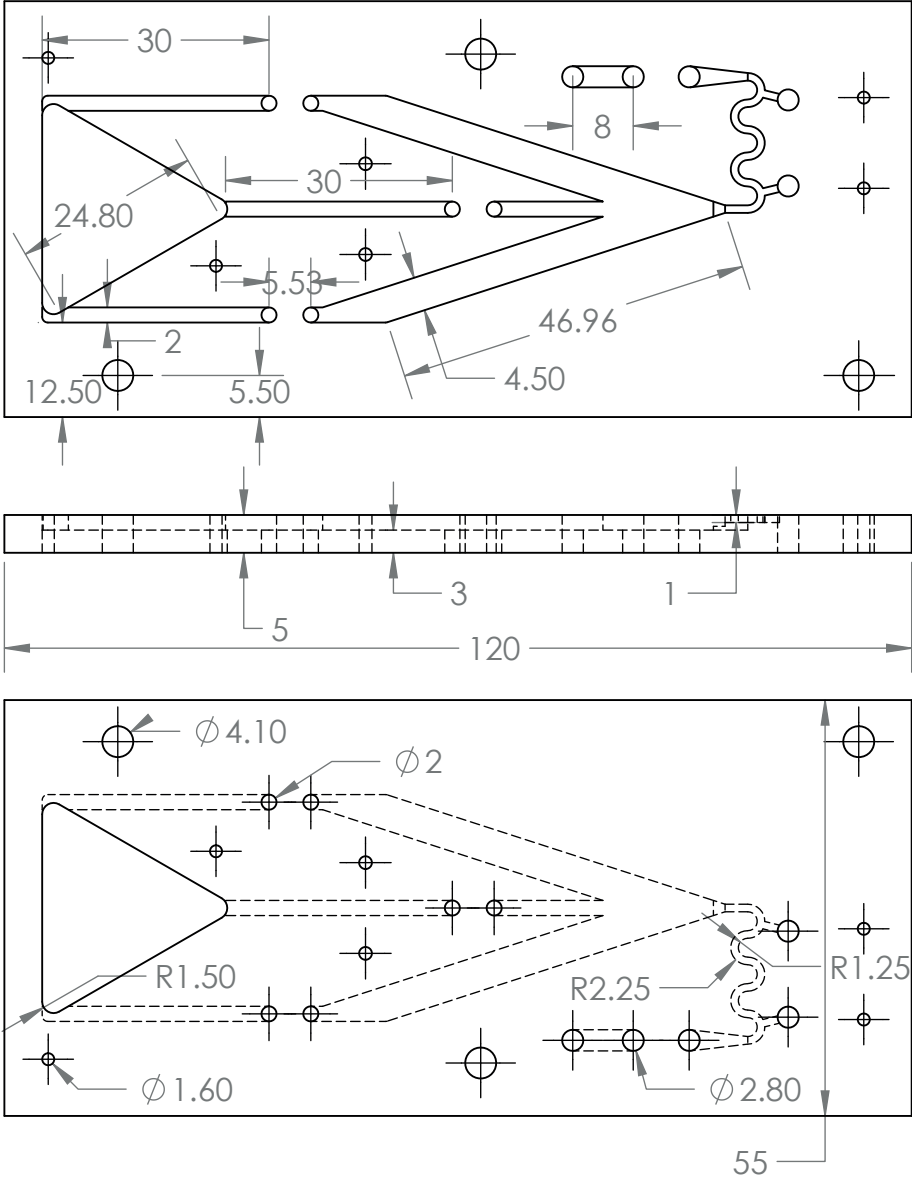
Figure 6.27 – Base of the metaloxide sensor platform. This component is tan in Figure 2.17. Labels are in millimeters.
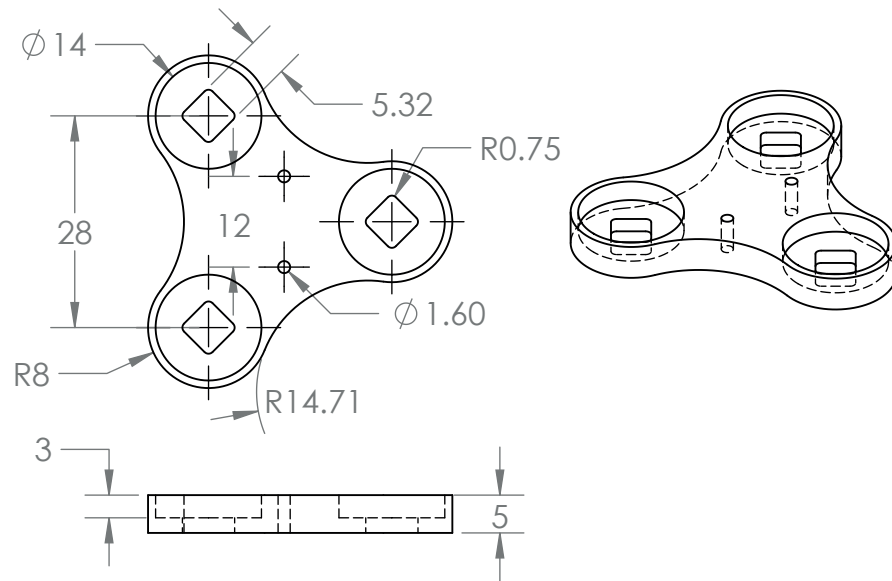
Figure 6.28 – Gas sensor lid of the metaloxide sensor platform. This component is green in Figure 2.17. Labels are in millimeters.
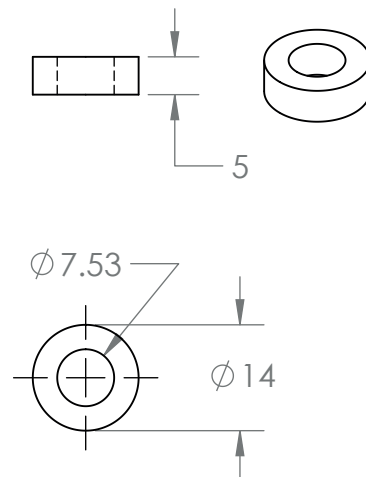
Figure 6.29 – Sensor holder for the metaloxide sensor platform. This component is green in Figure 2.17. The inner radius and thickness of material must be adjusted based on metal oxide sensor dimensions. Labels are in millimeters.
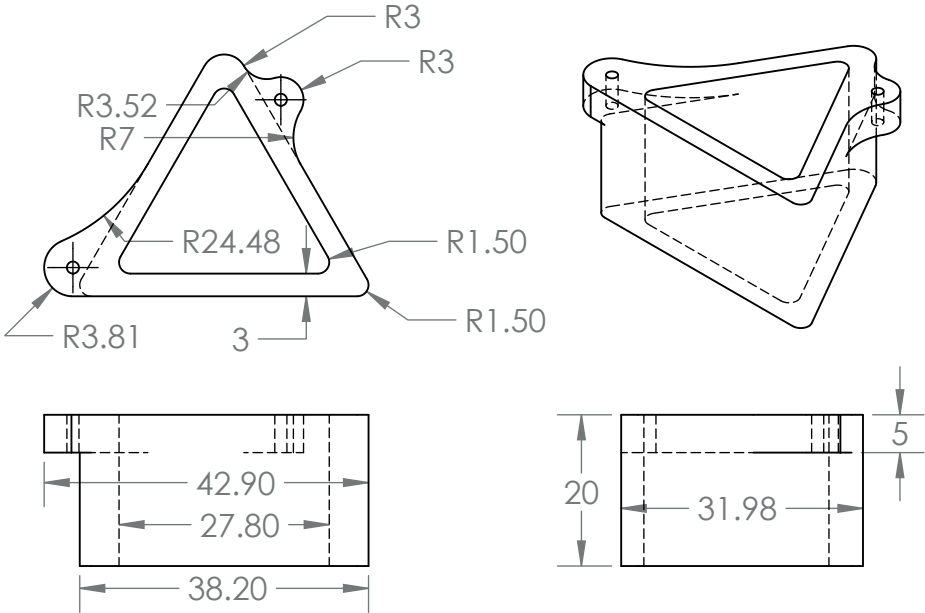
Figure 6.30 – Half of the preconditioning unit column for the metaloxide sensor platform. This component is purple in Figure 2.17. Labels are in millimeters.
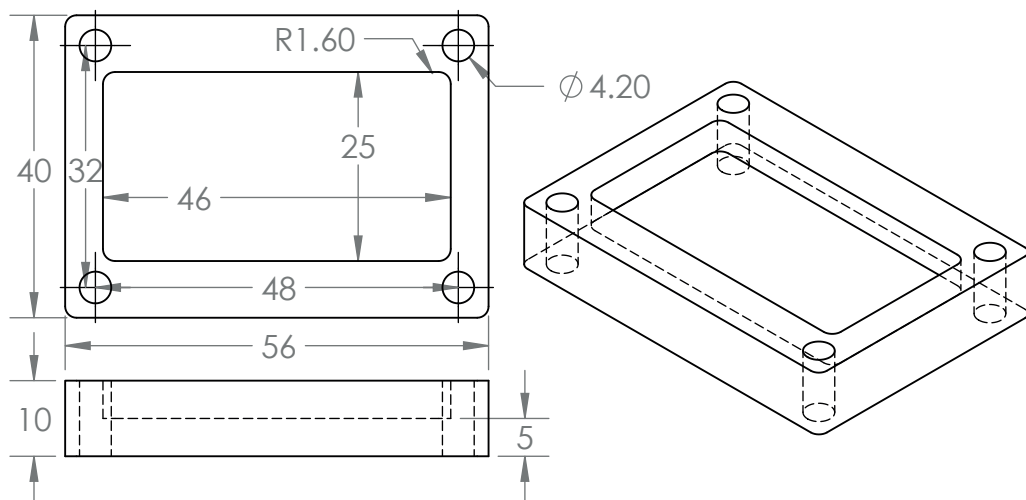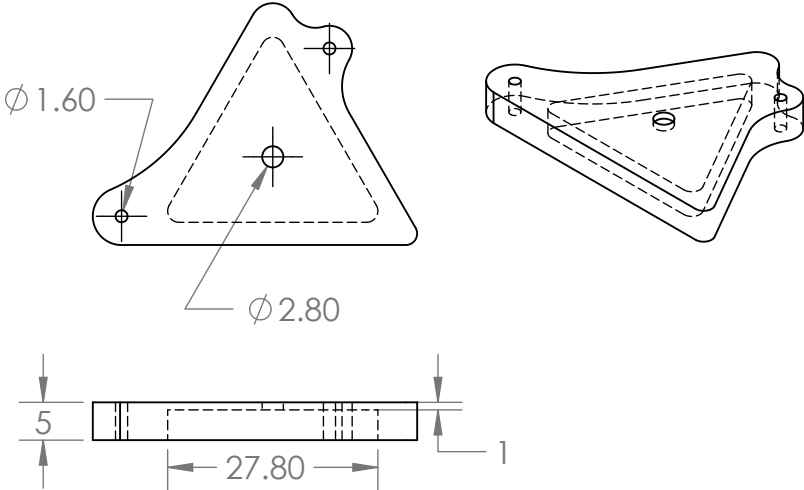

Figure 6.31 – Top of the preconditioning unit column for the metaloxide sensor platform. This component is purple in Figure 2.17. Labels are in millimeters.
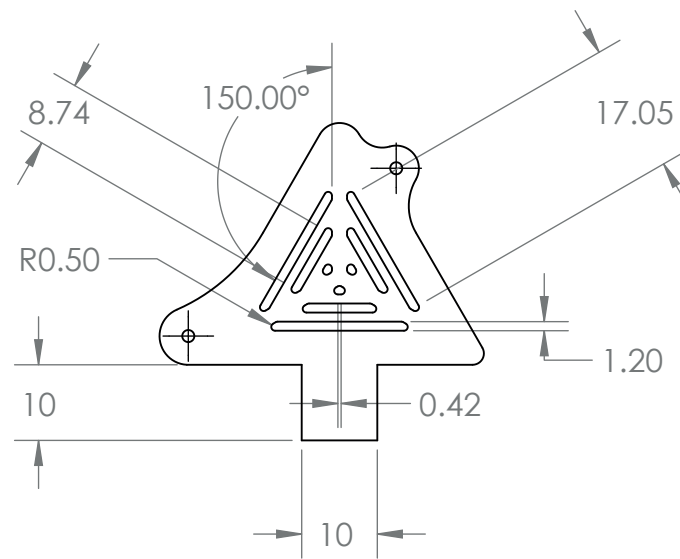
Figure 6.32 – PCB outline used in the preconditioning unit column for the metaloxide sensor platform. This component is dark green in Figure 2.17. Labels are in millimeters.

6.5 Latin Square Mathematics

Latin Squares, and Greco-Latin Squares, are used to determine the effects of single compo-
nents within a system using the minimum number of experiments. For example, imagine a
manager at a factory wants to increase productivity, but does not know if the worker, the
machine or the setting of the machine have significant effects on the number of items
produced. Moreover, the manager cannot simply test a single item in this group (i.e. the
setting) without having influence from the worker or the machine itself.

To solve this problem with the minimum number of experiments, the manager can set up a
system where the error from a specific component (i.e. worker) effects the results for every
other component equally (i.e. machine or setting), and then use a statistical analysis to
determine which effects are significant.

The steps involved are:

1. Number each item, and group them so that each item is used exactly once with each
   other item. For example:

		Worker 1	Worker 2	Worker 3
	1	1	3	2
Machine	2	3	2	1
	3	2	1	3

Setting

or

		Worker 1	2	3	4	5
	1	1	2	3	4	5
	2	2	3	4	5	1
Machine	3	3	4	5	1	2
	4	4	5	1	2	3
	5	5	1	2	3	4

Setting

2. Then data for each combination is collected. For example, this could be how many
   devices are made in a given day. For simplicity, let us use the 3 by 3 example, and assume
   our results are:

		Worker		
		1	2	3
	1	22	37	29
Machine	2	24	33	30
	3	23	35	32

Devices Made by worker

Note that the worker and machine values can be used to determine which setting the machine was on because each parameter is used exactly once with each other parameter.

3. The next step is to decompose the orthogonal components to create the model for the Latin Square design. Mathematically this takes the form:

$$Y_{ij(k)} = \mu + \alpha_i + \beta_j + \gamma_k + \epsilon_{ij(k)} \quad \text{for } i, j, k = 1, ..., m \tag{6.3}$$

where i, j and k represent the worker, the machine and machine's setting, respectively. Y is the result from an experiment, μ is the average of all results, α_i is the main effects factor for worker i, β_j is the main effects factor for a machine j, γ_k is the main effects factor for a setting k, $\epsilon_{ij(k)}$ is the residual or noise and m is the number of items of each type. In this case, $m = 3$. This equation becomes:

$$\begin{bmatrix} Y_{1,1} & Y_{2,1} & Y_{3,1} \\ Y_{1,2} & Y_{2,2} & Y_{3,2} \\ Y_{1,3} & Y_{2,3} & Y_{3,3} \end{bmatrix} = \begin{bmatrix} \mu & \mu & \mu \\ \mu & \mu & \mu \\ \mu & \mu & \mu \end{bmatrix} + \begin{bmatrix} \alpha_1 & \alpha_2 & \alpha_3 \\ \alpha_1 & \alpha_2 & \alpha_3 \\ \alpha_1 & \alpha_2 & \alpha_3 \end{bmatrix}$$

$$+ \begin{bmatrix} \beta_1 & \beta_1 & \beta_1 \\ \beta_2 & \beta_2 & \beta_2 \\ \beta_3 & \beta_3 & \beta_3 \end{bmatrix} + \begin{bmatrix} \gamma_1 & \gamma_3 & \gamma_2 \\ \gamma_3 & \gamma_2 & \gamma_1 \\ \gamma_2 & \gamma_1 & \gamma_3 \end{bmatrix} + \begin{bmatrix} \epsilon_{1,1} & \epsilon_{2,1} & \epsilon_{3,1} \\ \epsilon_{1,2} & \epsilon_{2,2} & \epsilon_{3,2} \\ \epsilon_{1,3} & \epsilon_{2,3} & \epsilon_{3,3} \end{bmatrix} \tag{6.4}$$

in matrix form.

Values for α, β, and γ are computed using the following formulas:

$$\alpha_i = \frac{1}{m} \sum_{j=1}^{m} Y_{i,j} - \mu \tag{6.5}$$

$$\beta_j = \frac{1}{m} \sum_{i=1}^{m} Y_{i,j} - \mu \tag{6.6}$$

$$\gamma_k = \frac{1}{m} \sum_{i=1}^{m} Y_{i,k} - \mu \tag{6.7}$$

and values for ϵ are solved by substituting all numerical values back into the matrix form of the equation or by computing residuals.

For our example problem this becomes:

$$
\begin{bmatrix} 22 & 37 & 29 \\ 24 & 33 & 30 \\ 23 & 35 & 32 \end{bmatrix} = \begin{bmatrix} 29.44 & 29.44 & 29.44 \\ 29.44 & 29.44 & 29.44 \\ 29.44 & 29.44 & 29.44 \end{bmatrix} + \begin{bmatrix} -6.44 & 5.55 & .89 \\ -6.44 & 5.55 & .89 \\ -6.44 & 5.55 & .89 \end{bmatrix}
$$

$$
+ \begin{bmatrix} -.11 & -.11 & -.11 \\ -.44 & -.44 & -.44 \\ .56 & .56 & .56 \end{bmatrix} + \begin{bmatrix} -.44 & 1.55 & -1.11 \\ 1.55 & -1.11 & -.44 \\ -1.11 & -.44 & 1.55 \end{bmatrix} + \begin{bmatrix} -0.45 & 0.56 & -0.11 \\ -0.11 & -0.45 & 0.55 \\ 0.55 & -0.12 & -0.44 \end{bmatrix}
$$

(6.8)

4. Once the model is found, a statistical test can be conducted using the equations below:

Source	Sum of Squares (ss)	Degrees of Freedom (df)	Mean Square (ms)	F value
μ (means)	$m^2\mu^2$	1		
α (worker)	$\sum_{i=1}^{m} m\alpha_i^2$	$m-1$	$\frac{1}{df_\alpha} ss_\alpha$	$\frac{ms_\alpha}{ms_\epsilon}$
β (machine)	$\sum_{j=1}^{m} m\beta_j^2$	$m-1$	$\frac{1}{df_\beta} ss_\beta$	$\frac{ms_\beta}{ms_\epsilon}$
γ (setting)	$\sum_{k=1}^{m} m\gamma_k^2$	$m-1$	$\frac{1}{df_\gamma} ss_\gamma$	$\frac{ms_\gamma}{ms_\epsilon}$
ϵ (residual)	$\sum_{i=1}^{m}\sum_{j=1}^{m} m\alpha_{i,j}^2$	$(m-1)(m-2)$	$\frac{1}{df_\epsilon} ss_\epsilon$	

After all of these values are calculated, the critical F-value for a given confidence level is determined using a lookup table. When the F-value for an item type is greater than critical F-value, then the null hypothesis is rejected, meaning that the items within a group (workers, machines or settings) are statistically different from each other. Alternatively, p-values can be calculated using the `anovan` function in MATLAB.

For our example problem, the resulting table is:

Source	Sum of Squares (ss)	Degrees of Freedom (df)	Mean Square (ms)	F value	P value
Mean (μ)	7803	1			
worker (α)	220	2	109.78	141.1	.007
machine (β)	2	2	0.78	1.0	.500
setting (γ)	12	2	5.78	7.4	.119
Residue (ϵ)	2	2	0.78	1.0	

Thus, there are significant differences between the workers.

Bibliography

J. Elston Ahlberg. Rates of Water Vapor Adsorption from Air by Silica Gel. *Industrial & Engineering Chemistry*, 31(8):988–992, 1939.

Aizpea Eceiza Alday. *IMPLEMENTACIÓN DE SISTEMA COMPACTO DE MEDIDA PARA SENSORES DE GAS CONDUCTOMÉTRICOS.* PhD thesis, Universidad de Navarra, 2014.

Thomas J. Allen and Rory P. O'Shea. *Building Technology Transfer within Research Universities: An Entrepreneurial Approach.* Cambridge University Press, 2014.

Alphasense Ltd. Application Note AAN 106: Humidity extremes: Drying out and water absorbtion. 44(12):1–7, 2015.

C Antoine. Tensions des vapeurs; nouvelle relation entre les tensions et les températures. *Comptes Rendus des Séances de l'Académie des Sciences*, 107:681–684, 778–780, 836–837, 1888.

A M Azad, S A Akbar, S G Mhaisalkar, L D Birkefeld, and K S Goto. Solid-State Gas Sensors - a Review. *Journal of the Electrochemical Society*, 139(12):3690–3704, 1992.

Dortmund Data Bank. Dortmund Data Bank. http://ddbonline.ddbst.de/AntoineCalculation/AntoineCalculationCGI.exe.

Uwe Bau, Franz Lanzerath, Manuel Gräber, Stefan Graf, Heike Schreiber, Niklas Thielen, and André Bardow. Adsorption energy systems library - Modeling adsorption based chillers , heat pumps , thermal storages and desiccant systems. *Proceedings of the 10th International ModelicaConference*, pages 875–883, 2014.

Guillaume B. Baur, Igor Yuranov, and Lioubov Kiwi-Minsker. Activated carbon fibers modified by metal oxide as effective structured adsorbents for acetaldehyde. *Catalysis Today*, 249: 252–258, 2015.

Kathleen Belanger, Janneane F. Gent, Elizabeth W. Triche, Michael B. Bracken, and Brian P. Leaderer. Association of indoor nitrogen dioxide exposure with respiratory symptoms in children with asthma. *American Journal of Respiratory and Critical Care Medicine*, 173(3): 297–303, 2006.

Bibliography

Robert Byron Bird, Warren E. Stewart, and Edwin N Lightfoot. Transport Phenomena, 2007.

Gt Orgi Bliznakov and Rosa Polikarova. On the Desorption of Ammonia from Silica Gel. *Journal of Catalysis*, 5(1):18–21, 1966.

George E P Box, William Gordon Hunter, and J Stuart Hunter. Statistics for Experimenters: An Introduction to Design, Data Analysis, and Model Building. *Wiley Series in Probability and Mathematical Statistics*, 1st:653, 1978.

J. F. Chang, H. H. Kuo, I. C. Leu, and M. H. Hon. The effects of thickness and operation temperature on ZnO:Al thin film CO gas sensor. *Sensors and Actuators, B: Chemical*, 84(2-3): 258–264, 2002.

Yuyu Chen, Avraham Ebenstein, Michael Greenstone, and Hongbin Li. Evidence on the Impact of Sustained Exposure to Air Pollution on Life Expectancy from China 's Huai River Policy. *Massachusetts Institute of Technology Department of Economics Working Paper Series*, 13 (15):1–53, 2013.

W Cheng. Methanol and Formaldehyde Oxidation Study over Molybdenum Oxide. *Journal of Catalysis*, 158(2):477–485, 1996.

COMSOL. Liquid Chromatography. Technical Report 1, COMSOL.

T. F. Cooke. Indoor Air Pollutants A Literature Review. *Reviews on Environmental Health*, 9(3): 137–160, 1991.

Linda Coyne, Cindy Kuhlman, and Nicole Zovack. The Stability of Sulfur Compounds , Low Molecular Weight Gases , and VOCs in Four Air Sample Bag Materials, 2011. http://www.skcinc.com/catalog/pdf/instructions/1805.pdf.

E. L. Cussler. *Diffusion: Mass Transfer in Fluid Systems*. Cambridge University Press, New York, 2nd edition, 1997.

Levi Yorgey Davidheiser. *The Adsorbtion of Ammonia by Silica Gel*. PhD thesis, Johns Hopkins University, Baltimore, Md., 1921.

Don DeVault. The Theory of Chromatography. *Journal of the American Chemical Society*, 65 (4):532–540, 1943.

E2v. MiCS Application Note 1 MiCS-2610 O3 Sensor Additional Information, 2007a. http://www.sgxsensortech.com/site/wp-content/uploads/2012/10/AN1-MiCS-2610-O3-Sensor-Additional-Information.pdf.

E2v. Pellistor Application Note 1 Pellistor Sensor Technology & Applications, 2007b. http://www.sgxsensortech.com/content/uploads/2014/08/AN1-Pellistor-Sensor-Technology-and-Applications1.pdf.

E2v. Introduction to Electrochemical (EC) Gas Sensors, 2007c. http://www.sgxsensortech.com/content/uploads/2014/08/Introduction-to-Electrochemical-EC-Gas-Sensors1.pdf.

E2v. Infrared Sensor Application Note 1 - A Background to Gas Sensing by NDIR, 2007d. http://www.sgxsensortech.com/site/wp-content/uploads/2012/10/AN1-A-Background-to-Gas-Sensing-by-Non-Dispersive-Infrared-NDIR1.pdf.

Daniel P Eisenberg. Neurotoxicity and Mechanism of Toluene Abuse. *The Einstein quarterly journal of biology and medicine*, (19):150–159, 2003.

European Environment Agency. New Sensing Technologies and Methods for Air-Pollution Monitoring. In *Cost Action EuNetAir*, number October, pages 3–4, Copenhagen, 2013.

European Union (EU). Air Quality Standards. (May 2011):2–3, 2015.

S. Fanget, S. Hentz, P. Puget, J. Arcamone, M. Matheron, E. Colinet, P. Andreucci, L. Duraffourg, Ed Meyers, and M. L. Roukes. Gas sensors based on gravimetric detection - A review, 2011. ISSN 09254005.

Figaro. TGS 2442 - for the detection of Carbon Monoxide, 2007. https://www.soselectronic.com/a{_}info/resource/c/figaro/TGS2442.pdf.

B A Finlayson. *Introduction to Chemical Engineering Computing*. 2006.

R.A. Fischer. *The Design of Experiments*. Hafner Publishing Company Inc., New York, 7th edition, 1960.

K. Y. Foo and B. H. Hameed. Insights into the modeling of adsorption isotherm systems. *Chemical Engineering Journal*, 156(1):2–10, 2010.

Tushar K. Ghosh and Anthony L. Hines. Adsorption of Acetaldehyde, Propionaldehyde, and Butyraldehyde on Silica Gel. *Separation Science and Technology*, 25(11-12):1101–1115, 1990.

James L. Gole and William Laminack. Nanostructure-directed chemical sensing: The IHSAB principle and the dynamics of acid/base-interface interaction. *Beilstein Journal of Nanotechnology*, 4(1):20–31, 2013.

S Golshan-Shirazi and Georges Guiochon. Analytical solution for the ideal model of chromatography in the case of a pulse of a binary mixture with competitive Langmuir isotherm. *The Journal of Physical Chemistry*, 2374(13):4143–4157, 1989.

Georges Guiochon and Bingchang Lin. *Modeling for Preparative Chromatography*. Acadmic Press, San Diego, 2003.

Emily Hammes, Jurgi Gonzalez-chavarri, Liam Henwood-moroney, Garcia Mandayo, Peter Ryser, and Helmut F Knapp. A Smart Air Quality Monitor for Energy Efficient Buildings. In *Smart Systems Integration*, Copenhagen, 2015. Smart Systems Integration.

Bibliography

A. V. Hill. The possible effects of the aggregation of the molecules of hæmoglobin on its dissociation curves. *Proceedings of the Physiological Society*, pages iv–vii, 1910.

Thomas F Icard. Sick Building Syndrome and Building-Related Illness Claims : Defining the Practical and Legal Issues. *The Construction Lawyer*, 14(4), 1994.

Noriaki Ikeda, Takahashi Hiroshi, Umetsu Kazuo, and Suzuki Tsuneo. The course of respiration and circulation in death by carbon dioxide poisoning. *Forensic Science International*, 41 (1-2):93–99, 1989.

Jun Izumi, Nariyuki Tomonaga, and Akinori Yasutake. Development on High Performance Gas Separation Process Using Gas Adsorption. *Mitsubishi Heavy Industries, Ltd. Technical Review*, 39(1):6–10, 2002.

Er Vibhor Jain, Er Gagan Bajaj, and Er Danda Avinash. Numerical Analysis of Silica Gel Bed Used In Desiccant Air Cooler and Dehumidifier. 3(6):640–644, 2013.

R Janssen. Towards energy efficient buildings in Europe. *The European Alliance of Companies for Energy Efficiency in Buildings*, page 74, 2004.

Stanley H. Jury and Harold R. Edwards. The silica gel-water vapor sorption therm. *The Canadian Journal of Chemical Engineering*, 49(5):663–666, 1971.

Shing-Lin Kuo, Enayat O Pedram, and Anthony L Hines. Analysis of Ammonia Adsorption on Silica Gel Using the Modified Potential Theory. *Journal of Chemical and Engineering Data*, 30(1):330–332, 1985.

K J Leckrone and J M Hayes. Efficiency and temperature dependence of water removal by membrane dryers. *Analytical chemistry*, 69(5):911–8, 1997.

Rick Lee and Bob Schmidt. Keeping Abrasive Dry: A Review of Recent Technology. *Journal of Protective Coatings and Linings*, pages 52–58, 1995.

Xin Li, Zhong Li, Qibin Xia, and Hongxia Xi. Effects of pore sizes of porous silica gels on desorption activation energy of water vapour. *Applied Thermal Engineering*, 27(5-6):869–876, 2007.

G.G. Mandayo, J. Gonzalez-Chavarri, E. Hammes, H. Newton, I. Castro-Hurtado, I. Ayerdi, H. Knapp, A. Sweetman, C.N. Hewitt, and E. Castaño. System to control indoor air quality in energy efficient buildings. *Urban Climate*, 14:475–485, 2015.

E.C. Markham and Arthur F. Benton. The Adsorbtion of Gas Mixtures by Silica. *Journal of the American Chemical Society*, 53(2):497–507, 1931.

Hiromitu Naono, Reiko Fujiwara, and Masahide Yagi. Determination of physisorbed and chemisorbed waters on silica gel and porous silica glass by means of desorption isotherms of water vapor. *Journal of Colloid and Interface Science*, 76(1):74–82, 1980.

150

Arpan Kumar Nayak, Ruma Ghosh, Sumita Santra, Prasanta Kumar Guha, and Debabrata Pradhan. Hierarchical Nanostructured WO 3 -SnO 2 for Selective Sensing of Volatile Organic Compounds. *Nanoscale*, (2):12460–12473, 2015.

K. C. Ng, H. T. Chua, C. Y. Chung, C. H. Loke, T. Kashiwagi, A. Akisawa, and B. B. Saha. Experimental investigation of the silica gel-water adsorption isotherm characteristics. *Applied Thermal Engineering*, 21(16):1631–1642, 2001.

K.; Oberbach, E.; Baur, S.; Brinkmann, and E Schmachtenberg. *Saechtling Kunststoff Taschenbuch*. Hanser, Munich, 2001.

OSHA. Occupational Safety and Health Standards. Toxic and Hazardous Substances. Air Contaminants. 1901.1000., 2006a. http://www.osha.gov/pls/oshaweb/owadisp. show{_}document?p{_}id=9991{&}p{_}table=STANDARDS.

OSHA. TABLE Z-1 Limits for Air Contaminants., 2006b. https://www.osha.gov/pls/oshaweb/ owadisp.show{_}document?p{_}table=STANDARDS{&}p{_}id=9992.

OSHA. Table Z-2 Toxic and Hazardous Substances, 2006c. https://www.osha.gov/pls/oshaweb/ owadisp.show{_}document?p{_}table=STANDARDS{&}p{_}id=9993.

OSHA. TABLE Z-3 Mineral Dusts, 2006d. https://www.osha.gov/pls/oshaweb/owadisp. show{_}document?p{_}table=STANDARDS{&}p{_}id=9994.

OSHA. Substance technical guidelines for formalin, 2013. https://www.osha.gov/pls/oshaweb/ owadisp.show{_}document?p{_}table=STANDARDS{&}p{_}id=10076.

Nello Pace, Enrique Strajman, and Elaine L. Walker. Acceleration of Carbon Monoxide Elimination in Man by High Pressure Oxygen. *Science*, 111(2894):652–654, 1950.

Frank G Pearce. *The performance of adsorbents in gas mask canisters by*. PhD thesis, Massachusetts Institute of Technology, 1946.

A. Pesaran and A. Mills. Moisture transport in silica gel packed beds - II. Experimental study. *International Journal of Heat and Mass Transfer*, 30(6):1037–1049, 1987a.

A. Pesaran and A. Mills. Moisture transport in silica gel packed beds - I.Theoretical study. *International Journal of Heat and Mass Transfer*, 30(6):1037–1049, 1987b.

A. A. Pesaran. *Moisture Transport in Silica Gel Particle Beds*. PhD thesis, University of California, Los Angeles, 1983.

R. F. Phalen and O. G. Raabe. Aerosol Particle Size as a Factor in Pulmonary Toxicity. In *Paper No. 23, AD-AO 11872*, pages 353–365. NTIS, U.S. Dept of Commerce, 1974.

Dallas Safriet. *Locating and Estimating Air Emissions From Sources of Formaldehyde (revised)*. U.S. EPA, Triangle Park, NC, 1991.

Bibliography

Jung Yang San and Gwo Donq Jiang. Modeling and testing of a silica gel packed-bed system. *International Journal of Heat and Mass Transfer*, 37(8):1173–1179, 1994.

R. Scott. *Physical Chemistry Resources Book 5: Thermal Analysis*. 2000.

Siemens Building Technologies. Demand-Controlled Ventilation. Technical Report January, Siemens, 2015.

K. S. W. Sing. Reporting physisorption data for gas/solid systems with special reference to the determination of surface area and porosity (Recommendations 1984). *Pure and Applied Chemistry*, 57(4):603–619, 1985.

David J. Tenenbaum. The Monster in the Closet: Mothballs' Link to Non-Hodgkin Lymphoma. *Environmental Health Perspectives*, 112(13):758–759, 2004.

T Tuomi, B Engstrom, R Niemela, J Svinhufvud, and K Reijula. Emission of ozone and organic volatiles from a selection of laser printers and photocopiers. *Applied occupational and environmental hygiene*, 15(8):629–634, 2000.

L. A. Wallace. Major sources of benzene exposure. *Environmental Health Perspectives*, 82 (about 200):165–169, 1989.

Ching Mei Wang, Kuei Sen Chang, Tsair Wang Chung, and Honda Wu. Adsorption equilibria of aromatic compounds on activated carbon, silica gel, and 13X zeolite. *Journal of Chemical and Engineering Data*, 49(3):527–531, 2004.

Benjamin A. Weinstock, Husheng Yang, Blayne L. Hirsche, and Peter R. Griffiths. Kinetic modeling of the adsorption rate of a gaseous adsorbate on a granular adsorbent by ultra-rapid-scanning fourier transform infrared spectrometry. *Langmuir*, 21(9):3915–3920, 2005.

WHO Regional Office for Europe. *WHO guidelines for indoor air quality*, volume 9. 2010.

World Health Organization. *WHO Air quality guidelines for particulate matter, ozone, nitrogen dioxide and sulfur dioxide: global update 2005: summary of risk assessment*. 2006.

N Yamazoe. Toward innovations of gas sensor technology. *Sensors and Actuators B-Chemical*, 108(1-2):2–14, 2005.

Husheng Yang, Benjamin A Weinstock, Blayne L Hirsche Ii, and Peter R Griffiths. Kinetics modeling of aldehyde adsorption rates on bare and aminopropylsilyl-modified silica gels by ultra-rapid scanning fourier transform infrared spectrometry. *Langmuir*, 21(4):3921–3925, 2005.

Carl L. Yaws. Thermal Conductivity of Liquid – Inorganic Compounds. In *Transport Properties of Chemicals and Hydrocarbons*, chapter 8, pages 396–402. Elsevier, 2009.

Zeynep Elvan Yildirim. A Study on Isotherm Characteristics of Adsorbent-Adsorbate Pairs Used in Adsorption Heat Pumps. Master's thesis, İzmir Institute of Technology, 2011.

EMILY ANN HAMMES

RESEARCH INTERESTS

Interested in tissue engineering, microfluidics and transport phenomena in biological systems
Prefers a balance between computational modeling, experimentation and device design

EDUCATION

École Polytechnique Fédérale de Lausanne (EPFL), Lausanne, Switzerland

Ph.D. in Advanced Manufacturing   *July 2016*

Illinois Institute of Technology (IIT), Chicago IL

Master, Biological Engineering   *July 2007*

    GPA: 3.4/4.0

B.S. Biomedical Engineering, Concentration: Cell & Tissue Engineering   *July 2006*

    GPA: 3.5/4.0 (High Honors)   Camras Scholarship (3/4 tuition, 5 years, including M.S.)

    Study Abroad: Finland (Fall 2003), France (Summer 2006) & Turkey (Summer 2007)

WORK EXPERIENCE

Designed, Modeled and Tested Sorption in a Gas Delivery System   *Feb 2012-June 2016*

    CSEM Central Switzerland

- Designed, constructed and tested the microfluidics and preconditioning unit for the Intasense air quality monitor
- Conducted experiments and modeled the sorption of humidity and toxic gasses on silica gel.

Modeling Mesenchymal Stem Cell Differentiation   *Sept 2009-December 2011*

    Max Planck Research Institute, Universität Magdeburg, Germany

- Developed quantitative models of stem cell differentiation

Modeling Stochastic Kinase Cascades   *June 2008-May 2009*

    École Polytechnique Fédérale de Lausanne (EPFL), Switzerland

- Modeled protein interactions within cells

Three-Dimensional Patterning in Poly(ethylene glycol) Hydrogels   *Sept 2005 -May 2007*

    IIT Department of Biomedical Engineering

- Created 3D Poly(Ethylene Glycol) (PEG) scaffolds using surface initiated non-contact photolithography

Inter-Professional Research Project: Engineering Novel Organisms   *Jan-Dec 2005*

    IIT Department of Biology

- Designed an oscillating metabolic pathway in multiple e-coli and conducted lab work to build the system

Understanding How the Nervous System Controls Unpracticed Movements   *Summer 2005*

    Marquette University Biomedical Engineering Department & The Rehabilitation Institute of Chicago

- Researched spinal cord and brain involvement during unpracticed human movement

MOST RELEVANT RESEARCH TECHNIQUES AND SKILLS

- Modeling sorption chemistry, transport phenomena and chemical reactions using Comsol and Matlab
- Manufacturing of microfluidic devices (laser cutting, milling etc)
- Using design of experiments to confirm that multiple systems are statistically identical
- Conducting biological and chemical experiments in tissue engineering and genetics
- Writing clear laboratory protocols and reports, experience working on multinational projects (European FP7)

PUBLICATIONS & CONFERENCE PRESENTATIONS

Journal Articles

G. G. Mandayo, J. Gonzalez-Chavarri, E. Hammes, H. Newton, I. Castro-Hurtado, I. Ayerdi, H. Knapp, A. Sweetman, C. Hewitt and E. Castaño, "System to Control Indoor Air Quality in Energy Efficient Buildings," Urban Climate, 2014.

Georgia Papavasiliou, Preedarat Songprawat, Victor Pérez-Luna, Emily Hammes, Megan Morris, Yu-Chieh Chiu, and Eric Brey, "Three-Dimensional Patterning of Poly(Ethylene Glycol) Hydrogels Through Surface-Initiated Photopolymerization," Tissue Engineering Part C: Methods, 2008

Invited Conference Presentations

G. G. Mandayo, J. Gonzalez-Chavarri, I. Castro-Hurtado, E. Castaño, T. Geiling, M. Hoffmann, E. Hammes, P. Ryser, H. Knapp, R. Heslop, J. Jones, P. Fitzpatrick and R. Bell, "System to Control Indoor Air Quality in Energy Efficient Buildings," EuNetAir, Copenhagen, 2013

E. Hammes and R. Findeisen, "Modeling Mesenchymal Stem Cell Differentiation," The US-Turkey Advanced Study Institute on Global Healthcare Challenges, Adrasan, 2010

Conference Proceedings

G. G. Mandayo, J. Gonzalez-Chavarri, I. Castro-Hurtado, I. Ayerdi, E. Castaño, E. Hammes, P. Ryser, H. Knapp, "The INTASENSE Project Approach for Toxic Gas Detection Indoors," International Congress on Architectural Envelopes, San Sebastian, 2015.

E. Hammes, J. Gonzalez-Chavarri, L. Henwood-Moroney, G. G. Mandayo, P. Ryser and H. F. Knapp, "The Transport Phenomena within the INTASENSE Indoor Air Quality Monitor Design," American Institute of Chemical Engineers, Austin, 2015.

E. Hammes, J. Gonzalez-Chavarri, L. Henwood-Moroney, G. G. Mandayo, P. Ryser and H. F. Knapp, "A Smart Air Quality Monitor for Energy Efficient Buildings," in Smart Systems Integration, Copenhagen, 2015.

E. Hammes and S. Schubert, "An Open Source Open Water Monitor," in Smart Systems Integration, Copenhagen, 2015.

E. Hammes and S. Schubert, "Built to Dive," European Conference on Scientific Diving, Stuttgart, 2015.

G. Papavasiliou, E. Brey, E. Hammes and V. Pérez-Luna, "A Technique for Generating Three-Dimensional Patterns in Poly(ethylene glycol) Hydrogels," Biomedical Engineering Society, Chicago, 2006

G. Papavasiliou, E. Brey, E. Hammes and V. Pérez-Luna, "Three-Dimensional Patterning in Poly(ethylene glycol) Hydrogels," International Society of Applied Cardiovascular Biology, La Jolla, 2006

S. Schindler-Ivens and E. Hammes, "How does the spinal cord compensate for reversal of pedaling direction?" Research Symposium of the National Science Foundation Research Experience for Undergraduates (REU) in Biomedical Engineering, Milwaukee, 2005

Conference Presentations

E. Hammes and S. Schubert, "Scuba Sensors," Chaos Communications Congress, Hamburg, 2014.

E, Hammes, J. Gonzalez de Chavarri, G. G. Mandayo, P. Ryser and H. F. Knapp, "Intasense—Fluidics Design," Building Test Expo, Brussels, 2014.

E. Hammes and R. Findeisen, "Modeling Mechanical Signal Transduction in Mesenchymal Stem Cell Differentiation," Systems Biology of Human Disease, Boston, 2010

Technical Reports

E. Hammes, P. Ryser and H. F. Knapp, "Air Pretreatment Platform for Indoor Air Qualtiy Monitoring," CSEM Scientific and Technical Report 2015, Neuchâtel, 2016.

E. Hammes, J. Gonzalez-Chavarri, L. Henwood-Moroney, G. G. Mandayo, P. Ryser and H. F. Knapp, "Air Pretreatment Platform for Indoor Air Quality Monitoring," CSEM Scientific and Technical Report 2014, Neuchâtel, 2015.